ANALYSIS OF A PROPOSED SIX INCH DIAMETER SPLIT HOPKINSON PRESSURE BAR

By

ELISABETTA LIDIA JEROME

A DISSERTATION PRESENTED TO THE GRADUATE SCHOOL
OF THE UNIVERSITY OF FLORIDA IN PARTIAL FULFILLMENT
OF THE REQUIREMENT FOR THE DEGREE OF
DOCTOR OF PHILOSOPHY

UNIVERSITY OF FLORIDA

1991

ACKNOWLEDGMENTS

I wish to thank my committee for their support and advice during this educational process. In particular I thank Dr. C. Allen Ross for his advice, support, and encouragement. Without him this effort would not have been possible. I would also like to thank my husband David for his patience and understanding during the many nights and weekends I spent at my desk or in front of the computer. I would like to acknowledge the financial support of the Air Force Engineering and Services Center at Tyndall Air Force Base. Finally, I wish to acknowledge the help and support of Sverdrup Technology Inc. during my educational endeavors.

TABLE OF CONTENTS

LIST OF FIGURES

page

Abstract of Dissertation Presented to the Graduate School of the University of Florida in Partial Fulfillment of the Requirements for the Degree of Doctor of Philosophy

ANALYSIS OF A PROPOSED SIX INCH DIAMETER SPLIT HOPKINSON PRESSURE BAR

By

Elisabetta Lidia Jerome

August 1991

Chairman: C. Allen Ross
Major Department: Aerospace Engineering, Mechanics and Engineering Science

The objective of this investigation was to determine whether a 6-inch diameter Split Hopkinson Pressure Bar (SHPB) is feasible; whether the assumptions made in a typical 2- to 3-inch SHPB still apply; and what changes, problems, and issues would be associated with an SHPB that size. The effort included a mathematical and a numerical analysis. Experimental data from a 2-inch SHPB were used to compare and validate analytical models.

A methodology based on the Pochhammer-Chree frequency equation was developed by the author to study the wave propagation and wave interaction in any size SHPB. Additionally, a second order accurate finite difference code was used to mathematically understand the wave motion in a typical bar.

The effects of friction and inertia were analyzed numerically, and general guidelines and corrections were developed.

This investigation concluded that a 6-inch SHPB is theoretically feasible and, in fact, identical to any existing system if the input pressure pulse duration is scaled appropriately.

The modified Pochhammer-Chree method can be used to assess the validity of any size SHPB and to study the wave interactions. If the specimen length and diameter are kept in the same order of magnitude, one need not worry about friction in the proposed 6-inch SHPB. A correction will be needed to account for inertia, especially at strain-rates of 50 to 100 sec^{-1} and above. The Split Hopkinson Pressure Bar has been and remains a reliable, accurate, and useful tool to study material response to loading, even for a new proposed system six inches in diameter.

CHAPTER 1

INTRODUCTION

Objective

The objective of this investigation is to determine whether a 6-inch diameter Split Hopkinson Pressure Bar (SHPB) is feasible; whether the assumptions made in a typical 2- to 3-inch SHPB still apply; and what major changes, problems and issues would be associated with an SHPB that size.

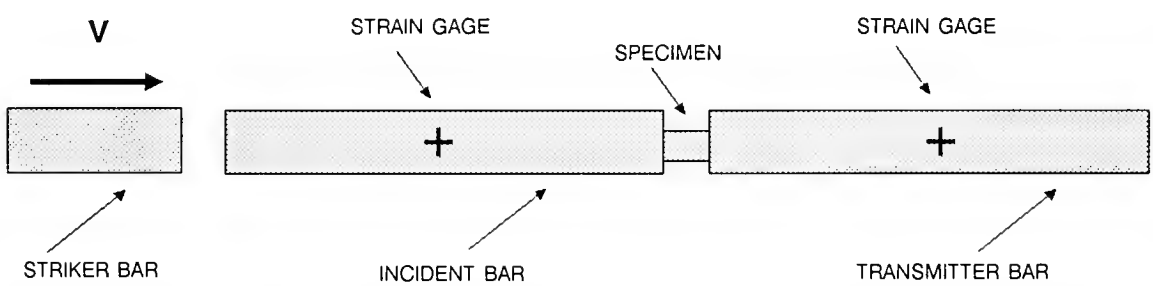

Figure 1. Compressive SHPB Schematic

Background

The Split Hopkinson Pressure Bar may be used to study materials at high strain-rates in tension, shear and compression. A compressive SHPB is shown schematically in Figure 1. An SHPB system consists of a specimen sandwiched between and in contact with two elastic bars--incident and transmitter bar. The incident bar is impacted by a striker bar at a known velocity

causing a pressure wave to travel down the bar. This wave is partially transmitted and partially reflected at the incident bar/specimen interface, and partially transmitted and partially reflected at the specimen/transmitter bar interface. Strain gages attached to the incident and transmitter bars record the strains associated with the reflected, transmitted, and incident pulses. From these strain data, stresses, strains, and strain-rates in the specimen can be computed as a function of time.

Although different sizes of SHPBs have been built, the largest one in existence in the USA is 3 inches in diameter. The main reason behind this size limitation is that it is generally assumed that the wave propagation in the bar is one-dimensional, implying a high length to diameter ratio. A simpler form of the SHPB has been around since the late 1940s, when techniques and instrumentation were not as sophisticated as they are today. Historically, there may not have been a need to test a material specimen larger than 3 inches in diameter. However, in recent times the need for more economical structures to resist impulsive loadings associated with earthquakes, accidental explosions, and effects of conventional explosives has prompted more research into strain rate effects on the properties of concrete. Considerable data have been generated in 2- to 3-inch diameter SHPB systems on concrete specimens containing small or scaled down aggregate. The question which arises from such small tests is, does the strain rate sensitivity, found for the small laboratory specimens, apply to the standard 6-inch diameter large aggregate test specimens which are cored or cast in the field? There is a need to use a 6-inch diameter SHPB type apparatus to test concrete specimens, which will match the concrete specimens which are cored directly in the field.

The SHPB has proven to be a very effective and useful tool to conduct high strain-rate material response studies since Kolsky [1] described its use in 1949. Detailed discussions of how a typical system works can be found in numerous papers including Hauser, Simmons and Dorn [2], Lindholm [3], Malvern and Ross [4], Robertson, Chou, and Rainey [5], and many others.

Because of the inherent difficulties associated with a system of this kind, an idealized one-dimensional wave theory is commonly assumed where stress is uniform over each cross section, plane cross sections remain plane during motion, and stress and strain are uniform throughout the length of the specimen. The above assumptions are adequate if the length of the bar greatly exceeds the diameter, in order to ensure no end effects and the loading pulse is much larger than the transit time of the specimen. However, factors like dispersion, radial and axial inertia effects, and friction between the specimen and the incident and transmitter bars can cause erroneous results if care is not used in either conducting the experiment or analyzing the data. Approximate corrections for the calculated one-dimensional stress have been formulated to account for inertial and frictional effects. Kolsky [6] introduced a correction for radial inertia. Davies and Hunter [7] discussed both friction and inertia effects. Other papers of interest on this subject are those by Rand [8], Dharan and Hauser [9], Samanta [10], Jahsman [11], Chiu and Neubert [12], and Young and Powell [13].

The original SHPB apparatus was devised to study materials in compression. More recently it was modified to test specimens in both tension and torsion. Examples of these techniques are discussed by Nicholas [14], Lawson [15], Baker and Yew [16], Jones [17], Okawa [18], Ross, Nash, and Friesenhahn [19], Rajendran and Bless [20], and Ross [21]. Follansbee and Frantz [22] used the Pochhammer-Chree frequency equation to correct the recorded pulses for dispersion as they travel down the bar assuming only the first longitudinal vibrational mode is excited.

Approach

Before undertaking any research it is imperative to know and understand what has already been done on the subject. This ensures no duplication of work and gives a good working foundation from which to start the research effort.

The wave propagation in an SHPB is governed by the equations of motion. Generally, it is assumed the motion is one-dimensional, and therefore is uniform in the radial and the circumferential direction. Although the one-dimensional wave theory has been shown to be accurate for the existing systems, a mathematical analysis is needed for the proposed 6-inch SHPB to assess whether this simple theory still applies. The two-dimensional axisymmetric cylindrical equations of motion need to be analyzed and solved (approximately), by various methods to understand the wave motion in a bar.

There are no known exact solutions to the two-dimensional wave propagation problem in a finite cylindrical bar, and therefore one must turn to a numerical scheme, namely a finite difference approximation. Modern computers make it possible to solve large problems in a reasonable amount of time. The plan was to first numerically simulate an existing SHPB in order to compare the results with experimental data and have confidence in the reliability of the numerical approximation. The second step would then be to simulate the proposed 6-inch system and gather information on the wave motion.

The final step will be a comprehensive look at the different methodologies, approximations, and assumptions to better understand the implications of increasing the size of the SHPB system. From this one can assess whether the data reduction of the current SHPBs still applies to the large bars, and what are the problems associated with a system two or three times the size of the existing ones.

CHAPTER 2

MATHEMATICAL BACKGROUND

SHPB Assumptions

As discussed earlier, a one-dimensional wave theory is generally assumed in the analysis of an SHPB. The one-dimensional theory assumes longitudinal spatial variations only. Applying Newton's law for a displacement u in the x direction of the diagram below, gives the equations of motion for an elastic system

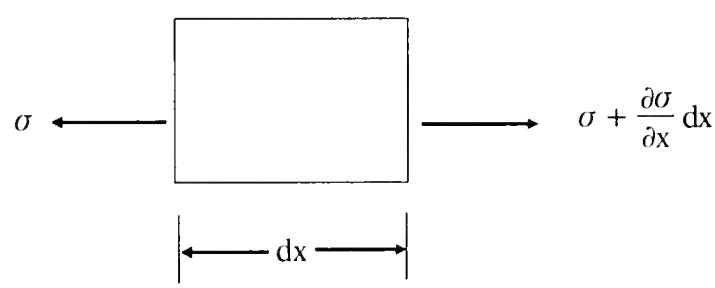

$$-\sigma A + (\sigma + \frac{\partial \sigma}{\partial x} dx)A = \rho A dx \left(\frac{\partial^2 u}{\partial t^2}\right),$$

or upon simplification

$$\frac{\partial \sigma}{\partial x} = \rho \frac{\partial^2 u}{\partial t^2} \tag{1a}$$

and Hooke's law

$$\sigma = E\,\varepsilon = \frac{\partial u}{\partial x} E,$$

where σ is the stress, E is Young's modulus, ε is strain, t is time, A is the cross-sectional area, and ρ is the density of the material. Equation (1a) can be rewritten as follows

$$\frac{\partial^2 u}{\partial t^2} = \left(E/\rho \right) \frac{\partial^2 u}{\partial x^2} \tag{1b}$$

where E/ρ is the familiar elastic wave speed squared, or $E/\rho = c_o^2$. The general solution to (1b) is of the form

$$u = f(x + c_o t) + g(x - c_o t)$$

corresponding to forward and backward propagating waves. Assuming $u = g(x - c_o t)$ only, differentiate u and obtain

$$\frac{\partial u}{\partial x} = g' \quad \text{and} \quad \frac{\partial u}{\partial t} = -c_o g'$$

where g′ denotes differentiation of the function w.r.t. the argument $(x\text{-}c_o t)$. Eliminating g′ between these two expressions yields

$$\frac{\partial u}{\partial t} = -c_o \frac{\partial u}{\partial x} = -c_o \varepsilon$$

Strains are usually measured in an SHPB experiment at some distance from the specimen. To obtain the interface displacements, these recorded strains must be time-shifted to give the strains at the interfaces, and then integrated over time to give

$$u_1 = \int_0^t -c_o (\varepsilon_i - \varepsilon_r)\, dt \quad \text{and} \quad u_2 = \int_0^t -c_o \varepsilon_t \, dt$$

where the subscripts i, r, and t indicate incident, reflected and transmitted. Additionally, u_1 and u_2 are the specimen's displacements at the incident and output bars interfaces respectively. The negative signs give positive displacements for compressive (negative) strains. Let L be the length of the specimen; then the average strain in the specimen is

$$\varepsilon_s = (u_2 - u_{1)}/L\,.$$

This is sometimes approximated for short specimens and slowly changing stress by assuming equal stresses at the two interfaces, which implies that

$$\varepsilon_t = \varepsilon_i + \varepsilon_r\,.$$

The specimen strain then becomes

$$\varepsilon_s = \left(-2c_o/L\right) \int_0^t \varepsilon_r dt$$

and the specimen strain rate is

$$\dot{\varepsilon}_s = (-2c_o/L)\,\varepsilon_r\,.$$

By using Hooke's law, the stresses on either face of the specimen are

$$\sigma_{s2} = E\left(\frac{A}{A_s}\right)\varepsilon_t \quad \text{and} \quad \sigma_{s1} = E\left(\frac{A}{A_s}\right)(\varepsilon_i + \varepsilon_r)$$

where $\frac{A}{A_s}$ is the ratio of the bar and specimen cross section areas. If the interface stresses are not assumed to be equal, then $\varepsilon_t \neq \varepsilon_i + \varepsilon_r$, and the specimen strain and strain rate are given by

$$\varepsilon_s = (-c_o/L) \int_0^t \left(\varepsilon_t - \varepsilon_i + \varepsilon_r\right) dt \quad \text{and} \quad \dot{\varepsilon}_s = (-c_o/L)\,\left(\varepsilon_t - \varepsilon_i + \varepsilon_r\right)\,.$$

There are some problems associated with such a simplified one-dimensional theory, even for long slender rods, and these problems are accentuated for larger diameter and shorter length SHPB systems. First, longitudinal waves are dispersive, (wave speed is a function of frequency), which means the waveform that is recorded at a distance from the specimen is not the same waveform that actually arrives at the specimen. Wave dispersion can be corrected for, but is time consuming and the correction methods are not exact. The one-dimensional theory also neglects stress and displacement variations across the cross section. Since strains are measured only at the surface, this can also lead to errors.

Equations of Motion

To assess the validity of this simple theory, one can study the equations of motion that govern the wave motion in a circular cross section SHPB. The equations of motion are given in tensor form as

$$\nabla \cdot \tilde{T} + \rho \tilde{b} = \rho \frac{d^2 \tilde{u}}{dt^2} \tag{2}$$

where $\tilde{T}$ is the stress tensor, $\tilde{b}$ are the body forces (which are usually safely neglected), and $\frac{d^2\tilde{u}}{dt^2}$ is the acceleration term. In cylindrical coordinates (Figure 2), equation (2) becomes

$$\rho \frac{\partial^2 u_r}{\partial t^2} = \frac{\partial \sigma_{rr}}{\partial r} + \frac{\sigma_{rr} - \sigma_{\theta\theta}}{r} + \frac{1}{r}\frac{\partial \sigma_{r\theta}}{\partial \theta} + \frac{\partial \sigma_{rz}}{\partial z}$$

$$\rho \frac{\partial^2 u_\theta}{\partial t^2} = \frac{\partial \sigma_{r\theta}}{\partial r} + \frac{1}{r}\frac{\partial \sigma_{\theta\theta}}{\partial \theta} + \frac{\partial \sigma_{\theta z}}{\partial z} + 2\frac{\sigma_{r\theta}}{r} \tag{3}$$

$$\rho \frac{\partial^2 u_z}{\partial t^2} = \frac{\partial \sigma_{rz}}{\partial r} + \frac{1}{r}\frac{\partial \sigma_{\theta z}}{\partial \theta} + \frac{\partial \sigma_{\theta z}}{\partial z} + \frac{\sigma_{rz}}{r}$$

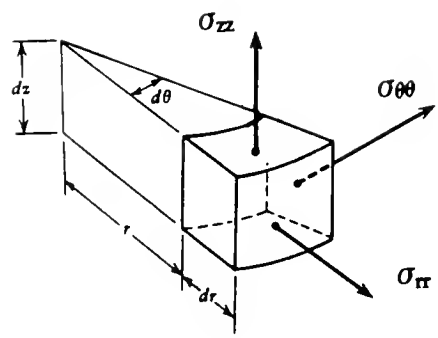

Figure 2. Cylindrical Coordinates

Equations (3) represent the three-dimensional motion in a cylindrical bar. The modes of vibration associated with an isotropic circular cylinder are in general very difficult to calculate and they depend on the specific boundary conditions as well as on the form of the input loading. If the axis of the cylinder coincides with the z-axis, two general types of vibrational modes exist. One set is symmetric and one is asymmetric. In this analysis, the assumption is made that since the striker bar impacts the incident bar squarely, then the motion should be axisymmetric. This means the solution is independent of theta; then u_θ, $\sigma_{r\theta}$ and $\sigma_{z\theta}$ vanish, and the second of equations (3) is satisfied identically. It also means that the only possible modes of vibration will be symmetric. Using Redwood's [23] notation, these modes will be called $M_{m,n}$ where m is either 1 (symmetric) or 2 (asymmetric) and n ranges from 1 (Young's modulus mode) to infinity. Therefore, in this study of an SHPB, only $M_{1,n}$ modes are considered. The constitutive relations for an elastic material can be written as

$$\sigma_{rr} = (\lambda + 2\mu)\frac{\partial u_r}{\partial r} + \lambda\left(\frac{u_r}{r} + \frac{\partial u_z}{\partial z}\right)$$

$$\sigma_{rz} = \mu \left(\frac{\partial u_r}{\partial z} + \frac{\partial u_z}{\partial r} \right)$$

$$\sigma_{zz} = (\lambda + 2\mu) \frac{\partial u_z}{\partial z} + \lambda \left(\frac{u_r}{r} + \frac{\partial u_r}{\partial r} \right) \tag{4}$$

$$\sigma_{\theta\theta} = r \frac{\partial \sigma_{rr}}{\partial r} + \frac{\partial \sigma_{rz}}{\partial z} + \sigma_{rr}$$

where λ and μ are Lame's constants. Making use of (4) and neglecting theta dependence, equations (3) can thus be reduced to only two equations

$$\rho \frac{\partial^2 u_r}{\partial t^2} = (\lambda + 2\mu) \left[\frac{\partial^2 u_r}{\partial r^2} + \frac{1}{r} \frac{\partial u_r}{\partial r} - \frac{u_r}{r^2} \right] + (\lambda + \mu) \frac{\partial^2 u_z}{\partial r \partial z} + \mu \frac{\partial^2 u_r}{\partial z^2}$$

$$\rho \frac{\partial^2 u_z}{\partial t^2} = \mu \left[\frac{\partial^2 u_z}{\partial r^2} + \frac{1}{r} \frac{\partial u_z}{\partial r} \right] + (\lambda + 2\mu) \frac{\partial^2 u_z}{\partial z^2} + (\lambda + \mu) \left[\frac{\partial^2 u_r}{\partial r \partial z} + \frac{1}{r} \frac{\partial u_r}{\partial z} \right] \tag{5}$$

The boundary conditions require no stress at the bar surface or

$$\sigma_{rr} = 0 \quad \text{and} \quad \sigma_{rz} = 0 \quad \text{at} \quad r = a$$

where a is the radius of the bar. Also at a free end, $\sigma_{rz} = 0$ and $\sigma_{zz} = 0$.

For a colinear impact of one bar against another, the initial conditions can be in the form of a step change in pressure

$$\sigma_{zz} = -PH(t), \ \sigma_{rz} = 0$$

where P is a uniform pressure and H(t) is the Heaviside step function, or as a harmonic displacement of $u_z = \sin\omega t$ and $\sigma_{rz} = 0$. The condition $\sigma_{rz} = 0$ is correct only if the two bars are of identical diameter and material, so that the interface is a plane of symmetry of the stress state, until a reflected wave

reaches the interface. Equations (5) have been solved for an infinitely long bar by Pochhammer and Chree for the propagation of sinusoidal waves and studied by numerous investigators over the years [6, 24, 25, 26, 27, 28, 29]. The solution is called the frequency equation and has the form

$$\begin{vmatrix} 2\gamma\frac{\partial}{\partial a}J_0(ha) & \left(2\gamma^2 - \frac{\omega^2\rho}{\mu}\right) J_1(\kappa a) \\ 2\mu\frac{\partial^2}{\partial a^2}J_0(ha) - \frac{\lambda\rho\omega^2}{\lambda + 2\mu}J_0(ha) & 2\mu\gamma\frac{\partial}{\partial a}J_1(\kappa a) \end{vmatrix} = 0 \qquad (6)$$

where $h^2 = (2\pi/\Lambda)^2 [\rho c_p^2/(\lambda + 2\mu) - 1], \kappa^2 = (2\pi/\Lambda)^2 [(\rho c_p^2/\mu) - 1]$, Λ = wavelength, $\gamma = 2\frac{\pi}{\Lambda} = \frac{\omega}{c_p}$, J_0 and J_1 are the zero and first order Bessel functions respectively, ω is the angular frequency, and c_p is the phase velocity.

Solutions of the Frequency Equation

There are an infinite number of solutions to Equation (6), each corresponding to a unique mode of vibration. The solutions are exact only for an infinitely long cylinder although, for a cylinder whose length greatly exceeds its diameter, the errors are small. Furthermore, the solutions are not explicit but rather a function relating the phase velocity c_p, the wavelength Λ, and Poisson's ratio v. Now (6) can be written in implicit form as

$$2\mu\gamma\frac{\partial}{\partial a}J_1(\kappa a)\, 2\gamma\frac{\partial}{\partial a}J_0(ha) - \left(2\gamma^2 - \frac{\omega^2\rho}{\mu}\right) J_1(\kappa a) \cdot$$

$$\left[2\mu\frac{\partial^2}{\partial a^2}J_0(ha) - \frac{\rho\lambda\omega^2}{\lambda + 2\mu}J_0(ha)\right] = 0 \qquad (7)$$

By making use of the following properties of Bessel functions,

$$\frac{\partial}{\partial a}\left(J_0(ha)\right) = -J_1(ha)$$

$$\frac{\partial}{\partial a}\left(J_1(ha)\right) = hJ_0(ha) - \left(J_1(ha)\right)/a\,,$$

equation (7) can be rewritten as

$$4\mu\gamma^2\left[(\kappa J_0(\kappa a) - J_1(\kappa a)/a)\,(-\kappa J_1(ha)) - \left((2\gamma^2 - \frac{\omega^2\rho}{\mu}\right) J_1(\kappa a)\right] \cdot$$

$$\left[2\mu\,(-hJ_0(ha) + J_1(ha)/a) - \frac{\lambda\rho\omega^2}{\lambda + 2\mu} J_0(ha)\right] = 0\,,$$

which finally becomes

$$\gamma^2\kappa\frac{J_0(\kappa a)}{J_1(\kappa a)} - \frac{1}{2}\frac{1}{a}(\kappa^2 + \gamma^2) + \left[\frac{1}{2}(\kappa^2 - \gamma^2)\right]^2 \frac{J_0(ha)}{hJ_1(ha)} = 0 \qquad (8)$$

Equation (8) has been solved numerically by several investigators [25, 27, 30]. It involves assuming a value of Poisson's ratio and then for varying values of frequencies, ranging from zero to some large number, equation (8) is numerically evaluated to obtain the values of the phase velocity. This turns out to be a very laborious task even with the aid of high speed computers. Results are usually shown in graphical form, namely in curves relating the phase velocity and the frequency, both in nondimensional form for general applicability. Figure 3 [22] shows the solution to equation (8) for a Poisson's ratio of .29. Only the first three vibrational modes are plotted namely $M_{1,1}$, $M_{1,2}$ and $M_{1,3}$. Recall that equation (8) only applies to symmetric vibrational modes. Mode $M_{1,1}$ is of most interest since it appears to be the only mode excited in a typical SHPB. As the frequency of this mode approaches zero, or as the wavelength approaches infinity, the phase velocity approaches ($\sqrt{E/\rho}$), which is the elastic, one-dimensional bar-wave

speed, c_o. As the frequency becomes very large, the phase velocity approaches c_r, the velocity of Rayleigh surface waves. Although it may not be clear from Figure 3, c_p, the phase velocity, approaches c_r from the down side, implying that the phase velocity reaches a minimum which is less than the Rayleigh wave speed at some intermediate frequency. Recall that

$$c_d^2 = \frac{\lambda + 2\mu}{\rho}, \qquad c_t^2 = \frac{\mu}{\rho}, \qquad c_o^2 = \frac{E}{\rho}$$

$$h^2 = (2\pi/\Lambda)^2 (\rho c_p^2/(\lambda + 2\mu) - 1) \quad \text{and} \quad \kappa^2 = (2\pi/\Lambda)^2 (\rho c_p^2/\mu - 1)$$

and it is easily shown that $c_o < c_d$ and for $M_{1,1}$ $c_p \leq c_o$. Then for the $M_{1,1}$ mode the parameter h is always imaginary since, for all frequencies, $c_p < c_d$ where c_d is the dilatational wave speed in an infinite medium.

For very low frequencies κ is real, but past roughly $\frac{a}{\Lambda} = 0.65$, when c_p becomes less than the shear wave speed in an infinite medium c_t, κ is imaginary. This means that at low frequencies ($\frac{a}{\Lambda} < 0.65$), the displacement is mainly due to plane transverse waves, since the set of dilatational waves exists only as a surface disturbance. At high frequencies the total displacement becomes increasingly like a pure surface disturbance [33].

Mode $M_{1,2}$ and higher may be of interest in a "larger" SHPB and at high frequencies. These modes have what are called cut-off frequencies, i.e., frequencies at which the phase velocity becomes infinite and no real disturbance propagates in that mode. From equation (8) this implies either that $\gamma = 0.0$ or that $J_1(\kappa a) = 0.0$. If $\gamma = 0.0$, equation (8) becomes

$$\frac{1}{2}\left(\frac{\omega_{co}}{c_t}\right)^2 \frac{1}{a} = \left(\frac{1}{2}\frac{\omega_{co}^2}{c_t^2}\right)^2 \frac{J_0(ha)}{hJ_1(ha)}$$

since

$$\kappa^2 = \frac{\omega^2}{c_p^2}\left(\frac{c_p^2}{c_t^2} - 1\right) = \omega^2\left(\frac{1}{c_t^2} - \frac{1}{c_p^2}\right)$$

and $\kappa^2 = \frac{\omega_{co}^2}{c_t^2}$ for $c_p = \infty$, where ω_{co} is the cut-off frequency.

Following the same reasoning $h^2 = \frac{\omega_{co}^2}{c_d^2}$, for $c_p = \infty$ and thus one can write

$$2\frac{c_t^2}{c_d^2} = \left(\frac{\omega_{co}}{c_d}a\right)\frac{J_0\left(\frac{\omega_{co}}{c_d}a\right)}{J_1\left(\frac{\omega_{co}}{c_d}a\right)} \tag{9}$$

If $J_1(\kappa a) = 0.0$, it can be said that

$$J_1\left(\frac{\omega_{co}}{c_t}a\right) = 0.0 \tag{10}$$

Equations (9) and (10) can now be used to determine the cut-off frequencies for any mode $M_{1,n}$.

From the solutions of the frequency equation, equation (8), it is possible to calculate the radial and longitudinal displacements for each mode at every frequency, and Poisson's ratio within the cylinder. Bancroft [25] calculated and plotted the amplitude of the longitudinal displacement and showed that they are (as expected) uniform for $\frac{a}{\Lambda} = 0.0$ and the motion is confined to the outside surface when $\frac{a}{\Lambda}$ approaches infinity. This agrees with the observations made earlier about mode $M_{1,1}$ response in general.

Numerous other approximate methods of varying degrees of complexity have been developed to mathematically treat an SHPB system. They fall somewhere in between the simple one-dimensional theory and the two-dimensional, coupled differential equations just presented. Unfortunately,

those that show good agreement with the Pochhammer-Chree solution have very complicated descriptive equations, while those simple equations agree with the exact theory only over a very limited frequency range.

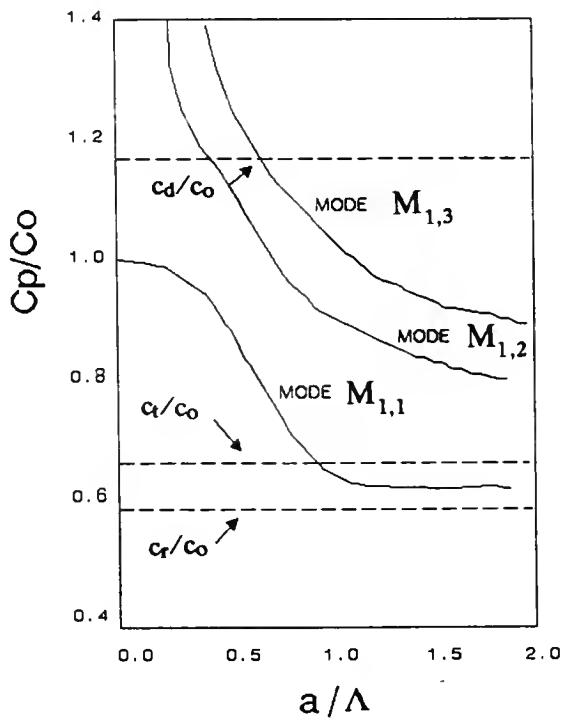

Figure 3. Pochhammer-Chree Solutions for First Three Modes.

When computers were not readily available and usable, a large number of approximate theories were developed. Most important to this study are the different methods and approaches used to derive these theories. As already discussed, the simplest analysis is to assume purely axial stress, uniform over each cross section. This leads to the familiar one-dimensional wave equation in terms of the axial displacement u_z,

$$\frac{\partial^2 u_z}{\partial t^2} = E/\rho \frac{\partial^2 u_z}{\partial z^2}, \tag{11}$$

which predicts that waves of all frequencies travel at the same constant velocity $c_o = \sqrt{E/\rho}$. A better approximation to this theory introduces a correction for the radial motion by considering the inertia of the cross section [23]. The approach involves the use of Hamilton's principle which states that the first variation of the integral of the Lagrangian, (T - V), with respect to time is zero. Specifically

$$\delta \int \left(T - V\right) dt = 0 \tag{12}$$

and (T - V) can be expressed as

$$\int_0^L \left[\underbrace{\frac{1}{2}\rho A\left(\left(\frac{\partial u_z}{\partial t}\right)^2 + (\upsilon R)^2\left(\frac{\partial^2 u_r}{\partial z\,\partial t}\right)^2\right)}_{\text{kinetic energy}} - \underbrace{\frac{1}{2} EA\left(\frac{\partial u_z}{\partial z}\right)^2}_{\text{potential (strain) energy}}\right] dz \tag{13}$$

where L is the length of the cylinder, R is the radius of gyration about the z-axis, υ is Poisson's ratio, and the velocities in the z and r directions are respectively

$$\frac{\partial u_z}{\partial t} \quad \text{and} \quad \frac{\partial u_r}{\partial t}$$

But u_r can be assumed in this approximation to be of the form $\left(-\upsilon\, r \frac{\partial u_z}{\partial z}\right)$ so that

$$\frac{\partial u_r}{\partial t} = -\upsilon r \frac{\partial^2 u_z}{\partial z\,\partial t}.$$

The result of substituting equation (13) into (12) and solving via integration by parts is as follows

$$\rho \left[\frac{\partial^2 u_z}{\partial t^2} - (\upsilon R)^2 \frac{\partial^4 u_z}{\partial^2 z \, \partial^2 t} \right] = E \frac{\partial^2 u_z}{\partial z^2} \tag{14}$$

This equation gives a better approximation of the exact theory than equation (11) at low frequencies. However, for short wavelengths the errors become considerable.

A third approximate theory developed by Love [29] is based on the exact characteristic equation (8), where the Bessel functions are expanded in a power series. If a, the radius of the cylinder, is small enough so that ha and Ka are small compared to unity, then powers of ha and Ka higher than the second can be neglected. That is

$$J_0(\kappa a) = 1 - \tfrac{1}{4} (\kappa a)^2$$

$$J_1(\kappa a) = \tfrac{1}{2} (\kappa a)$$

and the phase velocity becomes

$$c_p = \sqrt{\frac{E}{\rho}} \left(1 - \frac{1}{4} \upsilon^2 \gamma^2 a^2 \right) \tag{15}$$

and may be rewritten as

$$\frac{c_p}{c_o} = 1 - \upsilon^2 \pi^2 \left(\frac{a}{\Lambda} \right)^2 \qquad \text{where} \quad c_o = \sqrt{\frac{E}{\rho}} \tag{16}$$

This theory agrees fairly well with the exact theory up to values of $\frac{a}{\Lambda} = 1$ but then rapidly diverges. The assumptions that κa and ha are small compared to unity imply that the wavelengths of the vibrations are large compared to the radius of the cylinder.

Another common theory was developed by Mindlin and Herrmann [26]. It considers shear stresses and strains by assuming first that the radial displacement is of the form

$$u_r = (r/a)\, u(z,t)$$

with $u_\theta = 0$ and $u_z = w(z,t)$. Forces and moments are then calculated from standard engineering mechanics formulae and corrected for shear and inertia by introducing factors K_1 and K_2. This leads to equations of the form

$$a^2 K_1^2 \mu \frac{\partial^2 u}{\partial z^2} - 8K_2^2 (\lambda + \mu)\, u - 4aK_2^2 \lambda \frac{\partial \omega}{\partial z} = \rho a^2 \frac{\partial^2 u}{\partial t^2}$$

$$2a\lambda \frac{\partial u}{\partial z} + a^2 (\lambda + 2\mu) \frac{\partial^2 \omega}{\partial z^2} = \rho\, a^2 \frac{\partial^2 \omega}{\partial t^2} \qquad (17)$$

By substituting

$$u = A \exp(-i\gamma z) \exp(i\omega t)$$

and

$$w = B \exp(-i\gamma z) \exp(i\omega t)$$

into equation (17), two equations in A and B are obtained, from which A and B can be eliminated to again obtain a characteristic equation which relates phase velocity and frequency for the first two modes. By adjusting K_2 and K_1, a very good approximation can be obtained for mode $M_{1,1}$. Mode $M_{1,2}$, on the other hand, shows considerable deviation from the exact theory.

Many other theories have been developed and, in general, their complexity is directly proportional to their accuracy. These analyses are important because of the insight they give into the response of a cylinder subjected to impulsive loading. Knowing how stresses and displacements are distributed is crucial to the study of wave propagation and SHPB systems.

Transient Behavior

Thus far, the discussion has been limited to continuous waves or at least to pulses more than just a few cycles in length. However, in an SHPB experiment, a very short pulse is propagated through the cylinder, giving rise to a transient behavior which cannot be completely determined from the continuous theories; therefore, a different approach must be taken. One way to tackle the transient problem is to use Fourier analysis. By decomposing the pulse into its continuous component, continuous wave theory can be used on each component at any point down the bar and the new pulse can be obtained by adding the pieces together again. This method is not exact, but it does give a close approximation, especially at some distance from the source.

Choosing a mathematical function that describes the input pulse and that can be represented by a reasonably simple Fourier series is very difficult. Davies [27] used a trapezoidal pulse while Kolsky [28] assumed an error function. In both cases the Pochhammer-Chree curves are used to obtain the phase velocity for each pulse, and in calculating the new shape of the wave-forms, only the fundamental mode $M_{1,1}$ was assumed to be excited.

Another approach taken by some investigators in studying transient behavior is based on the concept of "dominant groups" and the method of stationary phase. The idea is that if at the beginning everything is in phase, any time after that all waves are out of phase, and therefore interfere destructively. When the combined effects of all these waves are studied, the

main contribution comes from a small "dominant" group whose phase velocities, periods, and wavelengths are almost the same. By focusing on this special group, one can obtain approximate propagation of longitudinal, flexural, and torsional waves in a cylinder.

In this study a modified Pochhammer-Chree method is developed using the Fourier analysis approach. It is straightforward and a much simpler numerical simulation than the existing complicated computer codes. This new approach is presented in the next section.

CHAPTER 3

MATHEMATICAL AND NUMERICAL ANALYSIS

Scaling Laws

In order to analyze the propagation of waves in a cylindrical bar, one should ideally solve the three-dimensional equations of motion. Unfortunately, there is no known closed form solution to the problem. Even if axisymmetry is assumed, the two-dimensional equations of motion cannot be easily solved. The problem is further compounded when a different material is introduced, such as when a specimen is introduced in an SHPB. The addition of two interfaces between dissimilar materials creates reflections and transmissions which cause waves to superpose, cancel each other, and in general interact with each other in a very complicated way. Pochhammer and Chree independently solved the equations for the propagation of a sinusoidal wave in an infinite bar. The solution, discussed in chapter 2, is the so called frequency equation; it has an infinite number of solutions, one for each mode, and results in a function relating phase velocity, wave length and Poisson's ratio. These solutions are valid and exact for infinitely long bars. If the bar is long enough to eliminate end effects (approximately 10 diameter lengths) and if the interest is in the transient pulse in its first passage, then the infinite assumption is reasonable.

The Pochhammer-Chree solutions can be plotted in nondimensional form as shown in Figure 3. It is interesting to note that since $\Lambda = c_p T$, then $\frac{a}{\Lambda} = \frac{a}{c_p T}$ and thus $\frac{a}{\Lambda}\frac{c_p}{c_o} = \frac{a}{T c_o}$; where T is the pulse duration and is defined as $T = 2L_s/c_o$, where L_s is the striker bar length. Now if a is multiplied by a

constant factor and T is also multiplied by that same factor, then a plot of $\frac{a}{\Lambda}$ vs. $\frac{c_p}{c_o}$ will not change. What this means is that mathematically, under the assumptions made, if the diameter is multiplied by a constant and the duration of the input pulse is simultaneously multiplied by the same constant, then the solution for the original $\frac{a}{\Lambda}$ is the same for both $\frac{a}{\Lambda}$ values. This applies to a sinusodial, continuous input where the wavelength is constant, and travels at only one wavespeed relative to the bar radius: a long wave in a large bar will have the same wave speed as a short wave in a small bar, as long as $\frac{a}{\Lambda}$ stays constant.

What happens if the input is a transient pulse? A simple mathematical function can be chosen to describe this type of input which can be represented by a Fourier series. A transient pulse is composed of a spectrum of frequencies; the higher frequency components travel more slowly than the lower frequency components, and thus lag behind and cause the initial sharp pulse to spread. This spreading is called dispersion. The Pochhammer-Chree solutions give the velocity of each wave depending on its frequency. Thus, one may correct a given pulse for dispersion by representing the pulse by a series of frequency components, calculating how far each frequency component has traveled in a certain time, and then reassemble the pulse. This task basically amounts to correcting for phase changes within each term of the Fourier series. It is important to be able to correct for dispersion since the SHPB pulses are recorded on strain gages at distances typically 30 to 60 inches from the specimen. Interest is in the response at the specimen itself, but in many cases a strain gage cannot be physically placed there. The dispersion correction technique allows one to predict the shape of the pulse as it travels from the specimen to the strain gage.

Further, following the same kind of reasoning as for the continuous wave case, $\frac{a}{\Lambda}\frac{c_p}{c_o} = \frac{a\pi}{n\Delta t c_o}$ can be written where n is the number of points taken to represent the transient pulse and Δt is the time interval between them. In essence, $n\Delta t$ is the period of the transient pulse, and if $\frac{a}{n\Delta t}$ stays constant, the case is analogous to the continuous case. This means as long as the bar radius and the input pulse length are increased or decreased by the same amount, the response characteristics of a SHPB system will not change.

This fact is important to this study because the main concern is the feasibility of a 6-inch SHPB system. What the Pochhammer-Chree equations show is that if the incident pulse is of large enough duration relative to the bar radius, then, as far as the longitudinal waves of the $M_{1,1}$ mode are concerned, there is mathematically no difference between a 2-, 3-, 6- or 60-inch diameter SHPB. One must then determine what pulse duration would be needed to make a new 6-inch system equivalent to the existing 2- and 3-inch bars and whether the stress, strain and displacement distribution of that pulse are satisfactory for a usable SHPB.

As mentioned earlier, for a typical SHPB system, a uniform stress and strain distribution is assumed, and only strains on the surface are measured. It is then very important to identify under which conditions the one-dimensional assumption is acceptable. Davies [27] computed the ratio of the longitudinal displacement at the surface to that of the longitudinal displacement along the bar axis and showed that for $\frac{a}{\Lambda}$ less than 0.1 their difference is less than 5 percent. Thus for a continuous pulse, with one value of Λ, one-dimensionality is assured if $\frac{a}{\Lambda} < 0.1$. On the other hand, a transient wave contains many different frequencies, and in fact the majority of the $\frac{a}{\Lambda}$ s will be greater then 0.1. Thus, if the transient wave f(t) is

represented with a Fourier series expansion, we would generally express it in a form such as

$$f(t) = \frac{A_o}{2} + \sum_{1}^{\infty} D_n \cos(n\omega_o t - \varphi'_n)$$

where A_o and D_n are Fourier coefficients and φ'_n is the phase angle which is a function of the wave speed and the wavelength. Specifically, from [31]

$$\varphi'_n = \varphi_n + \left(\frac{n\omega_o x}{c_o}\right)\left[\left(\frac{c_o}{c_n}\right) - 1\right]$$

where $n\omega_o$ is the angular frequency and c_n is the phase velocity of the nth component. Equation (8) and Figure 3 give the relationship between c_n and the frequency. The amplitudes in a Fourier series expansion are in decreasing order, meaning that A_o is the largest and D_{n+1} is less then D_n. Furthermore, the frequencies of each component are also in order, they start at zero and go to infinity. In summing the Fourier terms, each term will contribute less and less to the overall pulse. This is why truncating the series at some large number, say 55, results in a very small error. Also, at some point the nth component will have an $\frac{a}{\Lambda} = 0.1$. To ensure one-dimensionality in a SHPB the terms preceding the one with $\frac{a}{\Lambda} = 0.1$ must sum up to give almost the complete pulse. In other words, the amplitude D_n of the nth component having $\frac{a}{\Lambda} = 0.1$ must be a small fraction of the original amplitude A_o. Notice that it does not matter at which component $\frac{a}{\Lambda}$ reaches 0.1, but rather the value of the amplitude at that point must be small. If it is at the 10th or the 100th term in the Fourier series it makes no difference. The only question then is how small should this D_n amplitude be with respect to A_o, or what percentage of the whole pulse must be accounted

for when $\frac{a}{\Lambda}$ reaches 0.1. One way to answer this question is to look at the values for the existing SHPB systems at the University of Florida and at Tyndall AFB. A short computer code was written to calculate $\frac{a}{\Lambda}$ and Fourier amplitude values for an assumed trapezoidal input based on the Pochhammer-Chree solutions [32]. It was found (see Appendix B) that for each system the amplitudes of the Fourier components had fallen to 5-9 percent of the original value by the time $\frac{a}{\Lambda}$ reached 0.1. Therefore, a good minimum amplitude ratio to use for the proposed 6-inch system is about 10 percent. This would assure the one-dimensionality of the response.

In conclusion, because of the form of the equations involved, a pressure bar system can be mathematically scaled up or down to any degree, without affecting the characteristics of the wave motion. Analyses of the bars and input pulses used both at Tyndall AFB and at the University of Florida, showed that a 6-inch system would be equivalent to the existing 2- and 3-inch systems, if the input pulse duration was roughly 500 microseconds.

The length of the striker bar is related to the pulse duration as $T = \frac{2 L_s}{c_o}$, where c_o is the elastic wave speed and L_s is the striker bar length. The elastic wave speed c_o for steel is approximately 5080 m/sec. This means that for a 500 microsecond incident pulse in a steel SHPB, a 1.27 m (50-inch) long striker bar would be required.

Wave Propagation in an SHPB

Having an understanding of this very important fact, one can now turn to a more in-depth look at wave propagation in a cylindrical bar, to broaden the understanding of the overall problem. Three different methodologies were followed to study this problem. The goal was to compare and contrast

results, understanding the drawbacks, assumptions and reliability of each one. These three approaches were :

- A new numerical method developed by the author using the Pochhammer-Chree frequency solution and referred to as a modified Pochhammer-Chree method.
- A finite difference numerical simulation of the governing equations contained in an existing computer code.
- Experimental results from the SHPB at Tyndall AFB.

The following sections are a general description of these three approaches.

Modified Pochhammer-Chree Method

As previously discussed, Pochhammer and Chree independently solved the two-dimensional equations of motion for an infinitely long bar assuming a sinusoidal waveform. Their solution is what is referred to as the frequency equation for longitudinal motion of an elastic rod. It turns out to be a function relating Poisson's ratio, wavelength, and wave speed, and can be solved for each mode of a cylindrical bar for a particular material. This solution is neither simple nor explicit. Beginning with the Pochhammer-Chree frequency equation and assuming only the first mode ($M_{1,1}$) is excited, the wave speed of any wave of a given frequency in the bar of interest, since it is dependent only on its wavelength, can be calculated. Using this wavespeed and corresponding wavelength along with given material properties, the longitudinal and radial distribution of displacements and stresses may be determined from the assumed displacement functions for the "longitudinal" vibrations. One can now turn to the transient pulse being propagated in the bar and describe it in terms of Fourier series; that means representing the waveform by the sum of an infinite number of pulses, each one having a distinct amplitude, a distinct wavelength and traveling at a unique speed. This wave speed can be calculated from the frequency equation. Therefore, each piece of the input pulse can be followed as it travels down the bar, and at any time, the complete waveform can be reconstructed

numerically by adding up all the pieces. This methodology is currently being used to correct for dispersion in the SHPB at the University of Florida and at Tyndall AFB. To carry the logic a bit further, it appears one can still treat the pulses individually as they encounter the boundary between the specimen and the incident bar, partially reflect and partially transmit through, and eventually encounter the second interface where more reflections and transmissions take place. The basic assumption is that as the single Fourier component encounters an interface, its amplitude splits according to the characteristic impedance values of the two media, (which will be derived later), but it will maintain its original frequency and velocity. In other words, each wave component divides each time it encounters an interface, new components are formed each with a different amplitude, but all with the same frequency. Note also that the sum of these Fourier components produce the total incident, reflected, and transmitted pulses whose wavelengths will also not change.

The implications of this assumption are crucial to the conclusion that one can theoretically follow each wave component through multiple reflections, transmissions, and any length of travel, and at any time know its amplitude and location. With that information one can then reconstruct the pulse at any time or location and obtain the shape of the response.

A computer program has been written for an SHPB following the logic just described and is included in Appendix A. A trapezoidal input pulse was assumed to represent the longitudinal strain at $r = a$ and 2 meters from the specimen. Fifty-five terms were carried through in the Fourier analysis. At the onset all the terms in the series are assumed to be in phase and their relative phases are calculated as they travel down the bar. After multiple reflections, the pulses are reconstructed at the two strain gage locations on the incident and transmitter bars (both 1 meter from the specimen). At any interface between dissimilar materials, velocities and forces must be continuous. Assuming normal incidence waves only, in a perfectly elastic

medium, then the relationship between the incident, transmitted, and reflected stresses can be shown to be

$$\sigma_t = \left[2\, A_1 \rho_2 c_2/(A_2 \rho_2 c_2 + A_1 \rho_1 c_1)\right] \sigma_i$$

$$\sigma_r = \left[(A_2 \rho_2 c_2 - A_1 \rho_1 c_1)/(A_2 \rho_2 c_2 + A_1 \rho_1 c_1)\right] \sigma_i$$

where A is the bar cross-sectional area, ρ is the density, and c is the wavespeed. Subscripts 1 and 2 pertain to the two materials, and the wave is moving from material 1 to material 2. Each term in the Fourier series has a different wavespeed, and since only Mode $M_{1,1}$ is considered in the analysis, these wavespeeds are always less than or equal to the infinite elastic speed $\sqrt{E/\rho}$.

For the sake of consistency in comparing the various approaches, this effort was based entirely upon a compressive SHPB whose incident and transmitter bars are made of steel, and a work hardened aluminum specimen of varying dimensions was assumed. Thus, the characteristic impedance ρc is approximately three times greater in the bars than in the specimen. Consequently, an incident compressive wave will be reflected as a tension wave at the incident bar-specimen interface and the transmitted part will still be in compression. As this compressive pulse reaches the end of the specimen at the transmitter bar, it will be both reflected and transmitted in compression in accordance with the mismatch of characteristic impedances of the bar and the specimen. This means that a compressive wave is now "trapped" in the specimen. It loses amplitude at each reflection, but it remains compressive. It also means that every time the wave reaches the specimen-incident bar interface it will also transmit into the incident bar as a compressive pulse. The compressive pulse traveling out of the specimen into the incident bar superposes itself onto the reflecting tensile part and thus reduces its magnitude. As the compression pulse makes multiple reflections and

transmissions within the specimen, the magnitude of the original tensile reflection of the incident pulse is reduced by the magnitude of the transmitted compressive pulse from the specimen into the incident bar. The length of the compressive incident pulse is of finite time, which means the tensile reflection and the compressive transmission pulses are also of finite length, and in fact are of identical duration as the incident wave. This implies the wavelengths of these transient pulses do not change as they cross interfaces, only their amplitudes are changed.

These phenomena are clearly seen in experimental traces (see for example Figure 4), and in the Modified Pochhammer-Chree results (see for example Figure 5) obtained from the program discussed in the previous page; the reflected tensile wave starts out at a certain value, and then in the time required to transit twice the specimen length, it jumps to a lower level due to the arrival of the first portion of the compressive pulse from the specimen. The amplitudes of the reflected and the transmitted pulses add up to the amplitude of the incident pulse. In the experiment of Figure 4 the specimen was plastically deformed, while for Figure 5 the specimen remains elastic.

It should be mentioned at this point that in order to be able to directly compare the results, the dimensions of the bars and the locations of the strain gages were the same in all methodologies. Specifically, since the Tyndall SHPB is 2 inches in diameter and the gages are 40 inches on either side of the specimen, both the modified Pochhammer-Chree method and the finite difference method were run with those values. For the 6-inch SHPB, the numerical methods assumed strain gages 80 inches on either side of the specimen.

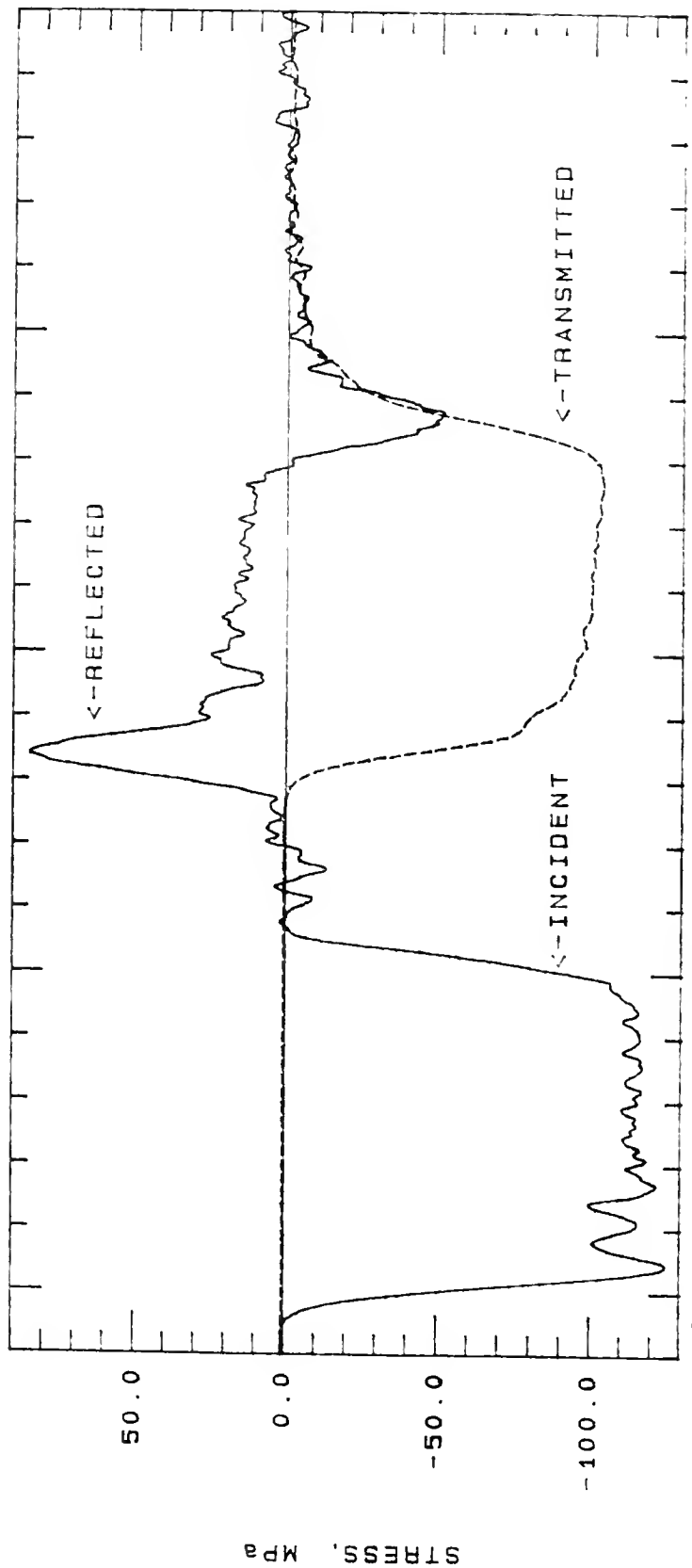

Figure 4. Tyndall 2-inch SHPB. Experimental Trace. Aluminum Specimen Length and Diameter 1.254 inch

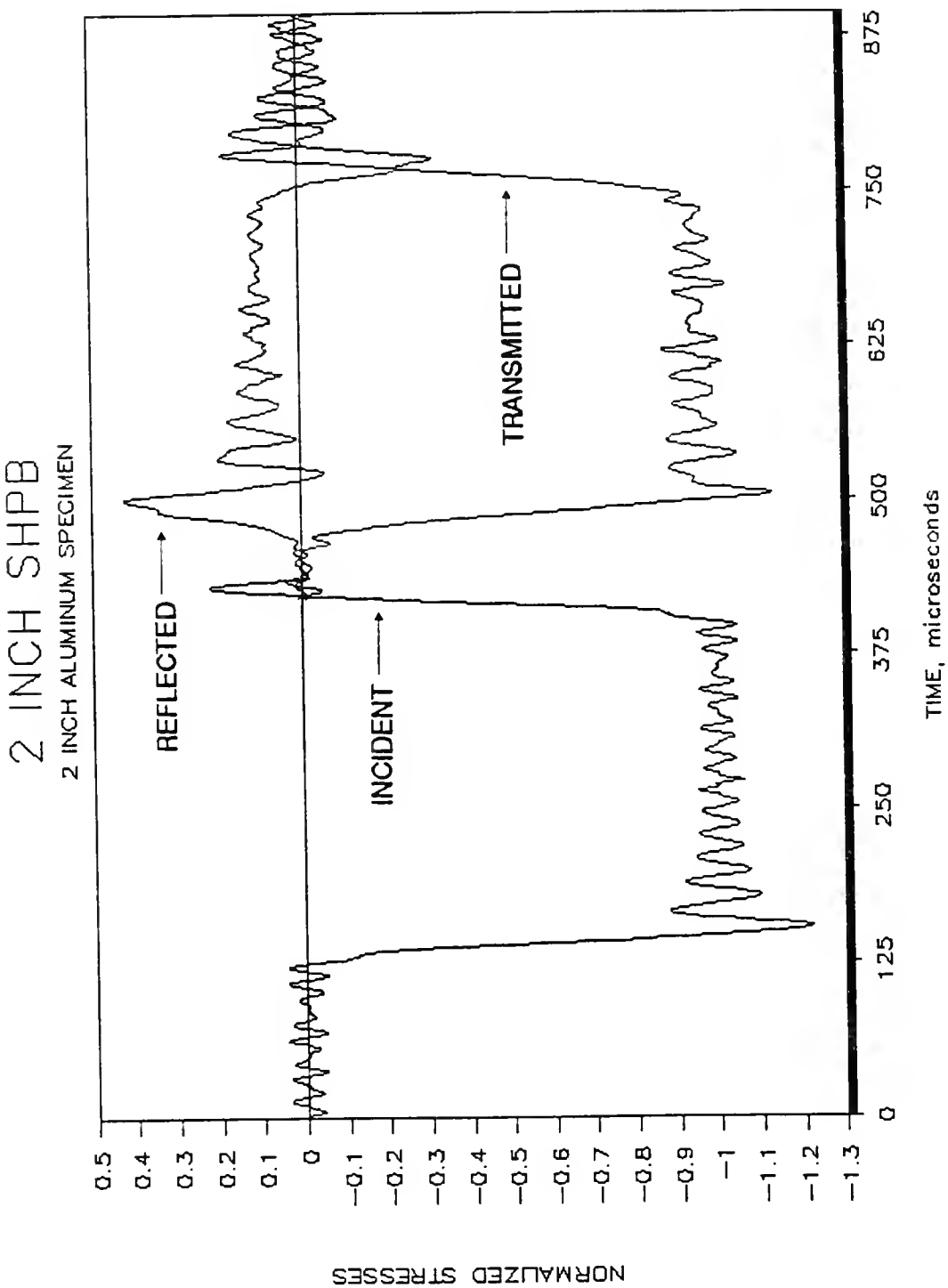

Figure 5. Modified Pochhammer-Chree Results. Incident Stress Normalized to 1.0

As mentioned earlier, the results of the Pochhammer-Chree frequency equation also lead to the variation of the stresses and displacements in the radial direction. These variations also depend on the wave speed and the wavelength of the pulse, and there are an infinite number of solutions each associated with a particular mode of vibration. After some tedious derivations [33] the amplitudes W(r) and U(r) of the assumed longitudinal and radial displacements $u_z = W(r) * f(t,z)$ and $u_r = U(r) * f(t,z)$ are

$$W(r) = i\gamma\hat{c}\,\frac{J_1(ha)}{ha}\left[\frac{ha\,J_0(hr)}{J_1(ha)} + \frac{(1-\beta x)}{(x-1)}\,\frac{\kappa a\,J_0(\kappa r)}{J_1(\kappa a)}\right]$$

$$U(r) = -\gamma\hat{c}\,\frac{J_1(ha)}{ha}\left[(\beta x-1)^{1/2}\,\frac{ha\,J_1(hr)}{J_1(ha)} - \frac{(1-\beta x)}{(x-1)}\,\frac{1}{(2x-1)^{1/2}}\,\frac{\kappa a\,J_1(\kappa r)}{J_1(\kappa a)}\right]$$

where $\hat{c}$ = a constant determined by the amplitude of vibration,

$$x = \left(\frac{c}{c_o}\right)^2 (1+\upsilon)\ ,\quad \beta = \frac{1-2\upsilon}{1-\upsilon}\ ,$$

$$h = \gamma(\beta x-1)^{1/2},\quad \kappa = \gamma(2x-1)^{1/2}$$

With this information the radial, shear, and longitudinal stresses can be calculated as

$$\sigma_{rr} = 2\mu\gamma^2\hat{c}\,\frac{J_1(ha)}{ha}\left[(1-x)\,ha\,\frac{J_0(hr)}{J_1(ha)} + (\beta x-1)\,\frac{a}{r}\,\frac{J_1(hr)}{J_1(ha)} +\right.$$

$$\left.\frac{\beta x-1}{1-x}\,\kappa a\,\frac{J_0(\kappa r)}{J_1(\kappa a)} - \frac{\beta x-1}{1-x}\,\frac{a}{r}\,\frac{J_1(\kappa r)}{J_1(\kappa a)}\right] f(t,z)$$

$$\sigma_{rz} = -2i\mu\gamma\hat{c}\,h\,J_1(ha)\left(\frac{J_1(hr)}{J_1(ha)} - \frac{J_1(\kappa r)}{J_1(\kappa a)}\right) f(t,z)$$

$$\sigma_{zz} = -2\mu\gamma^2\hat{c}\,\frac{J_1(ha)}{(ha)}\left[(1+x-\beta x)\,ha\,\frac{J_0(hr)}{J_1(ha)} + (1-\beta x)\,\kappa a\,\frac{J_0(\kappa r)}{J_1(\kappa a)}\right] f(t,z)$$

Again assuming only Mode $M_{1,1}$ is excited, the values of the wave speed for each component of the Fourier series under consideration can be calculated. Thus, if the bar is divided radially into a number of increments, it is possible to calculate the stress and displacement distributions in the bar at any point at any time. These calculations can be combined with those of the preceding discussion of the Modified Pochhammer-Chree equation and the result is a complete description of the elastic wave propagation in an SHPB .

Care must be taken when solving the equations involving Bessel functions numerically, since as the argument becomes negative, modified Bessel functions must be used. Specifically

$$J_0(ix) = I_0(x) \quad \text{and} \quad J_1(ix) = i\, I_1(x),$$

or in general ,

$$I_n(x) = (i)^{-n}\, J_n(ix)$$

Davies [27] showed that if the ratio $\frac{a}{\Lambda}$ is kept below 0.1 then the radial variation is less than 5%. In an SHPB there are an infinite number of pulses whose $\frac{a}{\Lambda}$ values span from zero all the way to infinity. As discussed earlier, it is sufficient to make sure that the amplitude of the Fourier components have fallen to a small fraction of the initial value, when the value of $\frac{a}{\Lambda}$ reaches and goes beyond 0.1. That is, most of the contributing components of the Fourier series must fall below $\frac{a}{\Lambda} = 0.1$.

A subroutine was added to the Modified Pochhammer-Chree program to calculate the radial variations for the longitudinal and the radial stresses. The results of the longitudinal stress for a 2-inch and a 6-inch bar are plotted in Figure 6. As expected, the lower (lower values of n), Fourier series terms

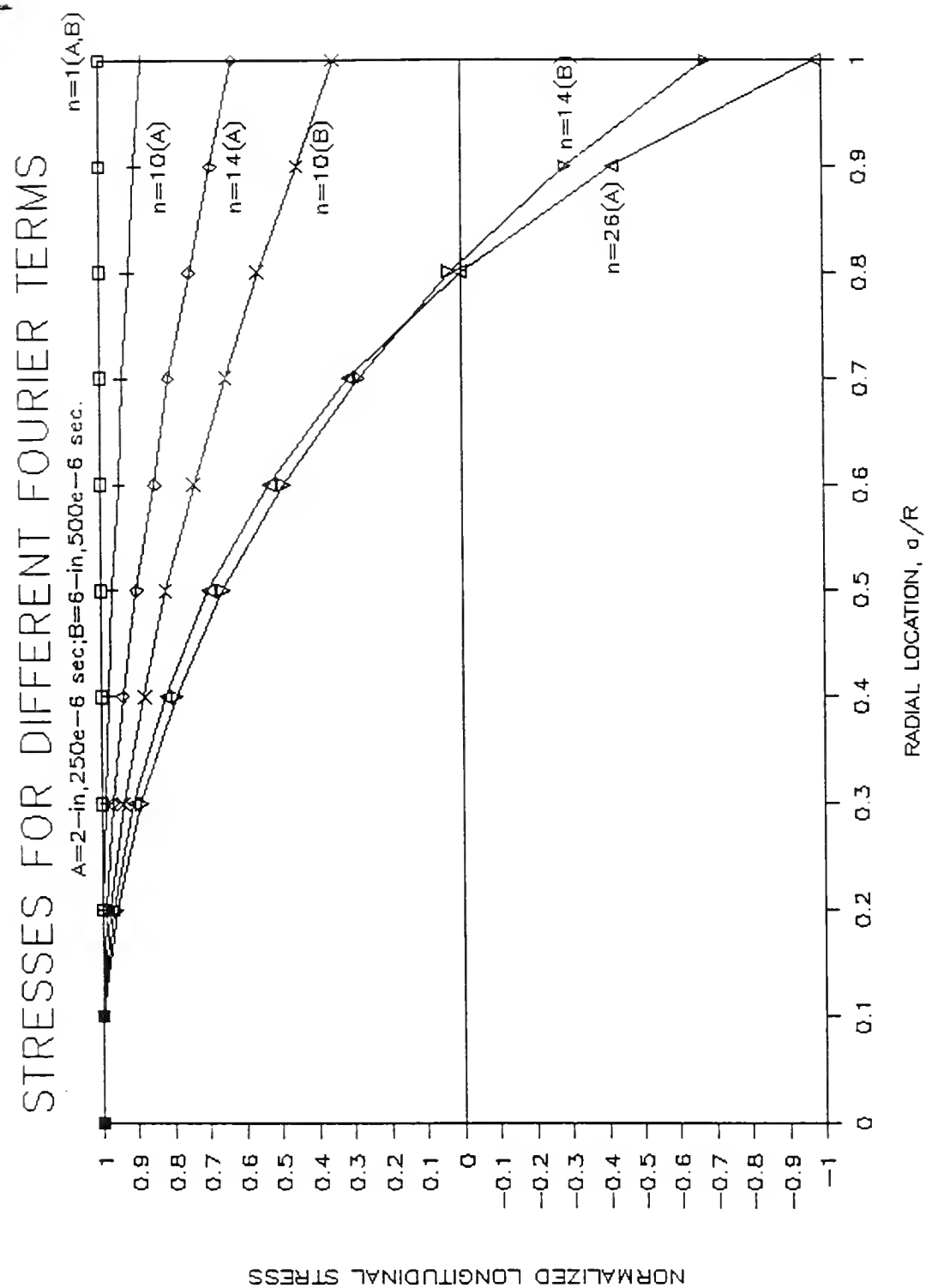

Figure 6. Normalized Longitudinal Stress Given as a Function of Radial Location for Several Fourier Terms

(the ones whose $\frac{a}{\Lambda}$ values are low), show a nearly uniform distribution of stress, while as the wavelengths become smaller (larger $\frac{a}{\Lambda}$), the radial variations become progressively greater to a point where they change sign. If the amplitudes of these higher terms have fallen to a very small value, then their contribution to the overall pulse will be negligible. Plots of the radial variations of reflected and transmitted stresses are shown in Appendix A for a 2 and a 6-inch SHPB (Figures 36 and 37). It is also apparent that as the diameter of the bar is increased and the input wavelength is kept the same, the stress will show uniformity for only a few terms. This fact is additional proof that the one-dimensionality of an SHPB is dependent on the ratio of the radius to the wavelength, and if kept the same as for the existing SHPBs, then the wave propagations should be mathematically identical.

Although the higher Fourier terms are highly nonuniform, their contributions are very small. Furthermore, if one normalizes the amplitude values of the radial and the shear stresses to those of the longitudinal stresses at the center, the results show the radial and shear stresses to be of many orders of magnitude smaller than the longitudinal values. This can also be observed in the finite difference calculations, and it is further proof of the one-dimensional nature of the wave propagation in the bar. Also, as expected, when the diameter of the bar is increased to 6 inches, the radial and shear stresses also increase, but remain in the same order of magnitude, and can thus still be safely neglected.

Finite Difference Numerical Simulation

The two-dimensional equations of motion in cylindrical coordinates can be solved using an existing hydrocode such as HULL [34]. HULL has a two-dimensional Lagrangian module that solves conservation of mass, momentum, and energy simultaneously with the definitions of the deformation tensor, constitutive relations, and the stress deviators. A centered

finite difference approximation is employed. The topic of constitutive relations is the most crucial as it includes the relationship between the elastic and plastic deviatoric strains and stresses, and the relationship between pressure, density, and internal energy. The accuracy of any hydrocode is highly dependent on the implementation of the constitutive relations.

In this effort only metals were considered, namely steel and aluminum. Both are modeled in HULL as elastic/plastic materials, although the stress levels were kept low enough to keep the steel bars in the elastic region. Both materials are also considered isotropic. Stresses are decomposed into a spherical and a deviatoric component, and the generalized Hooke's law is used. Yielding is treated following the von Mises criterion, which assumes that yielding starts when the combined-stress distortion energy equals the yield value of distorsion energy in a tension or compression test. Specifically, it relates the second deviatoric stress invariant to a specified yield function. Once yield is reached, the deviatoric stresses are corrected and reset to be normal to the yield surface in stress space. The total stresses can then be calculated. Using HULL, a trapezoidal pressure pulse was input on the incident bar and the specimen was specified as an elastic/strain-hardening material. The HULL output stations included the locations of the strain gages on the bars, plus one within the specimen itself. Sliding interfaces with no friction were used between the two materials for most calculations. To study the effects of friction, locked interfaces that allow no sliding to occur were used. The bars are made of steel and remain elastic at all times. The first runs were made to model as closely as possible the experimental data available for aluminum from the Tyndall AFB SHPB. Appendix D contains a HULL sample input file.

HULL was also run to investigate the complicated wave interaction phenomena at the specimen-bar interfaces, especially in cases when the specimen is smaller in diameter than the bars. The next step was to study the effects of a 6-inch diameter bar, with two input pulses. One input pulse with a wavelength long enough to give a one-dimensional response was used.

Additionally, one with a much shorter wavelength was used to show how the stresses and displacements vary in the radial direction, and disperse after a short travel, making the conventional SHPB analysis invalid.

Experimental Method

How does one know how good or even reliable the HULL output is? In order to answer this question, a direct comparison was sought between existing experimental data obtained at Tyndall AFB, and the calculated results from the HULL code. Specifically, numerous compression tests were run on aluminum 6061-T6511 specimens between steel incident and transmitter bars. The input pressure was varied to assess strain rate sensitivity, and stresses and strains were recorded at strain gages located in the incident and transmitter bars. It was found that (as already known) this particular aluminum is strain rate independent; that is, the stress strain curve is not affected by the rate at which the load is applied. This is very important because the HULL code does not take strain rate into account. Therefore, a comparison will be meaningful between the experimental data and the computer results for an aluminum specimen. The available data was obtained from a 2-inch diameter SHPB and varying specimen sizes. HULL was then run with a new material added to the material library to match as closely as possible the 6061-T6511 aluminum properties.

In particular, aluminum is modeled as an elastic/plastic material, and one would expect to observe that stress strain relationship in the output. One should be able to recreate the relationship between stress and strain since that is what the SHPB is designed and used for. The rationale was to prove the validity of the numerical tool by comparing existing data with the results of the code, and then move on to the proposed 6-inch bar and have the confidence to trust and draw conclusions from those results.

Comparison of Results

A number of compressive tests were conducted at Tyndall AFB using a 2- inch SHPB on aluminum specimens. The diameter and length of the specimen, as well as the input pressure were varied to assess their influence. The results for three cases are shown in Figures 7, 8, and 9. To compare experimental and numerical results, HULL was run matching as closely as possible the conditions in the Tyndall tests. One needs to realize however, that no matter how good the numerical model is, there are some parameters one cannot predict or reproduce. For example, the input pulse is not in reality a perfect square pulse, nor is it perfectly uniform along the cross section as numerically modeled. Furthermore, the constitutive equations for steel and especially for aluminum (which goes beyond yield in the course of the test), are theoretical models and by no means exact. Finally, the effects of friction are not included in the numerical scheme.

Having said that, one is then looking for a qualitative match in the data, more so than exact values of stresses or strains. What this means is that certain trends that have been observed experimentally should show up numerically. For example, as the specimen gets smaller compared to the incident bar, experimental results show that the transmitted stress also becomes smaller. Consequently, the reflected stress increases and its shape becomes more uniform as the initial high peak starts to blend in with the rest of the reflected pulse. The HULL calculations also show these phenomena. Although the actual amplitude values do not match, the relative change between tests does. In general, the experimental data gives higher transmitted stresses, but it does so consistently. Experimental results are shown in Figures 7, 8, and 9 and can be compared to the numerical results from HULL shown in Figures 10, 11, and 12. The results of the HULL calculations show very good agreement with the experiments, which point out the validity of the HULL code.

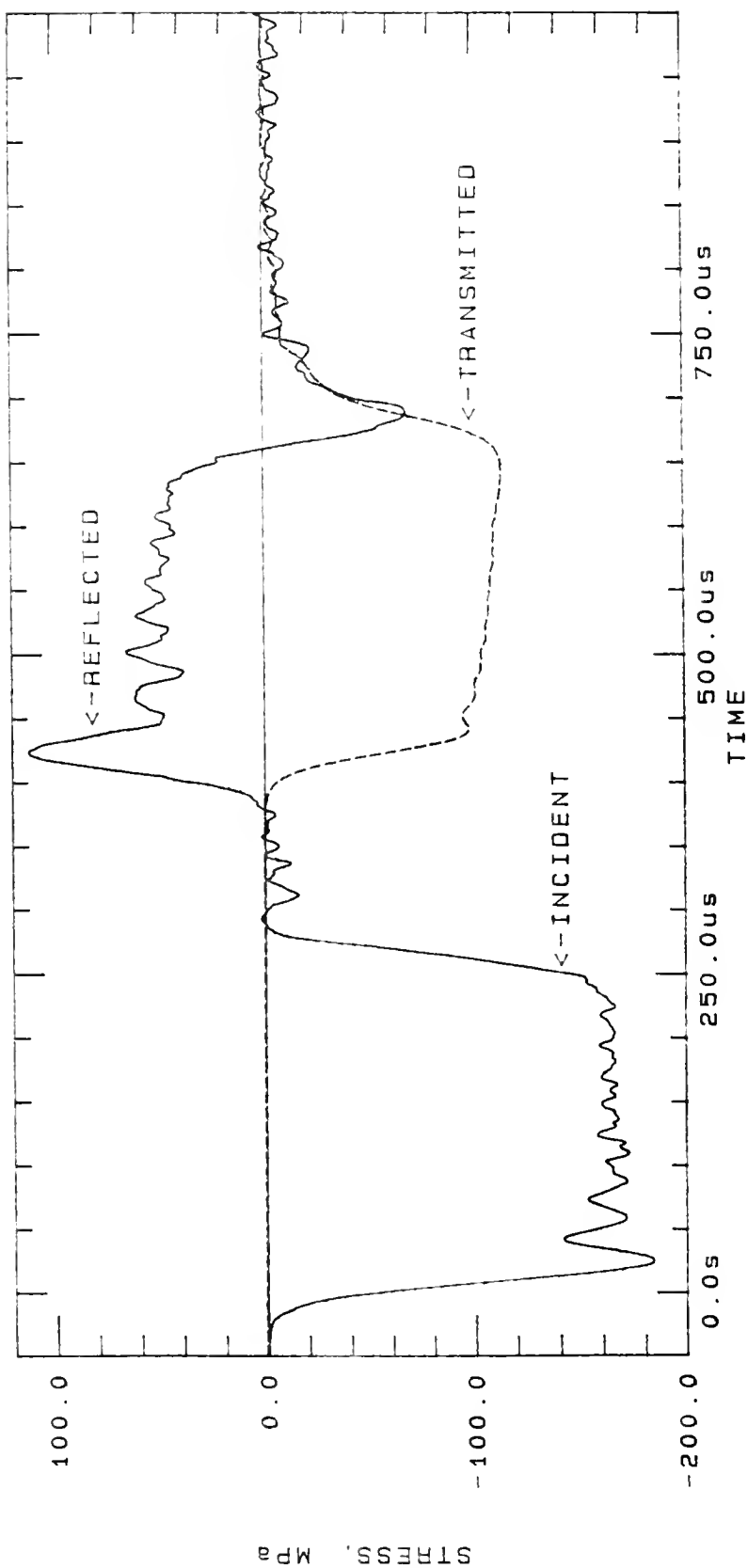

Figure 7. Experimental Results. 2-inch SHPB. Stress Pulses for a 6061-T6511 Aluminum Specimen, Diameter = 3.18 cm, Length = 3.18 cm

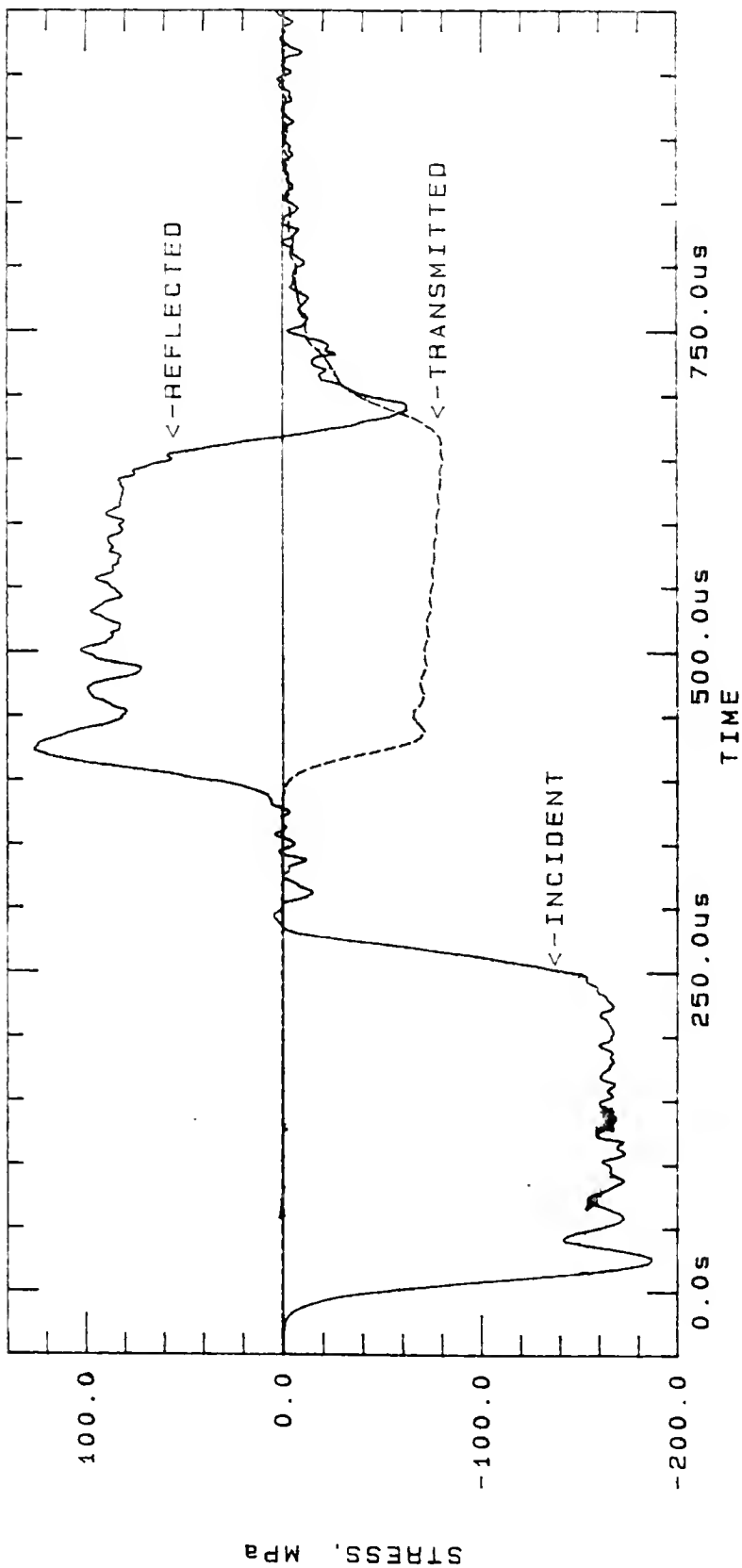

Figure 8. Experimental Results. 2-inch SHPB. Stress Pulses for a 6061-T6511 Aluminum Specimen, Diameter = 2.54 cm, Length = 2.54 cm

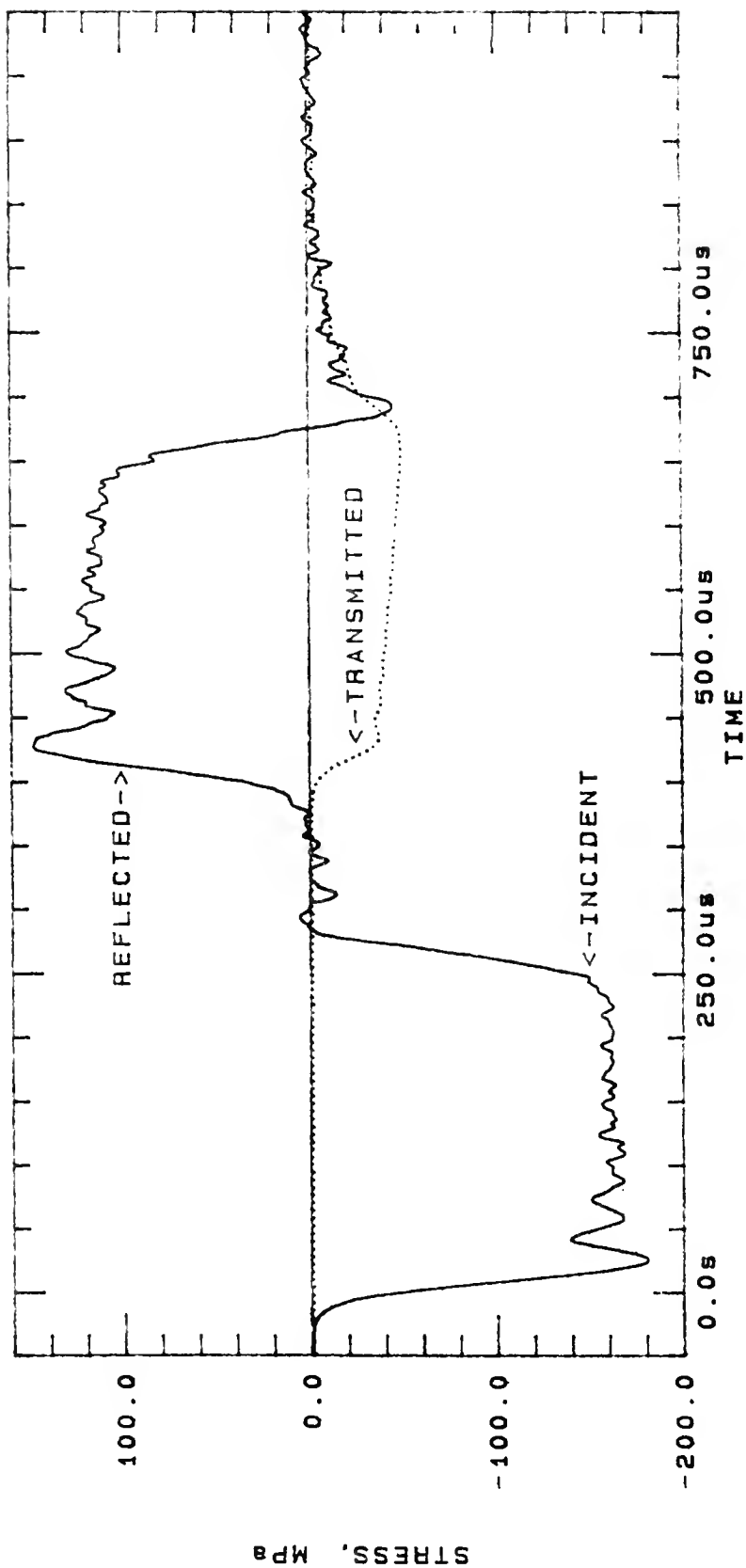

Figure 9. Experimental Results. 2-inch SHPB. Stress Pulses for a 6061-T6511 Aluminum Specimen, Diameter = 0.56 cm, Length = 0.56 cm

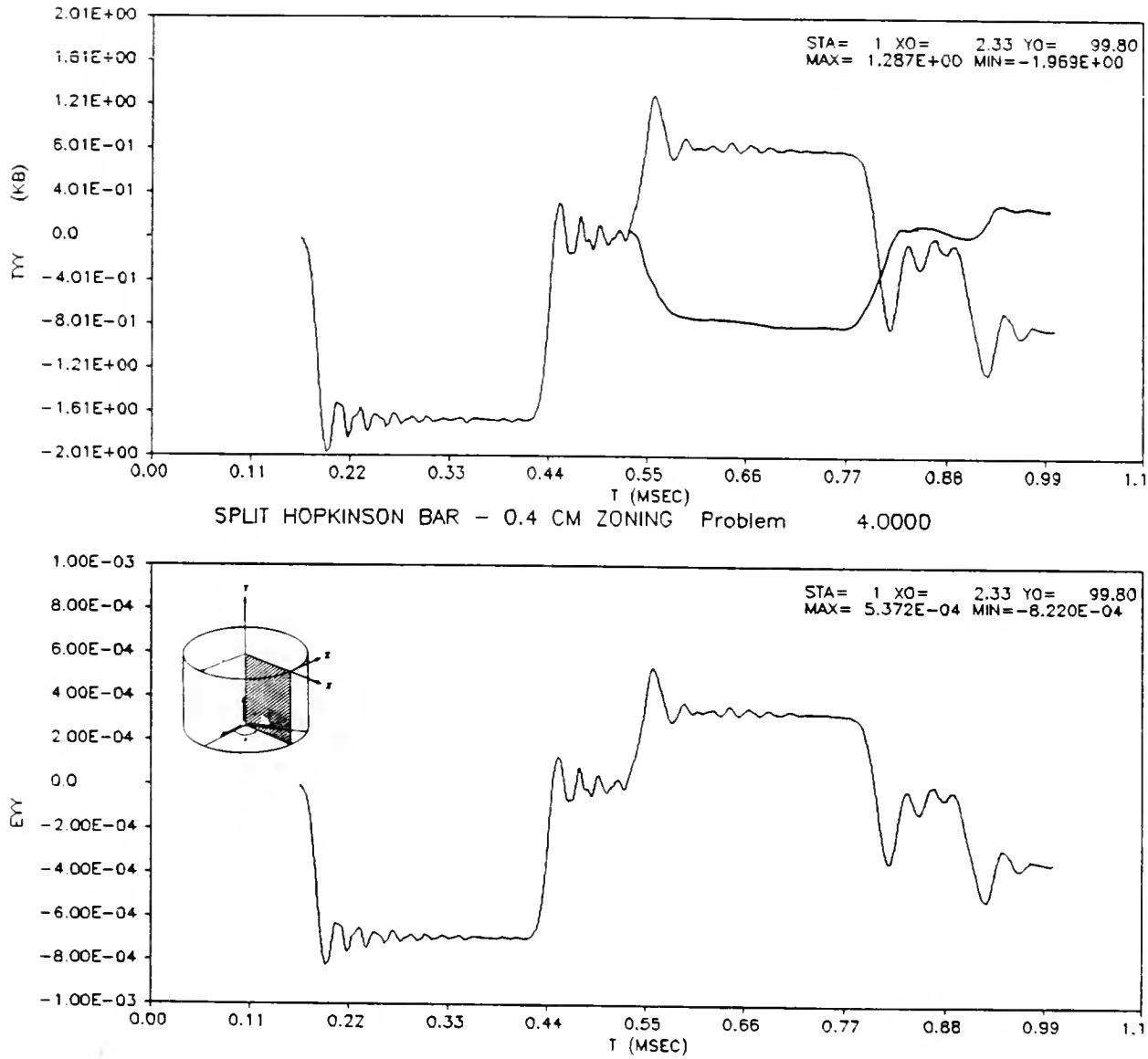

Figure 10. HULL Output. 2-inch SHPB. Stress (TYY) and Strain (EYY) Pulses for an Aluminum Specimen, Diameter = 3.18 cm, Length = 3.18 cm

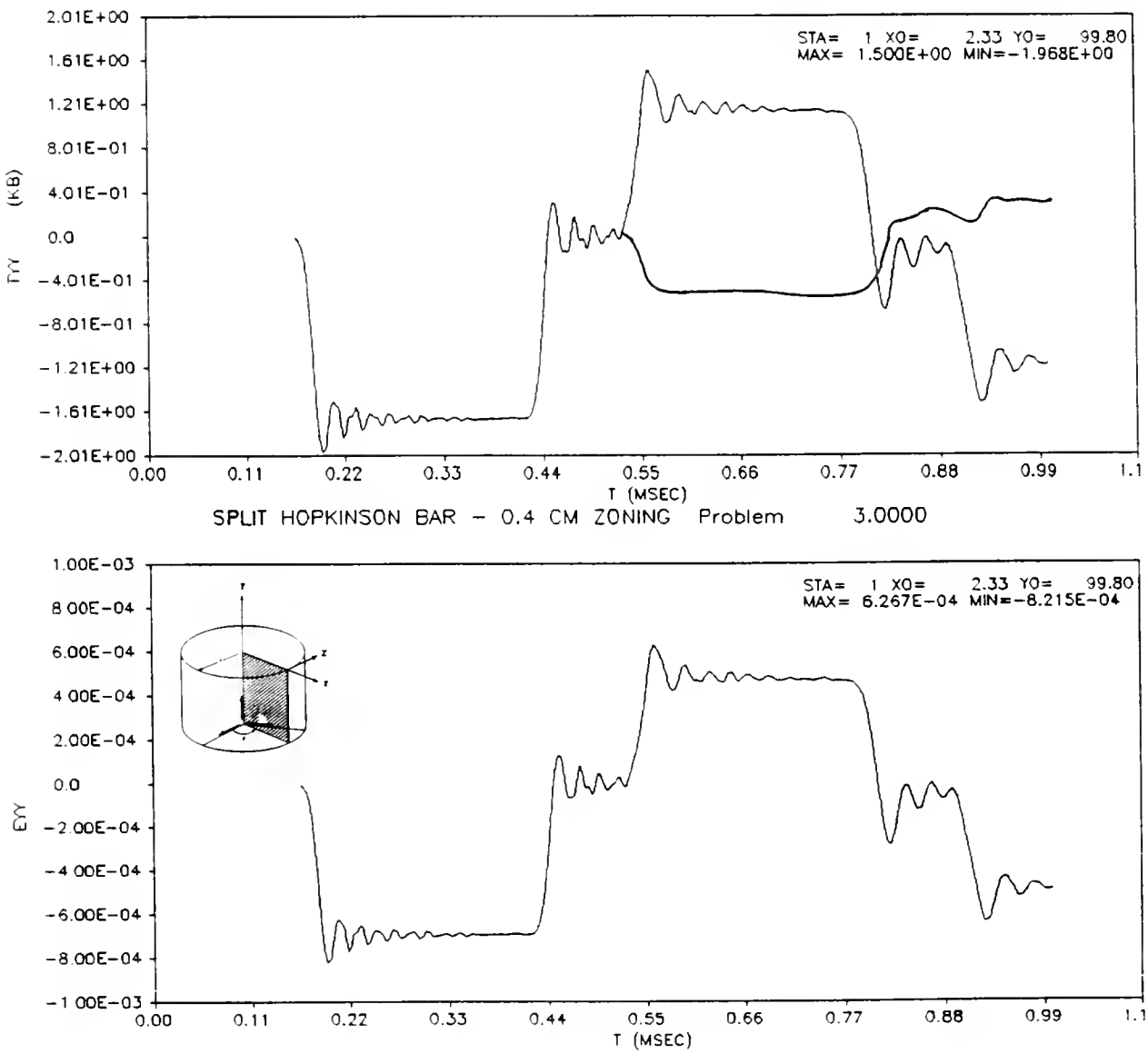

Figure 11. HULL Output. 2-inch SHPB. Stress (TYY) and Strain (EYY) Pulses for an Aluminum Specimen, Diameter = 2.54 cm, Length = 2.54 cm

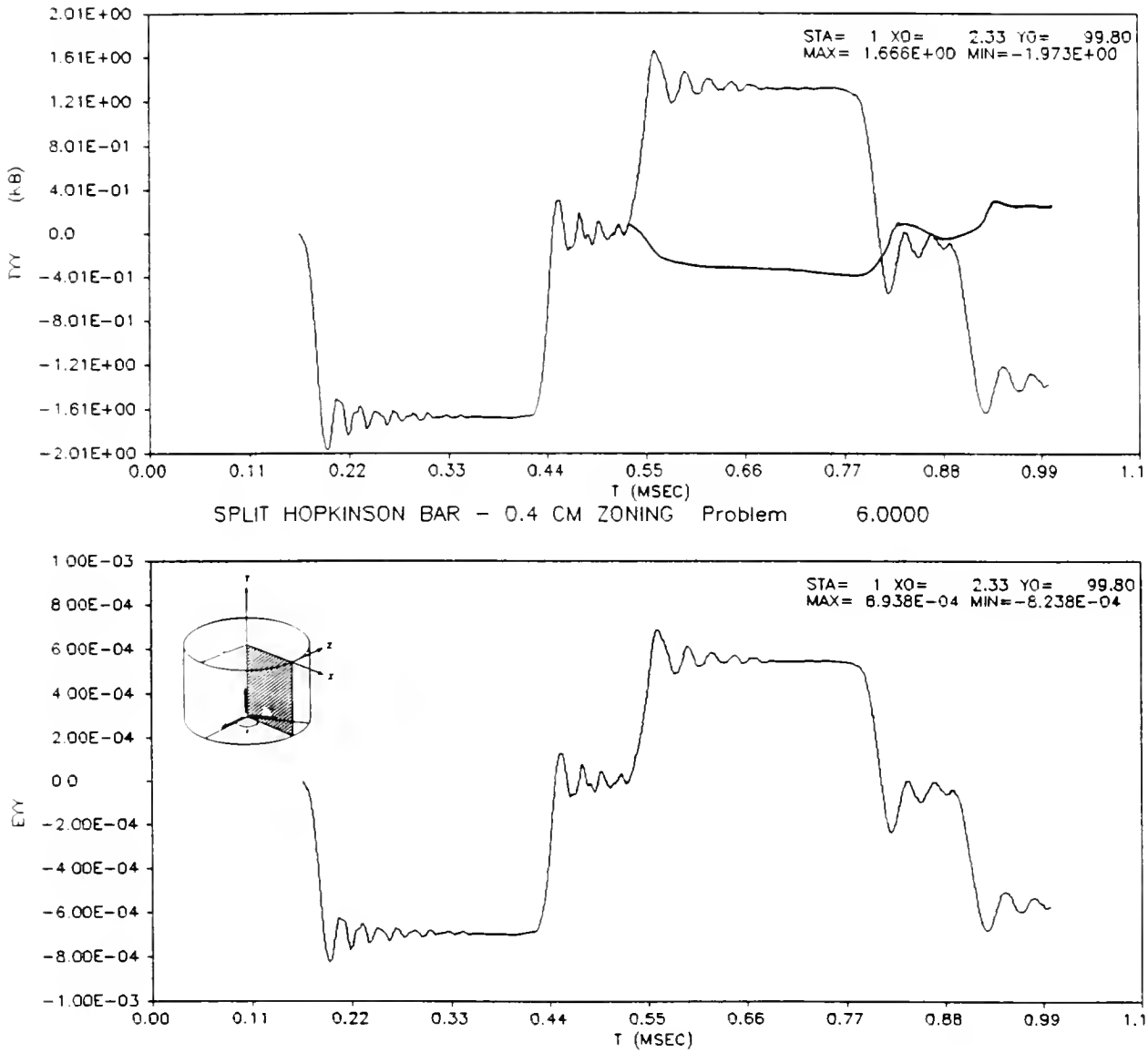

Figure 12. HULL Output. 2-inch SHPB. Stress (TYY) and Strain (EYY) Pulses for an Aluminum Specimen, Diameter = 0.56 cm, Length = 0.56 cm

It makes sense physically that as the specimen gets smaller, more and more of the incident pulse is reflected back, to the limit case when there is no specimen and the reflected trace is identical and reverse of the incident. It also seems reasonable that when the specimen diameter is less then half of the SHPB diameter, little of the incident pulse gets transmitted into the specimen, which means that even less of this transmitted pulse will get back to the reflected pulse and therefore its basic shape will not be changed. Hence the appearance of a distinct peak in the reflected trace is reduced when the specimen is small.

It has already been shown in Figure 5 that the Modified Pochhammer-Chree method also shows the characteristic "peak" in the reflected trace even though the solution is elastic. The only difference between an elastic and an elastic-plastic specimen is in the magnitude of the stress that may be applied. Therefore, the only difference in the shape of the traces in the modified Pochhammer-Chree method will be a higher compressive reflection out of the specimen, resulting in a lower reflective plateau after the initial "peak", than for the corresponding non-elastic case. To show this, three experimental tests were run with the same specimen configuration at different levels of stress; one level was kept in the aluminum elastic region, the other two exceeded the yield value for aluminum. Figure 13 shows how after the initial peak in the elastic case (top figure), the reflected pulse almost goes down to zero, while as the input stress is increased (middle and bottom figures), the plateau after the peak increases also.

Another issue to be explored experimentally and numerically is the effect of decreasing the pulse duration with respect to the diameter of the bar. As discussed, the equations governing an SHPB show that increasing the $\frac{a}{\Lambda}$ ratio will affect two important things. The first thing is that the pulse will disperse more; that is, the contribution from the slower traveling components will be greater, and the overall waveform will distort and spread out more as it travels. The second thing is that the wave propagation will be less one dimensional in nature, which means that the longitudinal stress will have

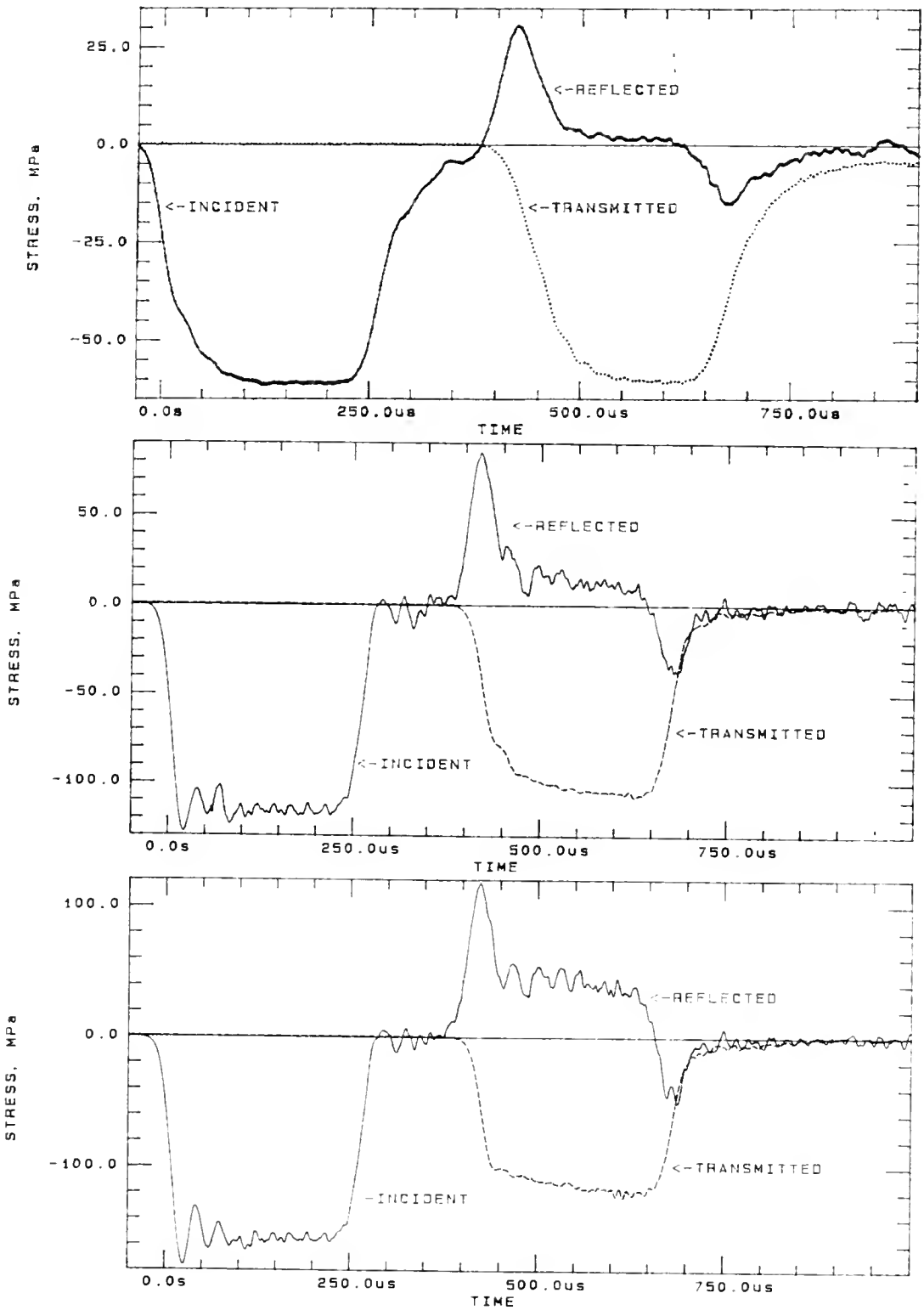

Figure 13. Experimental Traces at Three Incident Stress Levels (60 MPa-Top, 100 MPa-Middle, 167 MPa-Bottom). Specimen Diameter 1.253 in., Length = .625 in., 2-inch SHPB

larger variations along the radius and the radial and shear stresses will be less negligible as $\frac{a}{\Lambda}$ increases. Numerically one can observe the effects of decreasing the input wavelength by using HULL and the Modified Pochhammer-Chree method. The following runs shown in Table 1, were made to test the methodologies against what it is analytically believed to be true.

Table 1. HULL and Modified Pochhammer-Chree Runs

DIAMETER (inches)	WAVELENGTH (microseconds)	$\frac{a}{\Lambda}$	FIGURES
2	250	1/125	3, 14
6	750	1/125	15
6	500	3/250	16, 17
6	250	3/125	18, 19

Figures 5, 15, 16, and 18 show results from the Modified Pochhammer-Chree program, while Figures 14, 17, and 19 are HULL output traces. Notice that HULL appears to have two different coordinate systems from one figure to the next. The reason for this is that the runs were made on different computer systems (VAX and CRAY) and each system has a slightly different version of HULL. In one z is the longitudinal coordinate, and in the other, y is the longitudinal coordinate. This discrepancy should not cause confusion. It can be seen that the pulses disperse more when $\frac{a}{\Lambda}$ is greater. The results also confirm that if $\frac{a}{\Lambda}$ is the same, regardless of the bar

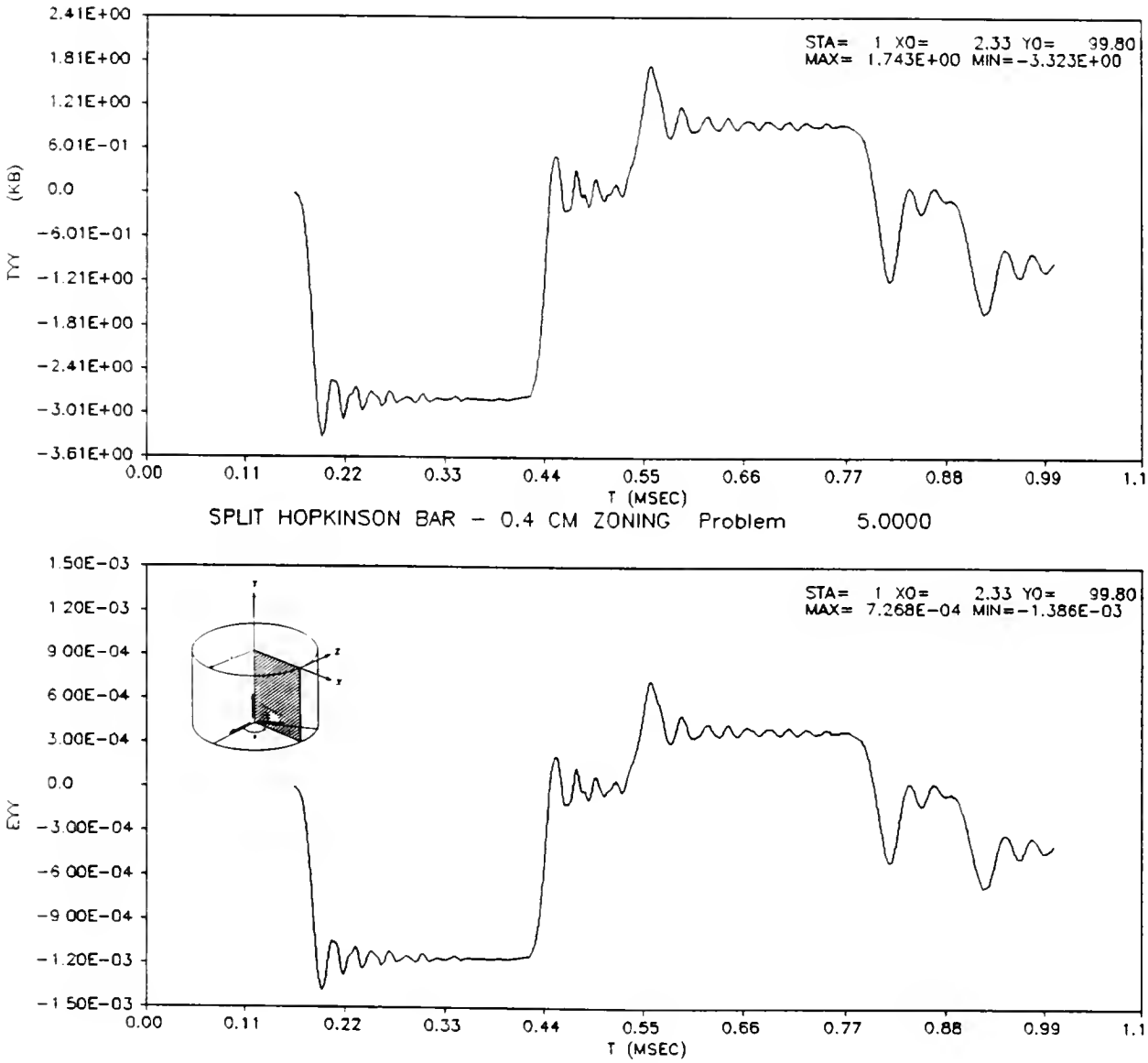

Figure 14. HULL Output. 2-inch SHPB. 2-inch Diameter and Length, Aluminum Specimen, 257 μsec Pulse

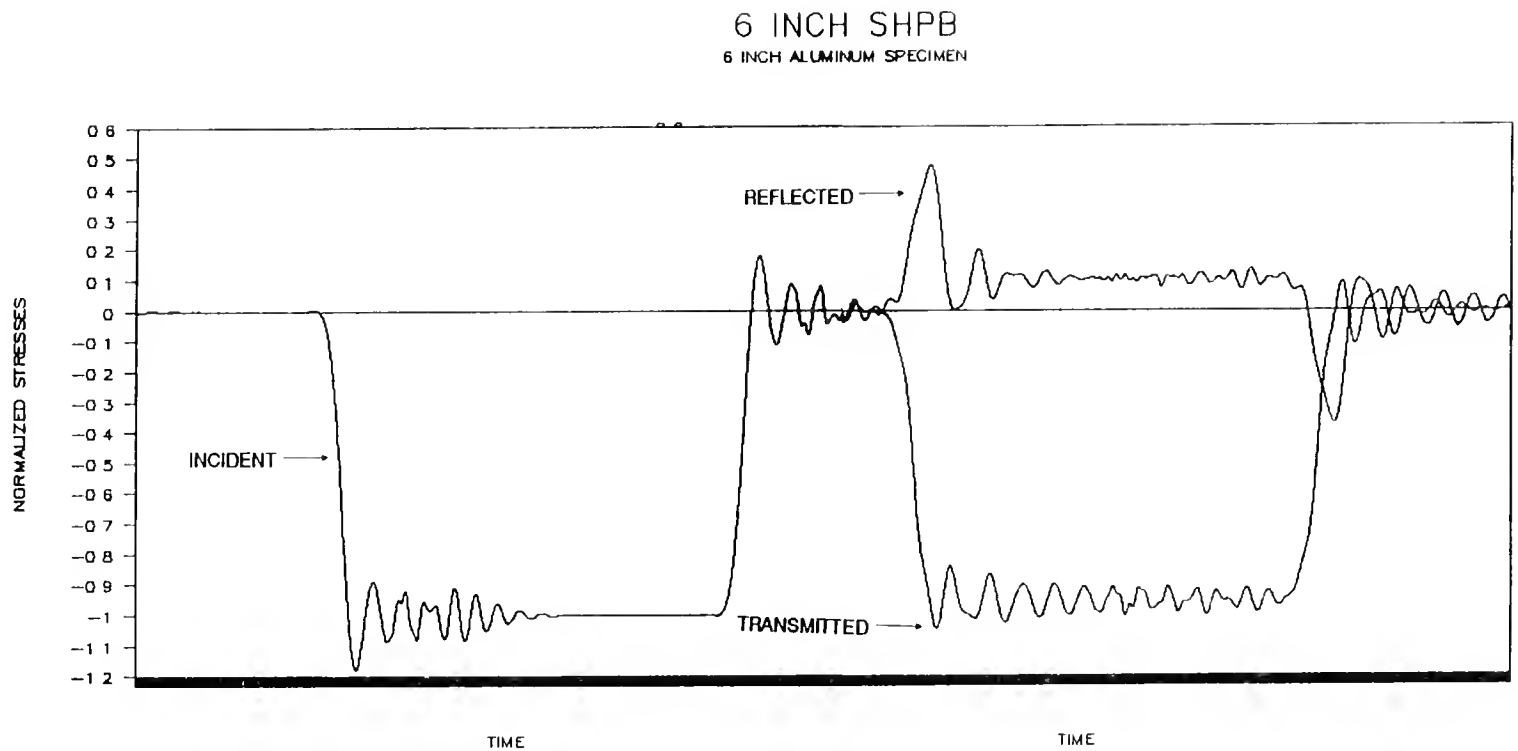

Figure 15. Modified Pochhammer-Chree Results. $\frac{a}{\Lambda} = \frac{1}{125}$, 6-inch SHPB. 750 μsec Pulse

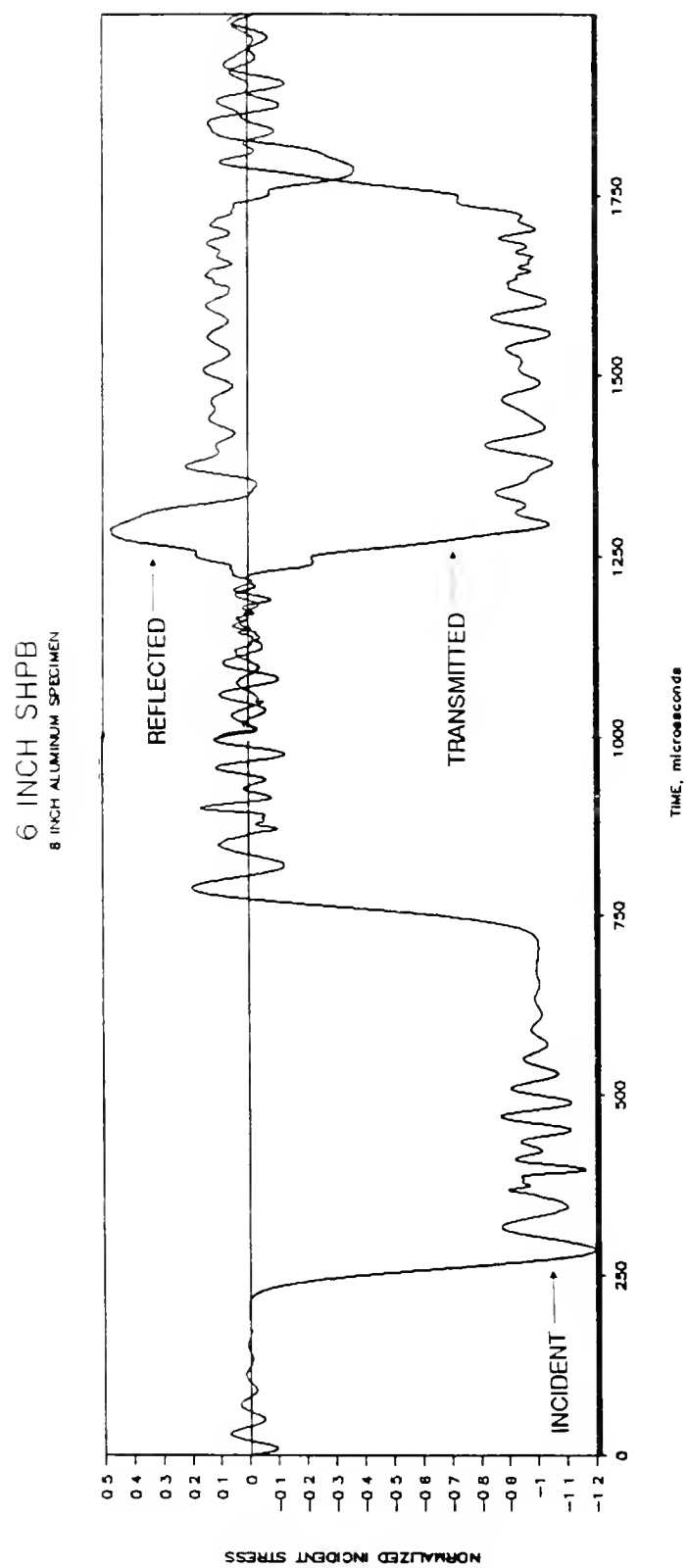

Figure 16. Modified Pochhammer-Chree Results. $\frac{a}{\Lambda} = \frac{3}{250}$, 6-inch SHPB. 500 μsec Pulse

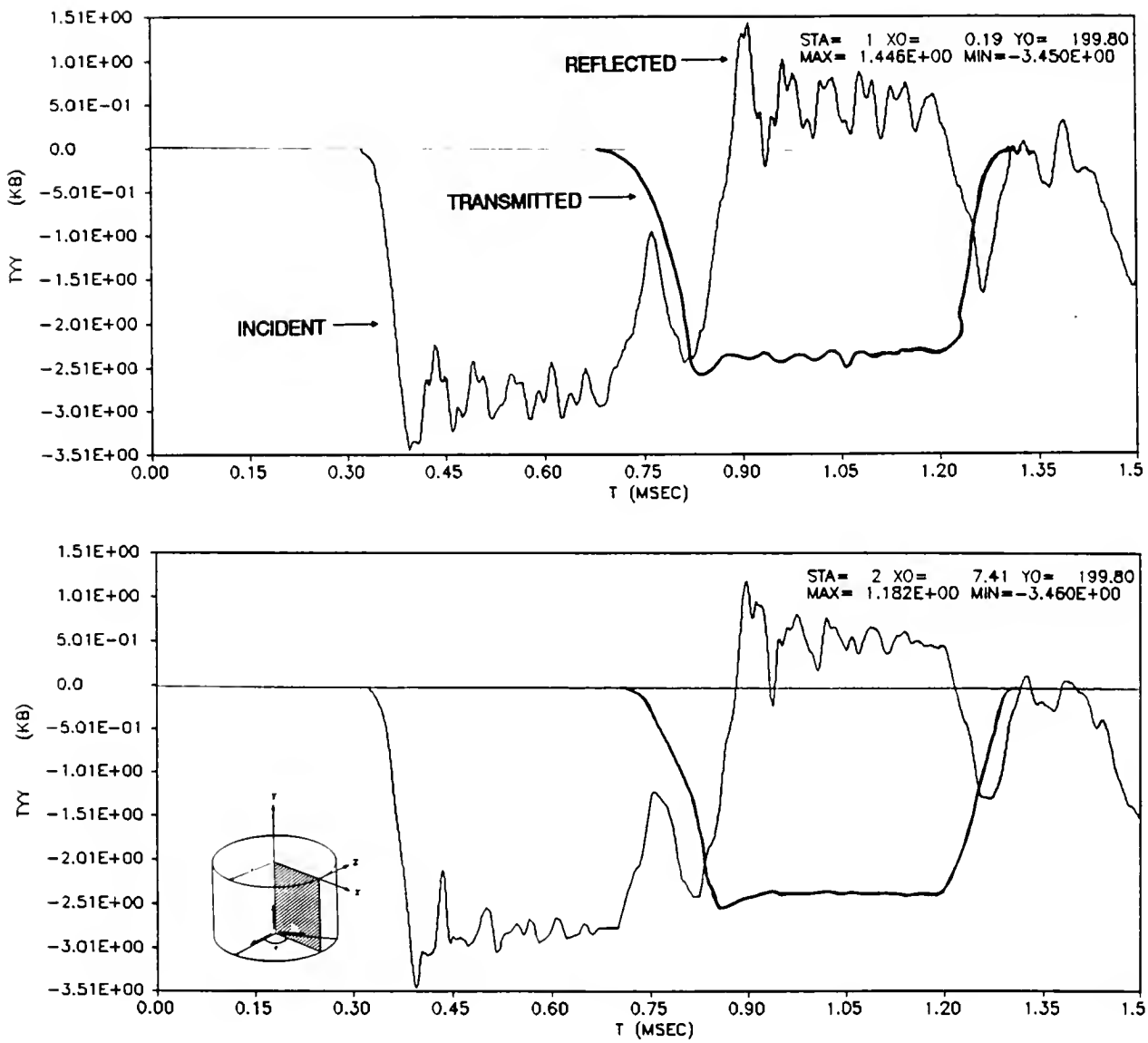

Figure 17. HULL Output. $\frac{a}{\Lambda} = \frac{3}{250}$, 500 μsec Pulse, Station 1 (Top) Bar Center, Station 2 (Bottom) Bar Surface

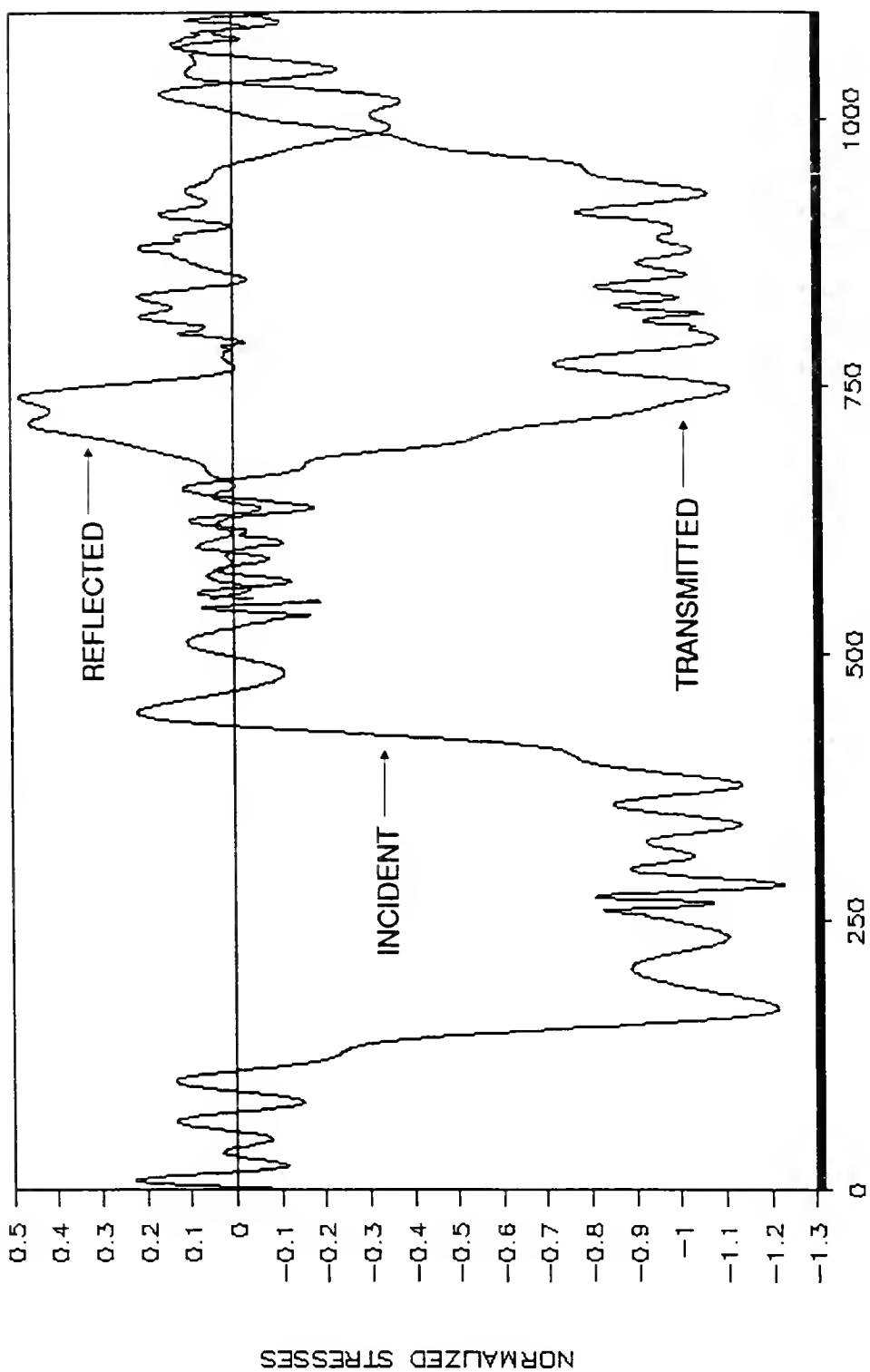

Figure 18. Modified Pochhammer-Chree Results. $\frac{a}{\Lambda} = \frac{3}{125}$, 6-inch SHPB. 250 μsec Pulse

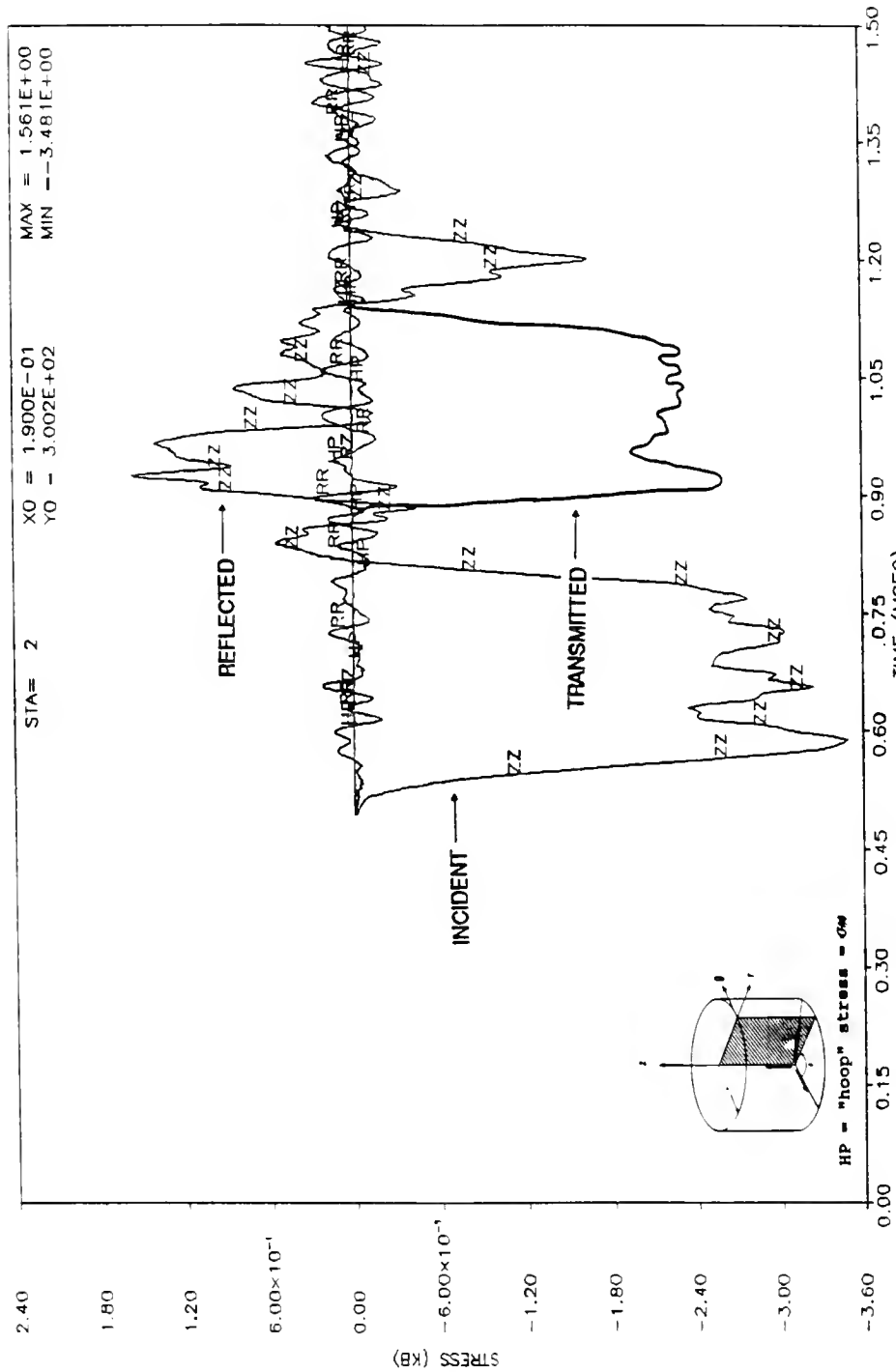

Figure 19. HULL Output at Incident Bar Strain Gage. $\frac{a}{\Lambda} = \frac{3}{125}$,
6-inch SHPB, 250 μsec Pulse

diameter, the waveforms are mathematically the same; this is shown in Figures 5 and 15. Figures 18 and 19 indicate that an input pulse of 250 microseconds for a 6-inch SHPB is not recommended. It appears dispersion becomes a problem, even after a very short time, and also the one-dimensionality of the motion is questionable. Experimentally, one can achieve different wavelengths by changing the length of the striker bar. The resulting waveforms for a 16-inch and a 25-inch striker bar are shown in Figure 20 (all three bar locations are on the incident bar). Notice the more pronounced dispersion for the shorter wavelength.

As discussed, along with more wave dispersion, the one dimensionality of the motion in a bar is also affected by the change of $\frac{a}{\Lambda}$ values. Again, one can turn to the two numerical schemes and observe how, as $\frac{a}{\Lambda}$ increases, the radial and shear stresses increase, and the longitudinal stress shows more variations along the radial direction. Figures 21, and 22 show all stress components on the surface of the incident bar at the strain gage location for a 2-inch bar and a 250 microsecond pulse, and a 6-inch bar with a 500 microsecond pulse. Incident and reflected stresses are shown. Although the radial and shear components of the stresses are higher for higher values of $\frac{a}{\Lambda}$, they nevertheless remain negligible when compared to the longitudinal stress. Figures 23, 24, and 25 show the pulses at the center and at the surface of the transmitter bar at the strain gage location. Figure 23 is the result of the modified Pochhammer-Chree method for a 2-inch bar and 250 microseconds. Figures 24 and 25 are HULL output for 250 and 500 microsecond input pulses respectively. Figure 23 shows a difference of about 1.5% between the two curves. The variation in stress along the cross section is roughly 5% for Figure 24 and 2.5% for Figure 25. Therefore, the uniformity of the longitudinal stress is degraded as $\frac{a}{\Lambda}$ is increased, although for the proposed 6-inch bar and a 500 microseconds pulse, the wave motion should be very close to one-dimensional.

distances from striker bar end :

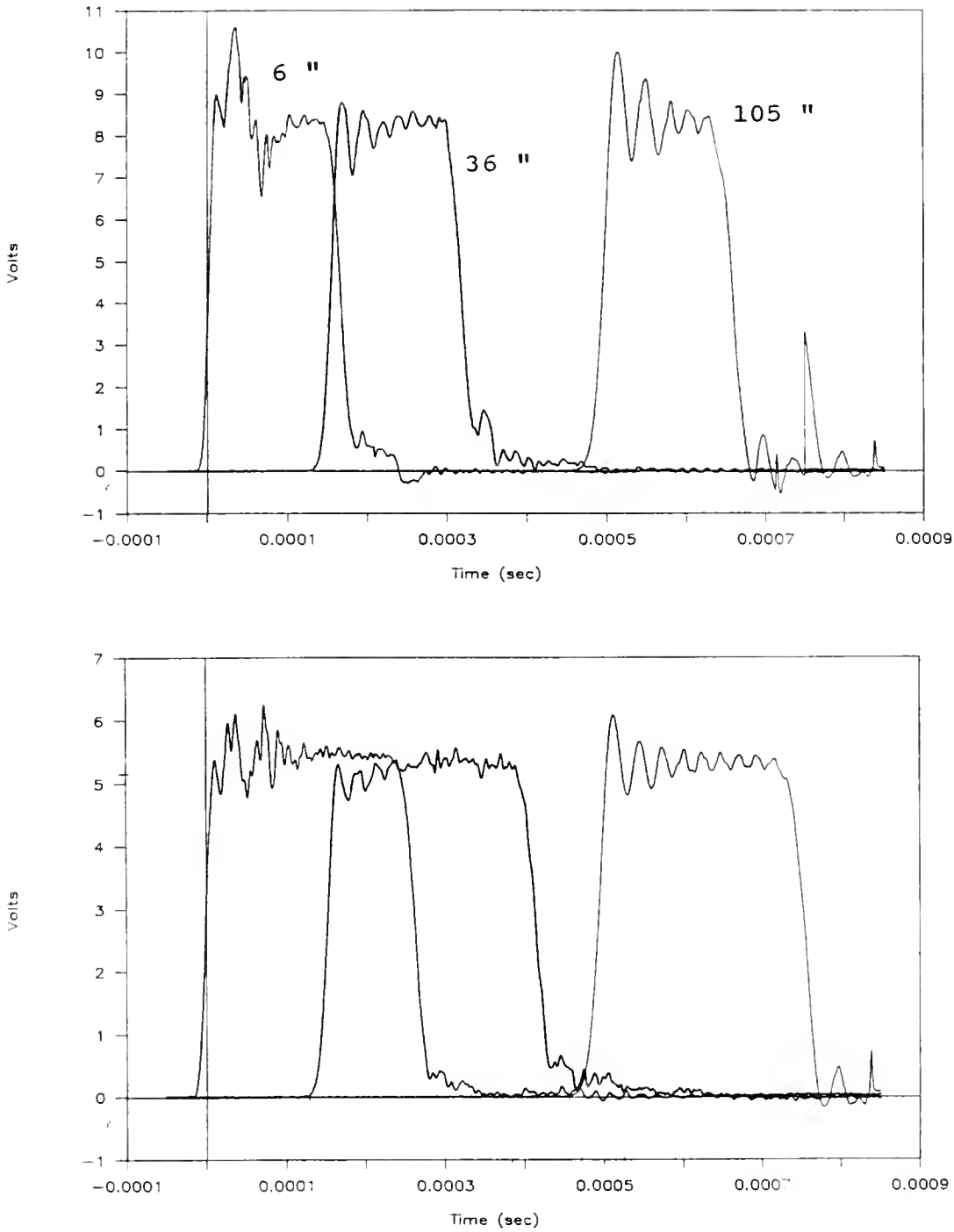

Figure 20. Experimental Traces at Three Incident Bar Locations for Two Striker Bar Lengths. 16-inch (Top) and 25-inch (Bottom), 2-inch SHPB

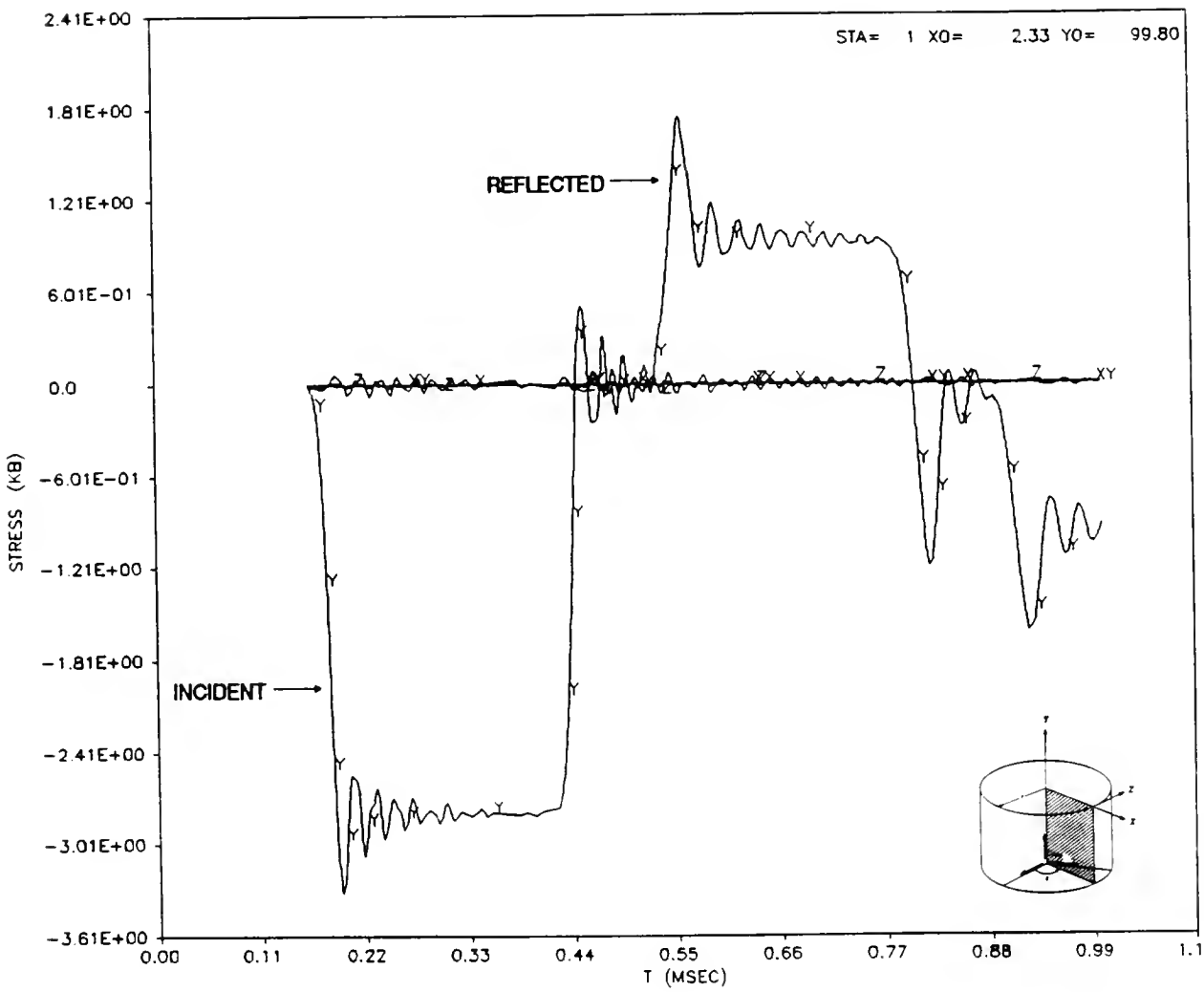

Figure 21. HULL Output. 2-inch Bar, 250 μsec Pulse, All Stress Components on the Surface at Incident Bar Strain Gage

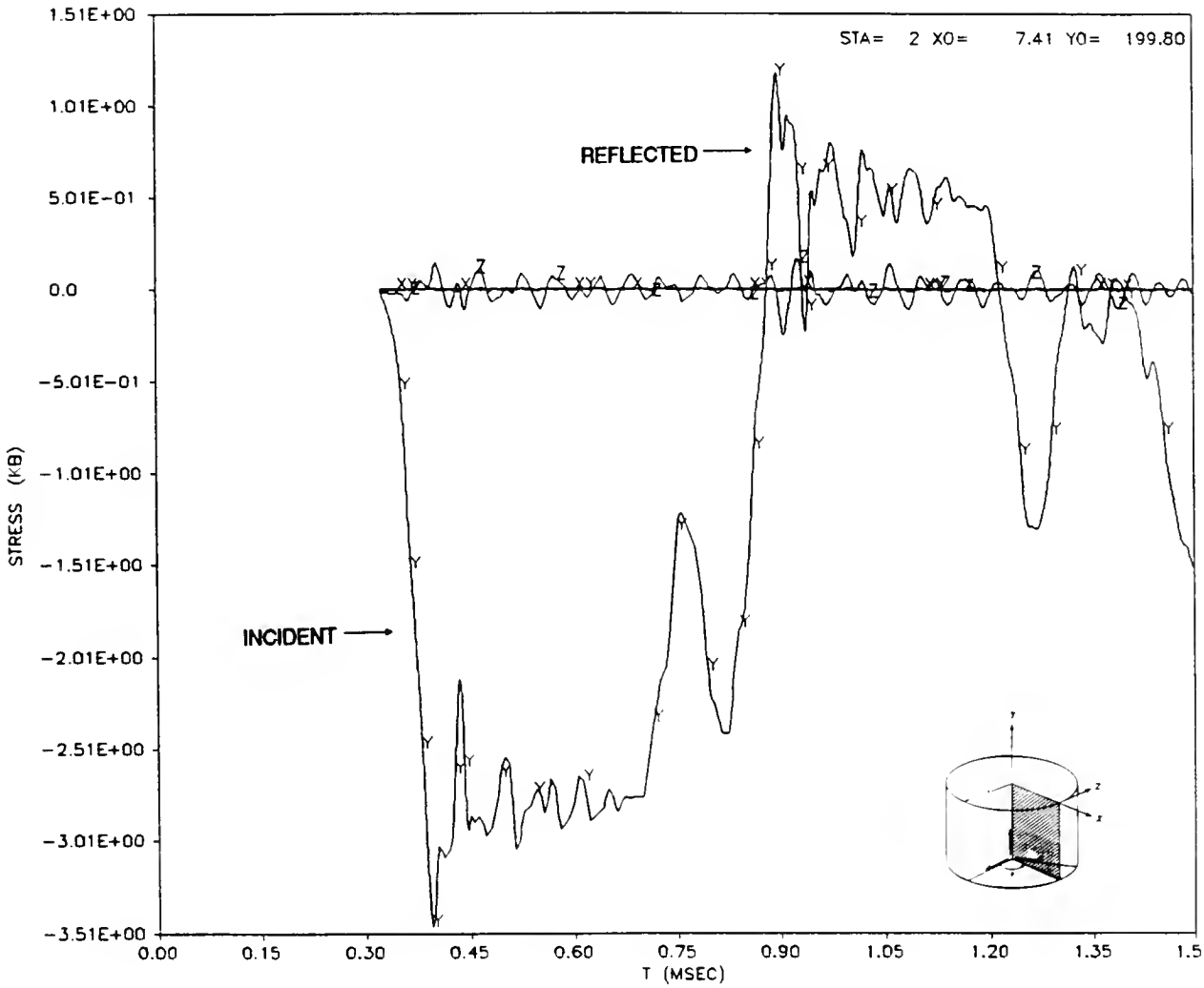

Figure 22. HULL Output. 6-inch Bar, 500 μsec Pulse, All Stress Components on the Surface at Incident Bar Strain Gage

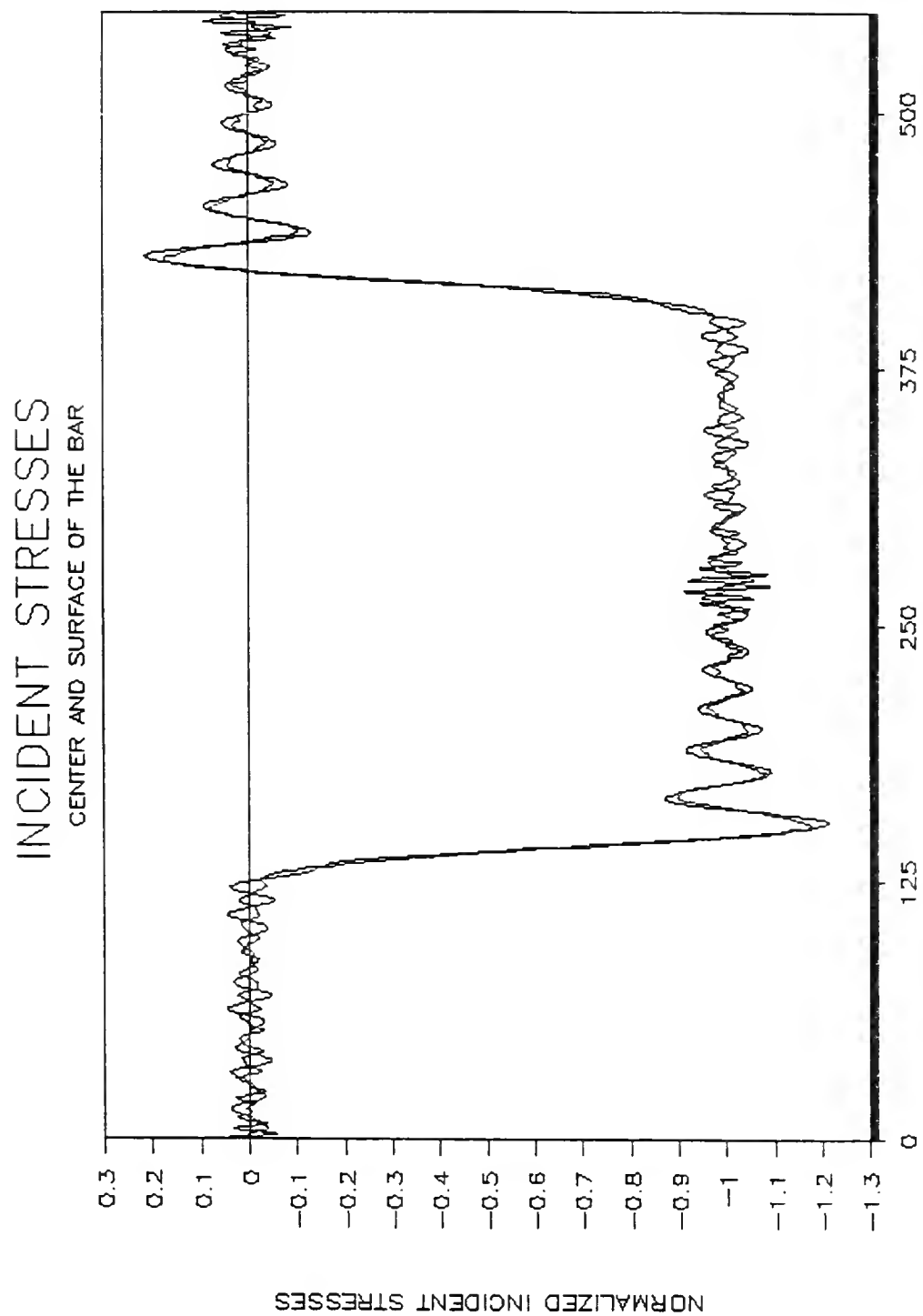

Figure 23. Modified Pochhammer-Chree Results at Incident Bar Strain Gage. 2-inch Bar

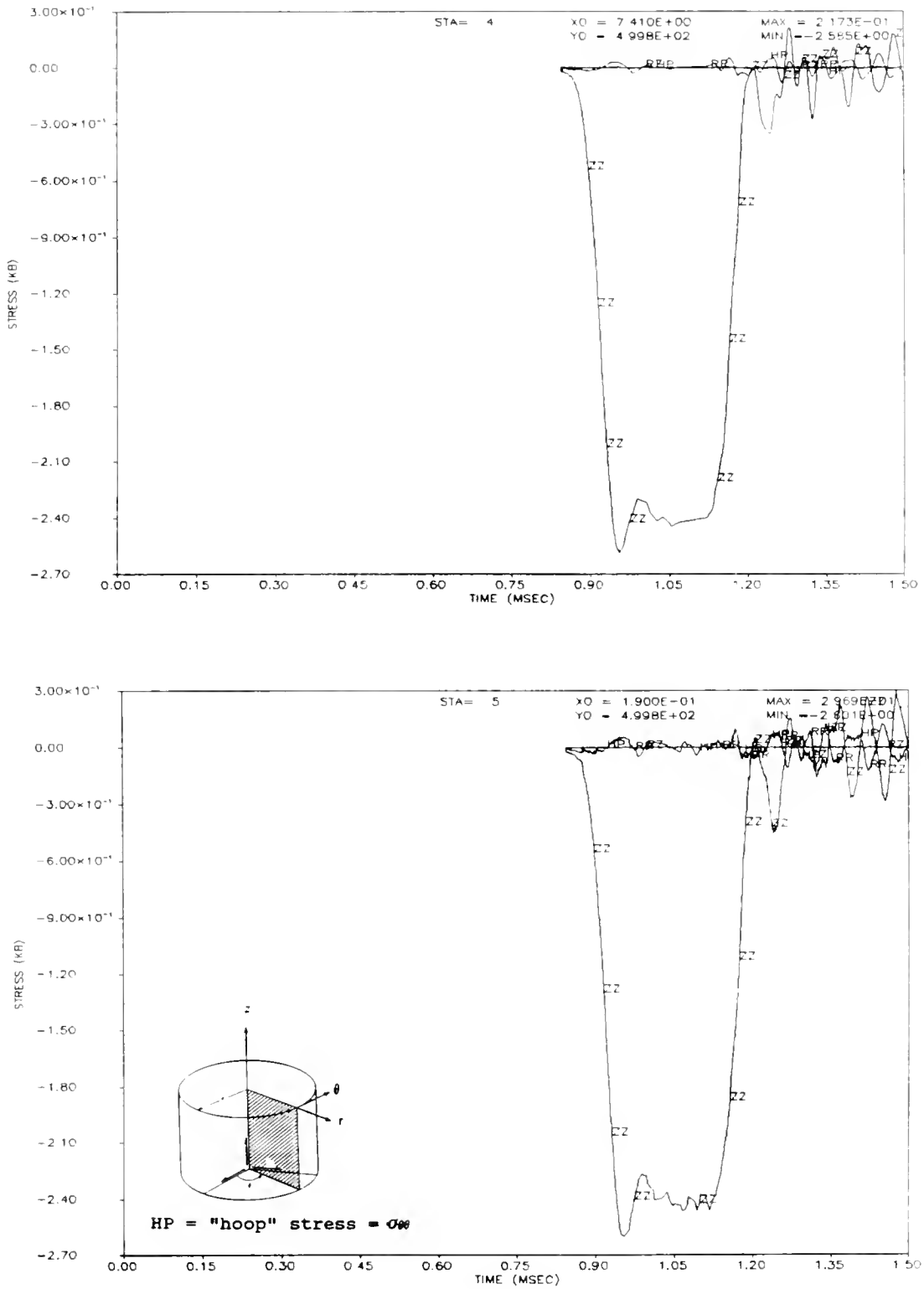

Figure 24. HULL Output. 6-inch Bar, 250 μsec Pulse.
Surface (Top) and Center (Bottom) Transmitted Stresses

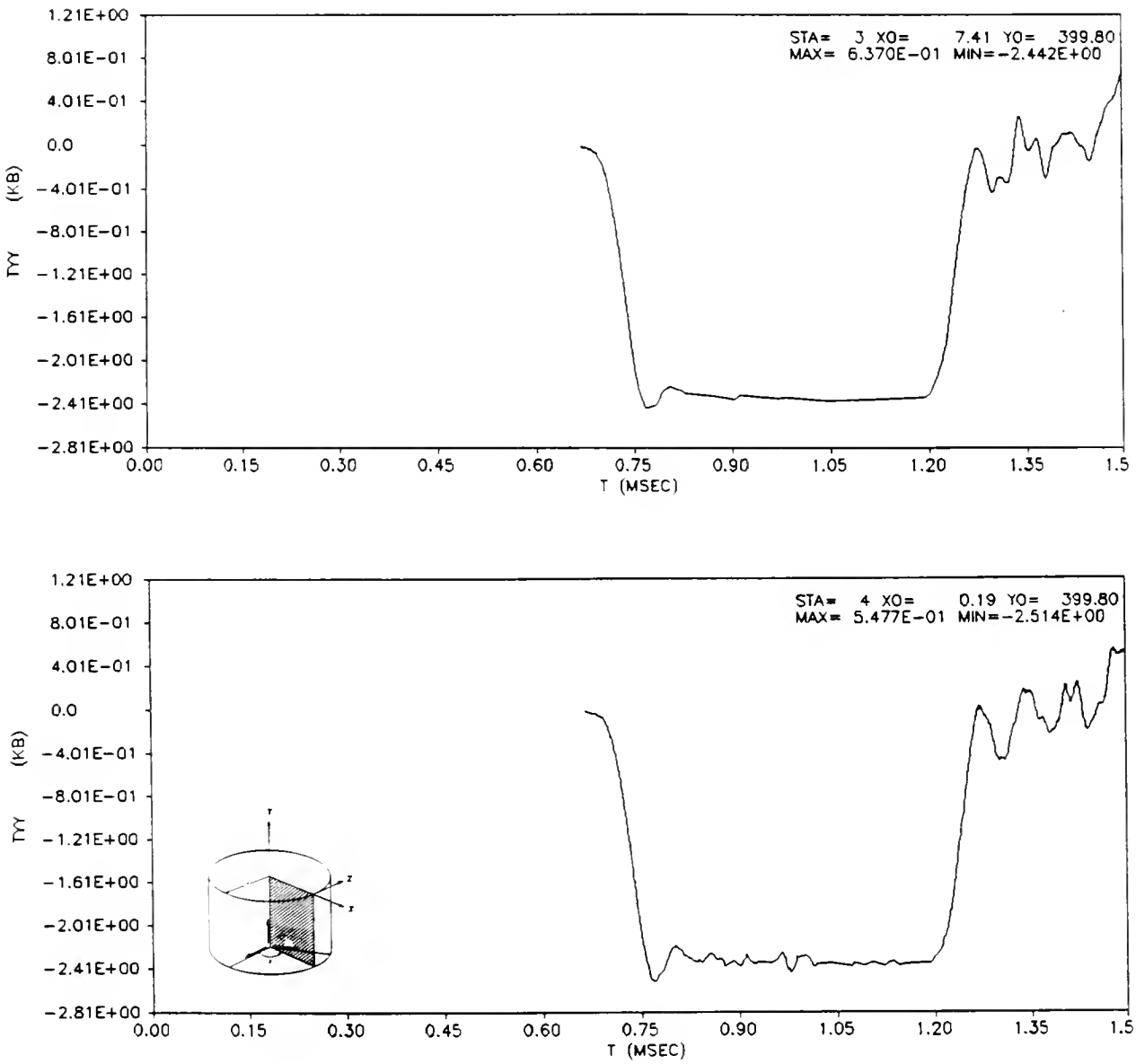

Figure 25. HULL Output. 6-inch Bar, 500 μsec Pulse.
Surface (Top) and Center (Bottom) Transmitted Stresses

A tool like HULL offers the advantage of being able to "look" at the wave response, stresses, accelerations, etc., anywhere in the bar. In particular, two questions regarding the operation of an SHPB have been of interest for some time. The first one has to do with the initial oscillations that are observed experimentally and whether they are due to something inherent to the equations of motion, or whether they are the result of some experimental characteristic like friction, or striker misalignment. The second question has to do with what really goes on at the interfaces between the specimen and the bars, especially when the specimen is smaller in diameter. To answer the first question one can look at the HULL stress output at points very close to the impacted ends. Figures 26 through 28 show curves for various diameter bars and various input pulses at two locations on the incident bar, one near the impacted end, and another one meter from it. The following observations can be made; in the cases where $\frac{a}{\Lambda}$ is larger, the oscillations in the input pulse are more pronounced and they take longer to damp out. Further, if one compares these results with the experimental traces (Figure 20), the similarity in the response is striking. Since the finite difference calculation does not take into account friction, misalignments, etc., it can be deduced that the so called "end effects" are due to inherent characteristics of the wave motion not to the way the experiment is carried out. That means higher frequency modes are excited at the impacted end of the bar. If one refers back to Figure 3, the cases with larger $\frac{a}{\Lambda}$ show more oscillations because the response is further to the right on the x-axis, and thus more modes of vibrations are possible. Nevertheless, as predicted by Davies [27] and others, these high frequency modes damp out quickly, so that after about ten diameter lengths the only mode of vibration present is mode $M_{1,1}$.

The second question presents more of a problem; the wave interaction at the bar-specimen interfaces is extremely complicated, especially if the specimen yields at some point during the process. Looking at the stress

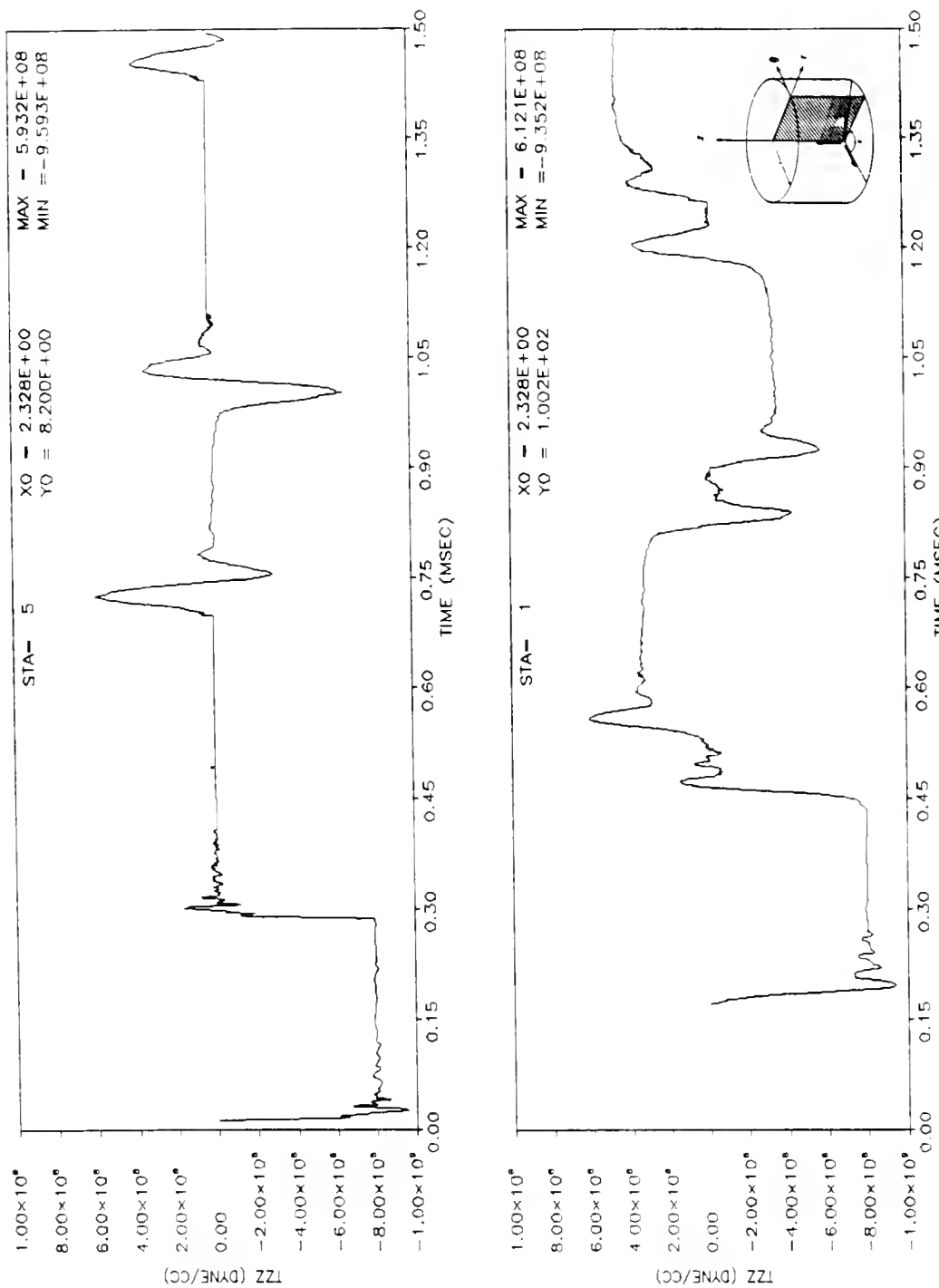

Figure 26. HULL Output. 2-inch Bar, Longitudinal Stress Near the Impacted End (Top) and at the Strain Gage Location (Bottom)

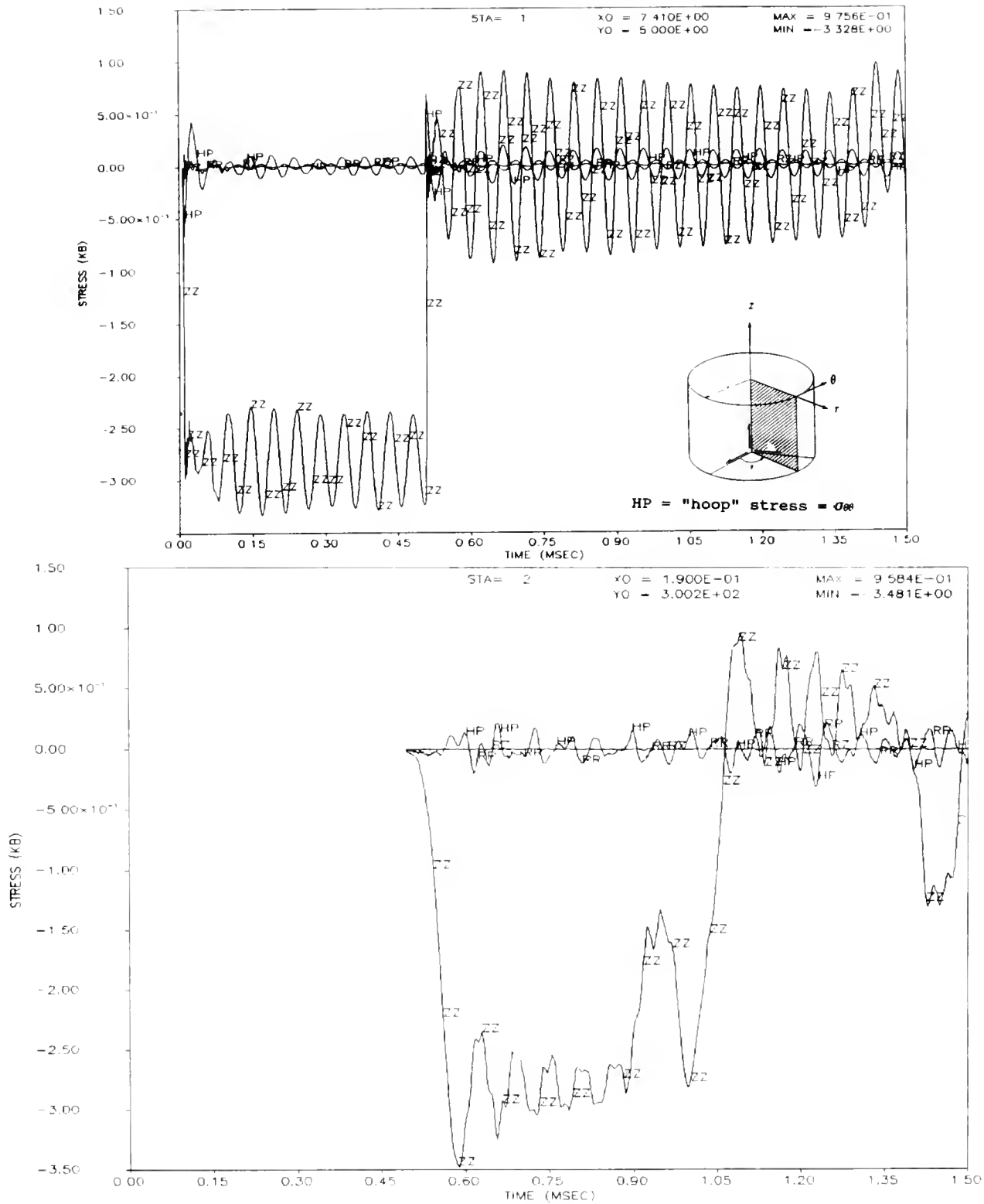

Figure 27. HULL Output. 6-inch Bar, All Stresses Near Impacted End (Top) and at the Strain Gage Location (Bottom)

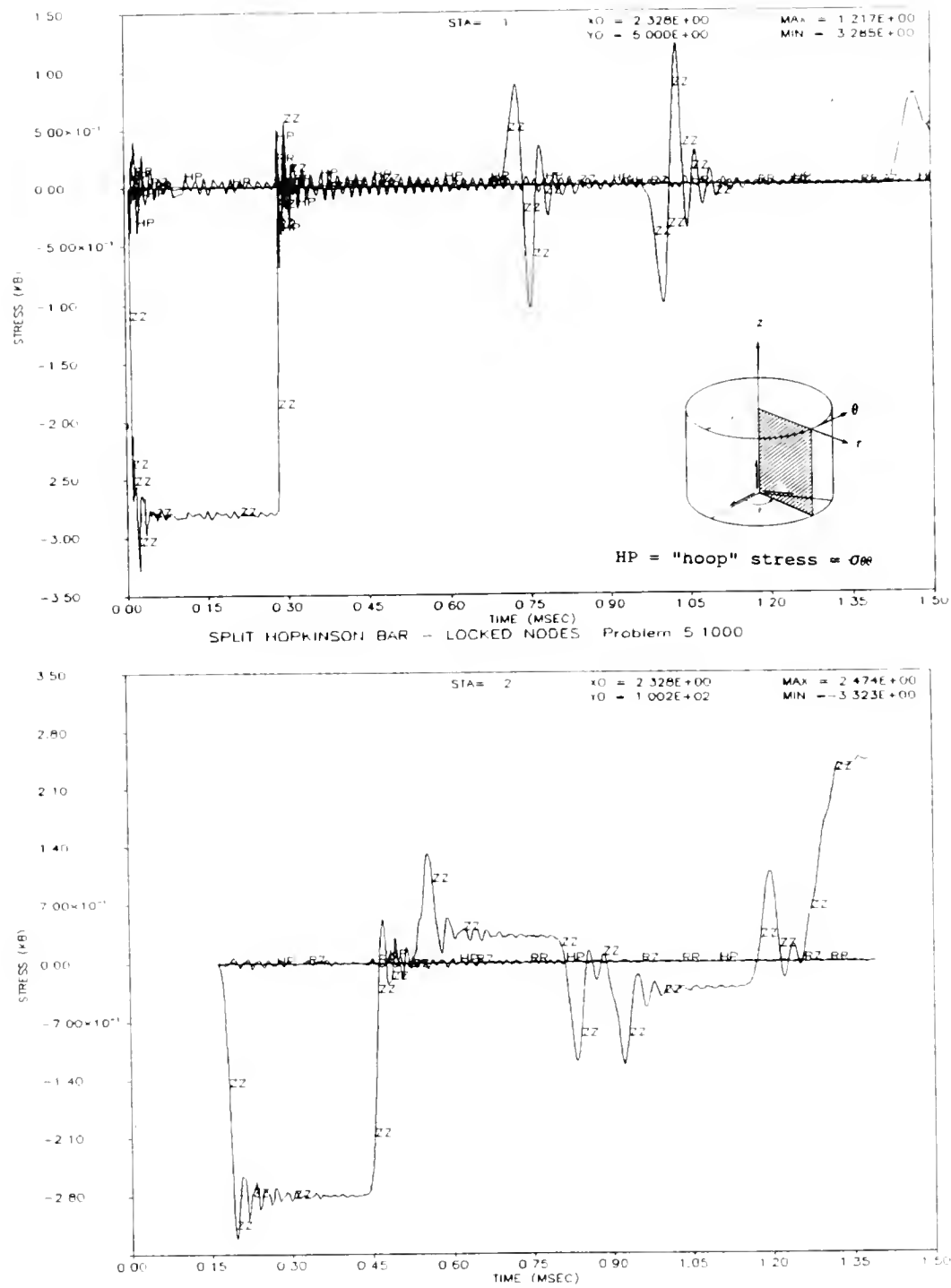

Figure 28. HULL Output. 2-inch Bar, All Stresses Near the Impacted End (Top) and at the Strain Gage Location (Bottom)

components along one such interface from a HULL calculation, it is very difficult to make any definite statement. To help in the understanding of the complicated stress wave interaction, Figure 29 shows the important features and magnitudes of all stress components along the incident bar-specimen interface. The longitudinal stress (uniform and in compression, of magnitude 167 MPa sometime prior to this interface), at the interface varies from almost zero at the bar surface to 100 to 80 MPa at the center. Shear and radial stresses become of the same order of magnitude as the longitudinal stress. What is worth noticing is that at the center $\sigma_{\theta\theta}$ or the "hoop" stress is very large, in fact larger than the input stress. Also at this point the displacements in the longitudinal and radial direction are small. It appears then, that shear and circumferential stresses play an important role at the edge where the specimen ends against the bar face. In a sense, the incoming stress has to "squeeze" itself through a smaller cylinder therefore it is not surprising to find other than longitudinal stresses at the interface. What is remarkable is how quickly it recovers to an almost uniform state of stress within the specimen only one centimeter from the interface (Figure 30), and in the transmitter bar at the strain gage location (Figure 31), where the longitudinal stress is the only non zero component. Figures 30 and 31 correspond to the same SHPB as in Figure 29. Notice that $\sigma_{\theta\theta}$ in Figure 30 is only about 50 MPa while it peaked at 220 MPa at the interface; that amounts to a reduction of 77% in one centimeter. Appendix C contains more HULL output traces which can further explain the above discussion.

Finally, Bertholf and Karnes [23] pointed out that the first interface between the bar and the specimen effectively filters out most of the oscillations in the incident pulse, and thus in the cases when these oscillations are large for one reason or another, it is wise to use only the transmitted stress to calculate the response in the specimen. The analytical tools also show this filtering effect of the specimen, and it appears the use of the transmitted pulse only, may be a worthwhile alternative for the proposed 6-inch SHPB.

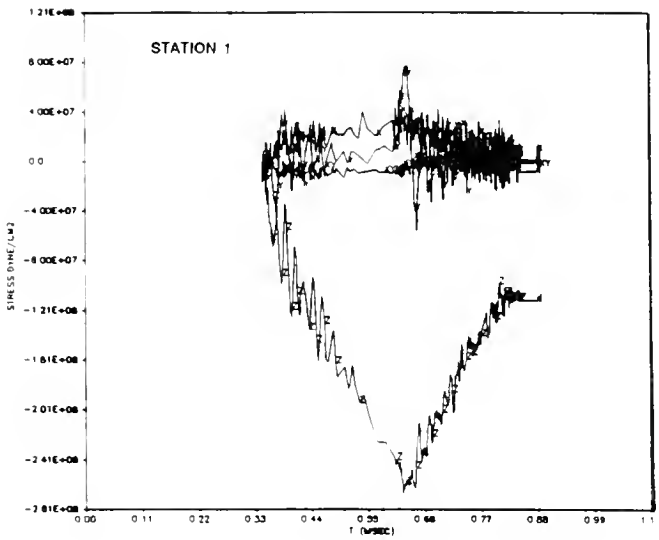

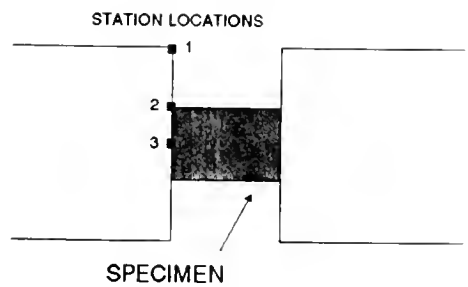

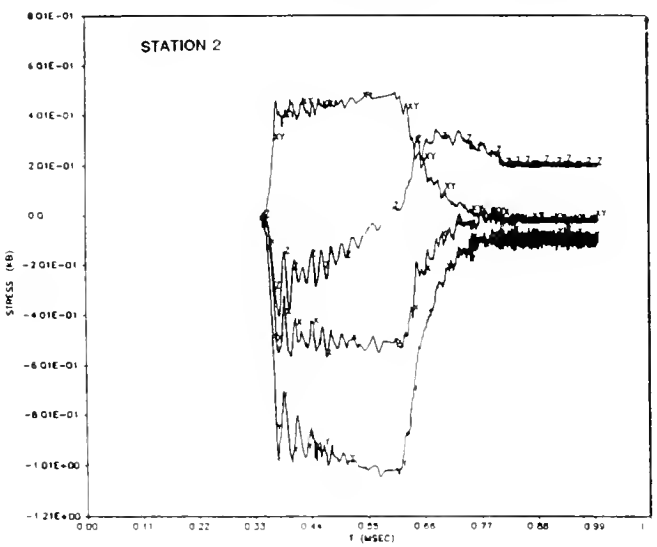

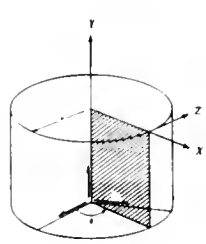

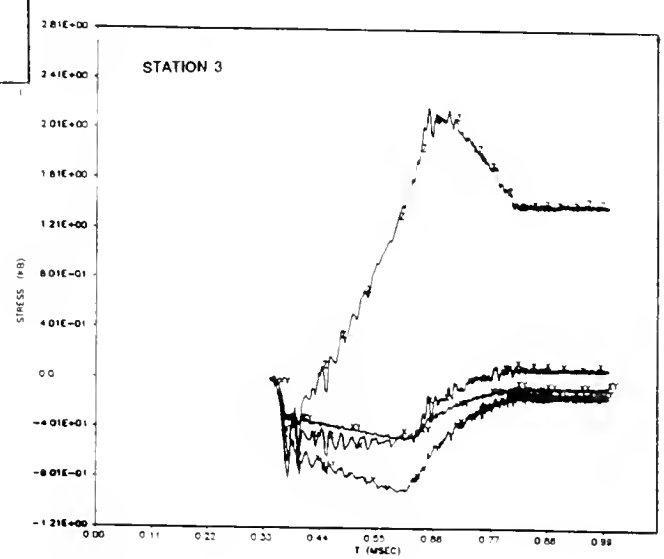

Figure 29. HULL Output. 2-inch Bar, All Stresses at Three Locations at the Bar-Specimen Interface

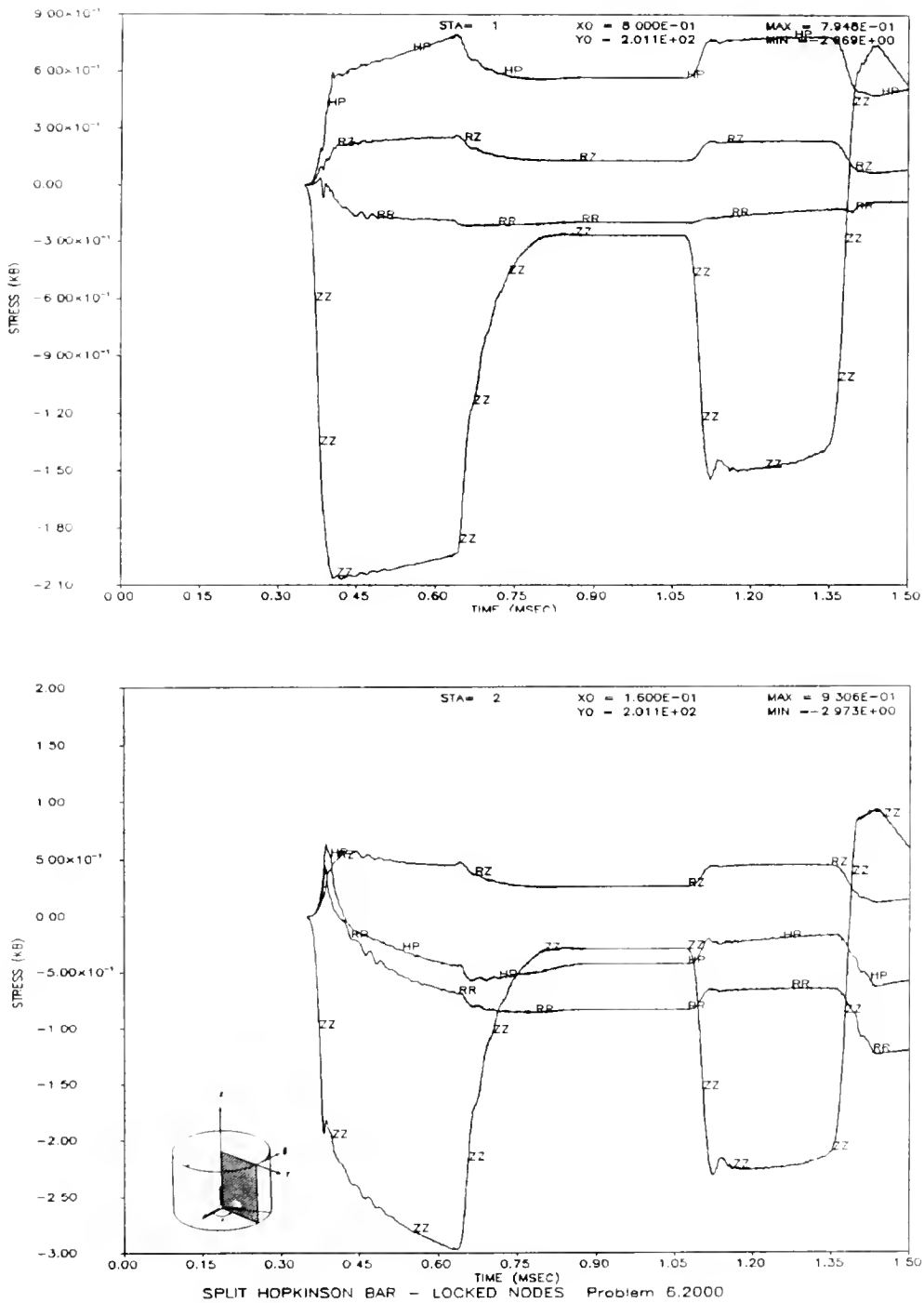

Figure 30. HULL Output. 2-inch Bar, Stresses in Aluminum Specimen at Two Locations Near the Surface (Top), Near the Center (Bottom). Compare with Figure 29

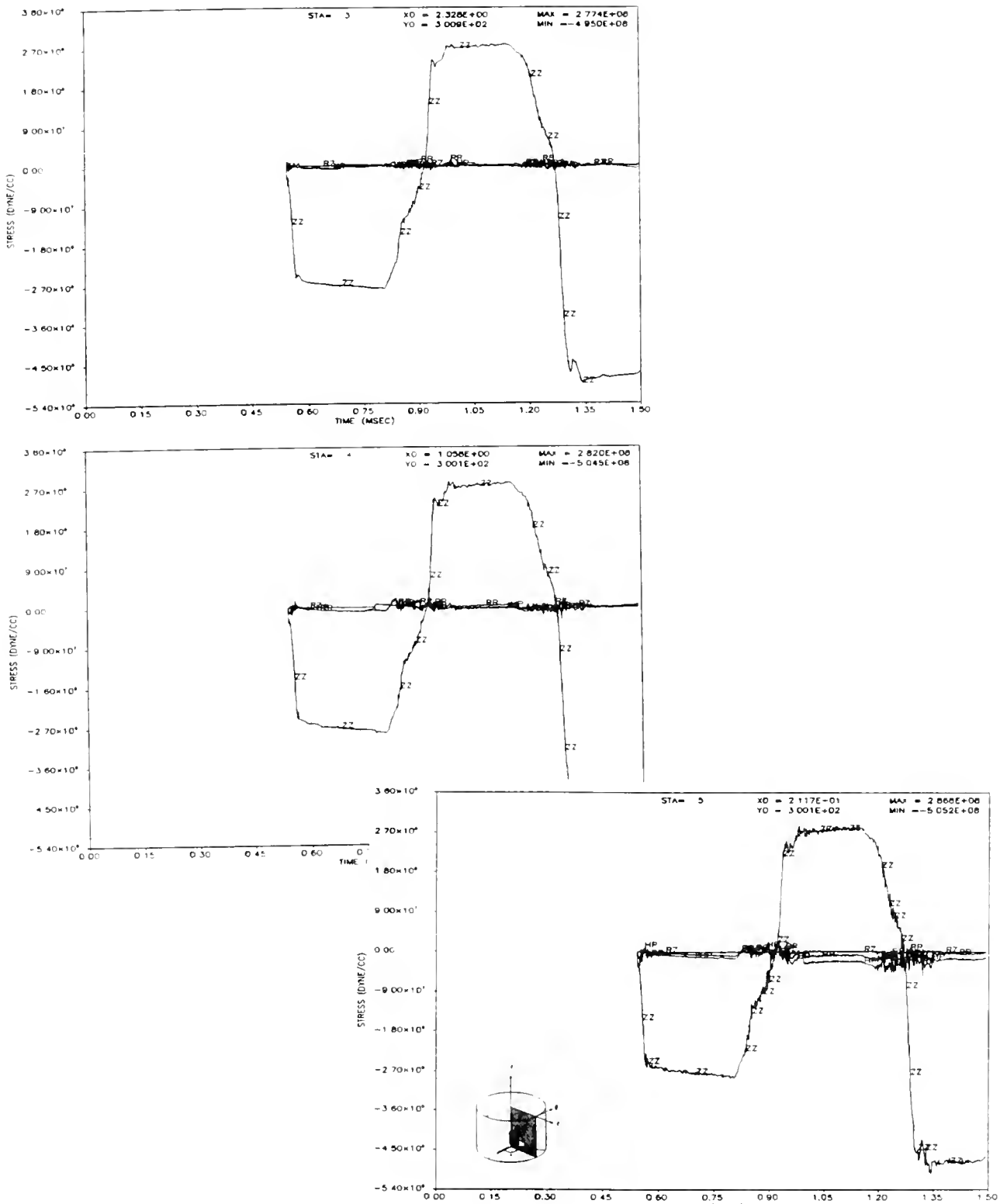

Figure 31. HULL Output. 2-inch Bar, Transmitted Stresses at Three Radial Locations. Surface (Top), Middle (Middle), Center (Bottom). Compare with Figure 29

The two analytical methodologies used have advantages and disadvantages, and the use of one over another depends on the particular need and application. The finite difference solution is the most accurate if the constitutive relationships of the materials involved are adequate. It is also the most time consuming and expensive. The Modified Pochhammer-Chree method developed in this study gives a good qualitative look at the wave propagation in a typical SHPB in a very short time. It can be reliably used to assess the one-dimensionality of the elastic wave motion, as well as dispersion effects and cross sectional variations and values of all the stress components. It is a tool that can also be used to investigate if a particular experimental setup is affected by friction or inertia by predicting what would happen in the absence of friction and inertia. Furthermore, a typical HULL calculation took anywhere between three and six central processing unit (CPU) hours on a CRAY Y-MP computer at an average cost of $800.00 per job! The modified Pochhammer-Chree method takes seconds to run on most machines at an average cost of less than $2.00. Although the Modified Pochhammer-Chree method assumes a purely elastic response, it does not affect its usefulness since one would not use any of these analytical tools to investigate true material response, but rather to study the reliability of a certain SHPB configuration. These numerical codes are not intended to replace the experimental method, but rather to study the validity of the data reduction, the implications of a geometric change, the effects of a different input pulse, and so on. After all, if the true constitutive relations of the specimen material were known one would not need to study its response with an SHPB. The Modified Pochhammer-Chree method can give the results it was designed to give with any elastic specimen, as long as the characteristic impedance of the material and the bars are known.

Inertia and Friction Effects

The analytical methods discussed are useful tools to study the wave propagation of any SHPB, and within their limitations and assumptions can assess the one dimensionality and therefore the usefulness of different bar sizes and configurations. However, the reliability of an SHPB can be influenced by radial and axial inertia and by friction between the specimen and the elastic bars. Neither the modified Pochhammer-Chree method nor the finite difference code HULL take those into account. Approximate corrections have been derived to account for the effects of radial and axial inertia [7] and friction [8]. The objective of this investigation is to understand when and how inertia and friction become important factors and whether the SHPB diameter is a key parameter on inertia and/or friction contributions. In other words, one would like to know whether increasing the diameter of a SHPB will increase the effects of inertia or the effects of friction.

Inertia effects become more pronounced as either the initial stress in the input bar becomes high, or the strain rate is increased [24]. The former causes very large stress and strain gradients which from the equations of motion, make the inertia term become important [35]. High strain-rates do not appear to cause inertia effects per se, rather the way the higher strain-rates are achieved can cause inertia effects to become important. Specifically, if one increases the input stress to obtain a higher strain-rate, and this input stress is in the form of a step function, then apparently the combination of high input stress, and the oscillations caused by radial waves resulting from the short rise time of the input, causes inertia effects to become quite important. Bertholf and Karnes [24] eliminated one of these two causes by, numerically, using a ramp input function with a much longer rise time. Their results show that doing this effectively eliminates the inertia effects, even though the same levels of strain rates were achieved. This means that the magnitude of the input stress is not a major cause of inertia effects, rather

the short rise time associated with the high input seems to significantly contribute to inertia effects. Therefore, since in an SHPB one is limited to a step input pressure, there appears to be a maximum achievable strain rate beyond which the validity of the experimental data becomes questionable. Bertholf and Karnes calculated a maximum allowable strain rate for their SHPB. They claim that since their numerical calculations are based on constitutive equations which are rate independent, their results can be applied directly to different diameter systems. For a 1-inch diameter bar, a length L over diameter d (L/d) = 0.3 in the specimen, and a step input stress, Bertholf and Karnes calculated a maximum strain rate of 400 1/sec. For a ramp input, this value is much higher for the reasons discussed earlier. If the diameter is increased by a factor n, then the new maximum strain rate is 400/n 1/sec. This scaling cannot be applied directly to the proposed 6-inch bar because the L/d of the specimen will not necessarily be 0.3. In fact it will be about one for concrete specimens to ensure the same aggregate density in all directions. Therefore one needs to go back to the equations that Davies and Hunter [7] derived to calculate the contribution of inertia based on the kinetic energy due to both axial and radial motion. Their result is

$$\sigma_s = \sigma_b + \rho_s \left(\frac{L^2}{6} - v_s^2 \frac{d^2}{8} \right) \frac{d^2 \varepsilon}{d t^2} \tag{19}$$

where σ_b is the measured stress, subscript s pertains to the specimen and $\frac{L^2}{6}$ and $v_s^2 \frac{d^2}{8}$ are the axial and radial inertia contributions respectively. Equation (19) can be rewritten in nondimensional form as

$$\frac{\sigma_s - \sigma_b}{\sigma_b} = \frac{d^2 \varepsilon / d t^2}{\sigma_b} \frac{\rho_s d^2}{6} \left[\left(\frac{L}{d} \right)^2 - 3/4 \, v_s^2 \right] \tag{20}$$

The left hand side is the error in the measured stress. If one assumes a nominal Poisson's ratio of 0.3, the contribution of the term L/d can be calculated relative to Bertholf and Karnes L/d of 0.3. This leads to the conclusion that for a nominal L/d = 1.0, the error in the measured stress will increase by a factor of 40. This means that the maximum strain-rate they calculated should be reduced even further. This would lead to unacceptably low strain-rates. Therefore, the thing to do is accept the errors due to inertia effects, and correct them using equation (19) in the data reduction algorithm.

Furthermore, if one looks at typical strain rate plots from actual SHPB experiments, it appears that in most cases the strain rate very quickly levels off to some constant value. What that means is that the derivative of the strain rate will eventually approach zero, and it may be that the inertia effects will not be as important after the initial 100 or so microseconds.

Friction presents more of a problem in the sense that its effects are not easily quantifiable or easy to predict. It is shown from numerical calculations that the measured stress will be larger than the true stress, resulting in an artificially high strength in the material being analyzed. But how much? Early work and studies done by Davies and Hunter [7] and by Samanta [10] show that in general, if the diameter and the length of the specimen are of the same order of magnitude, then friction contributes to only a few percent error. It appears that the important parameter is the ratio of the area constrained by friction over the volume of material in the specimen. In other words, a thin specimen will be more affected by friction than a thick one. Since the area constrained by friction is $\pi d^2/2$ (two faces) and the volume is $\pi d^2 L/4$, then the key parameter in determining friction effects is 2/L. The larger this value the greater the error due to friction. This means that increasing the diameter of the SHPB bars and specimen will not worsen friction effects. Although an exact value for friction effects is not obtainable, one can assess the order of magnitude of the error by running HULL with "locked" interfaces between the bars and the specimen, and then

compare the results with the other runs where the interfaces were friction-less. (There is no option in HULL for modeling friction). The results then bound the friction problem as the "locked" case represents a worst case scenario. Figures 32 and 33 show the transmitted stress for a 2-inch bar with zero and infinite friction, respectively. Figures 34 and 35 show the same thing for a 6-inch bar. As expected, the cases with infinite friction show a higher transmitted stress, implying an artificially higher strength in the specimen. It is interesting to notice that the error due to friction in the 2-inch bar is about 16.4% and in the 6-inch bar is only 5.6%. This agrees with the criterion derived above which states that the error is proportional to 2/L. It appears the larger SHPB set up will be less susceptible to friction in light of the fact that the specimen length will be increased along with the diameter. However, one should not imply from this that friction introduces errors in the existing systems of the order of 10-20%. That figure is an upper bound for a case where the specimen is attached to the bars. In reality, the friction coefficient will be somewhere less then 1.0, especially if care is taken in lubricating the ends. Therefore, the errors due to friction are negligible in typical SHPBs and will be so also for a proposed 6-inch system. If, however, one was to test thin specimens, then the data reduction should take friction effects into account.

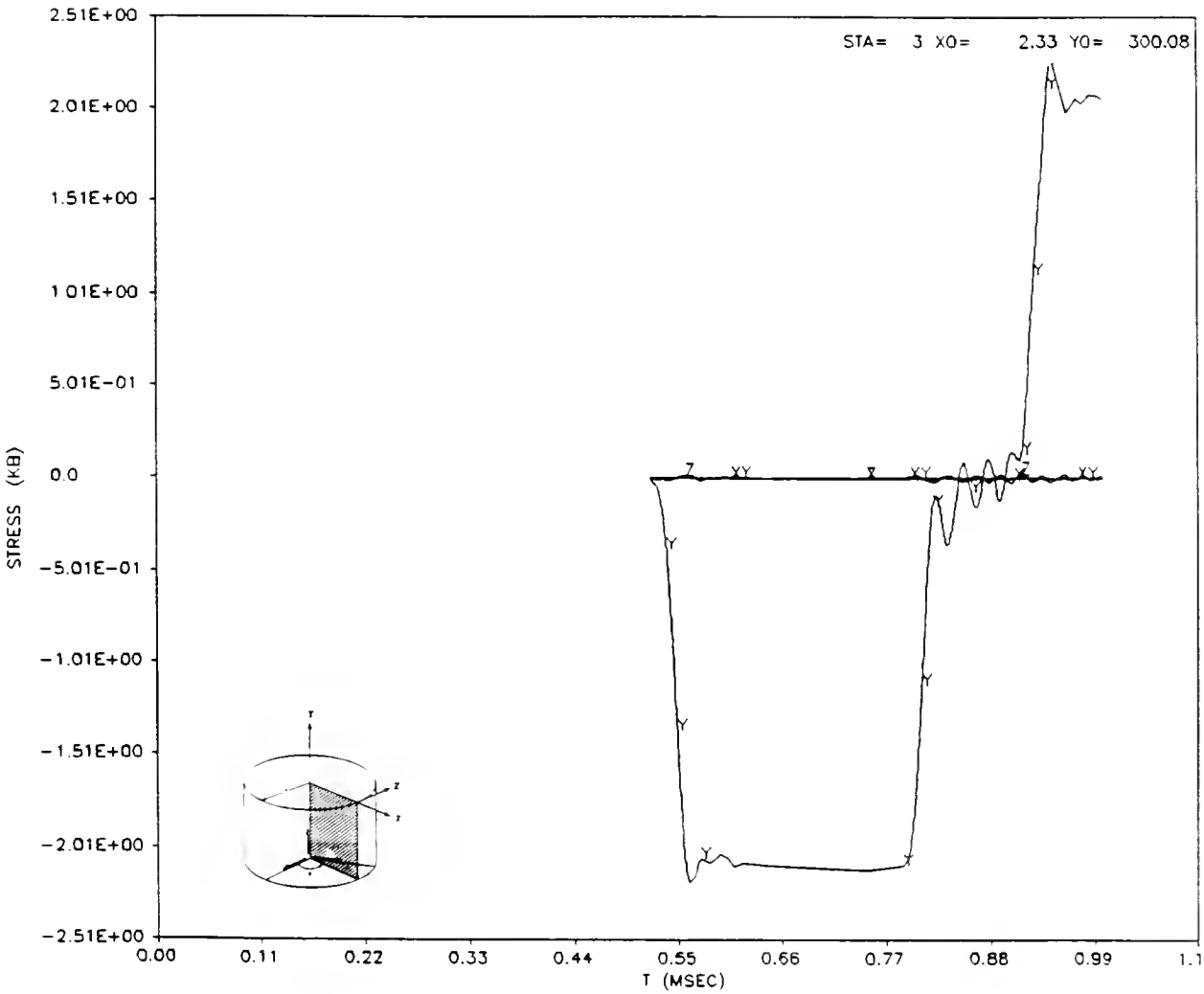

Figure 32. HULL Output. 2-inch Bar, Transmitted Stress with Zero Friction Between Specimens and SHPB

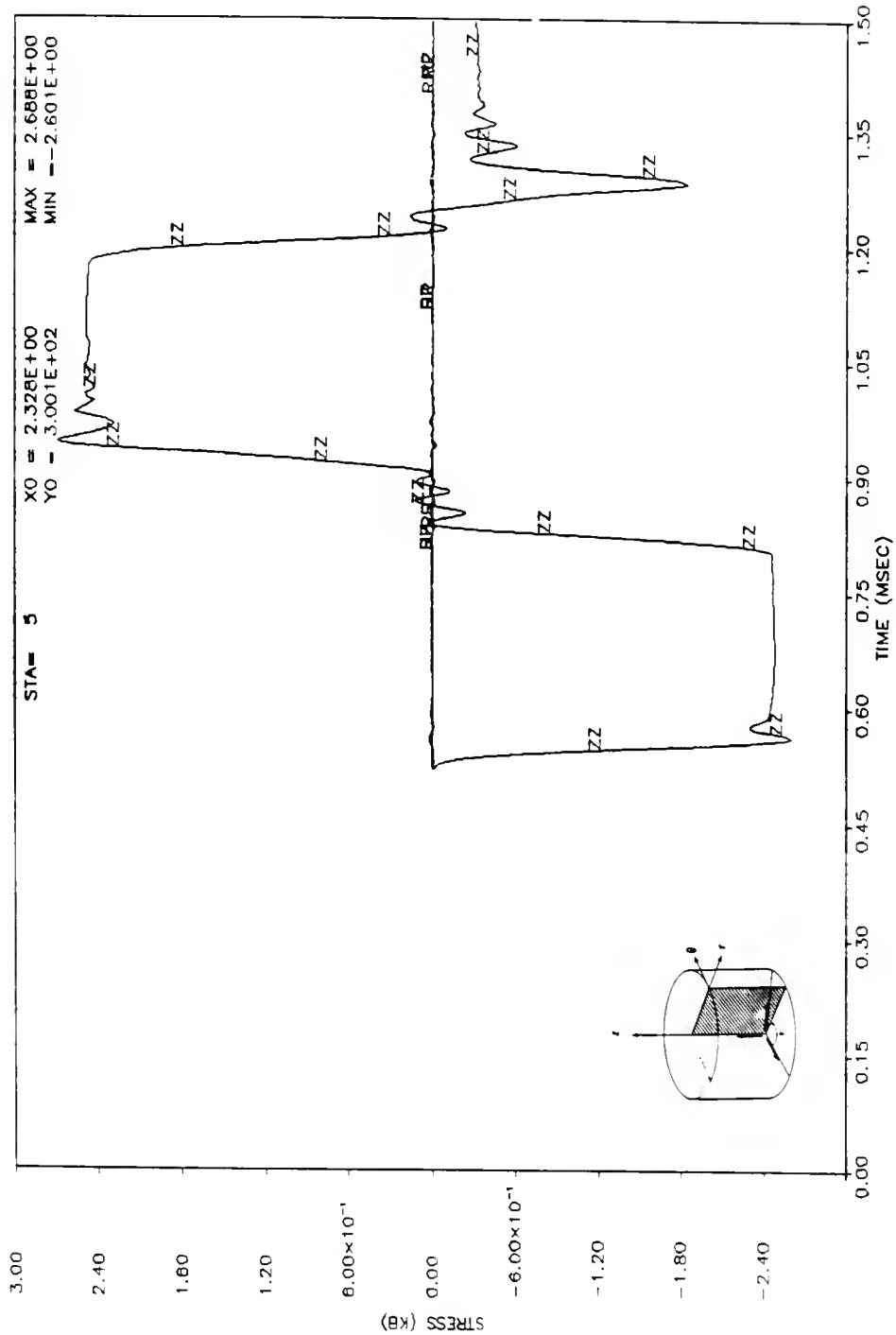

Figure 33. HULL Output. 2-inch Bar, Transmitted Stress with Infinite Friction Between Specimen and SHPB

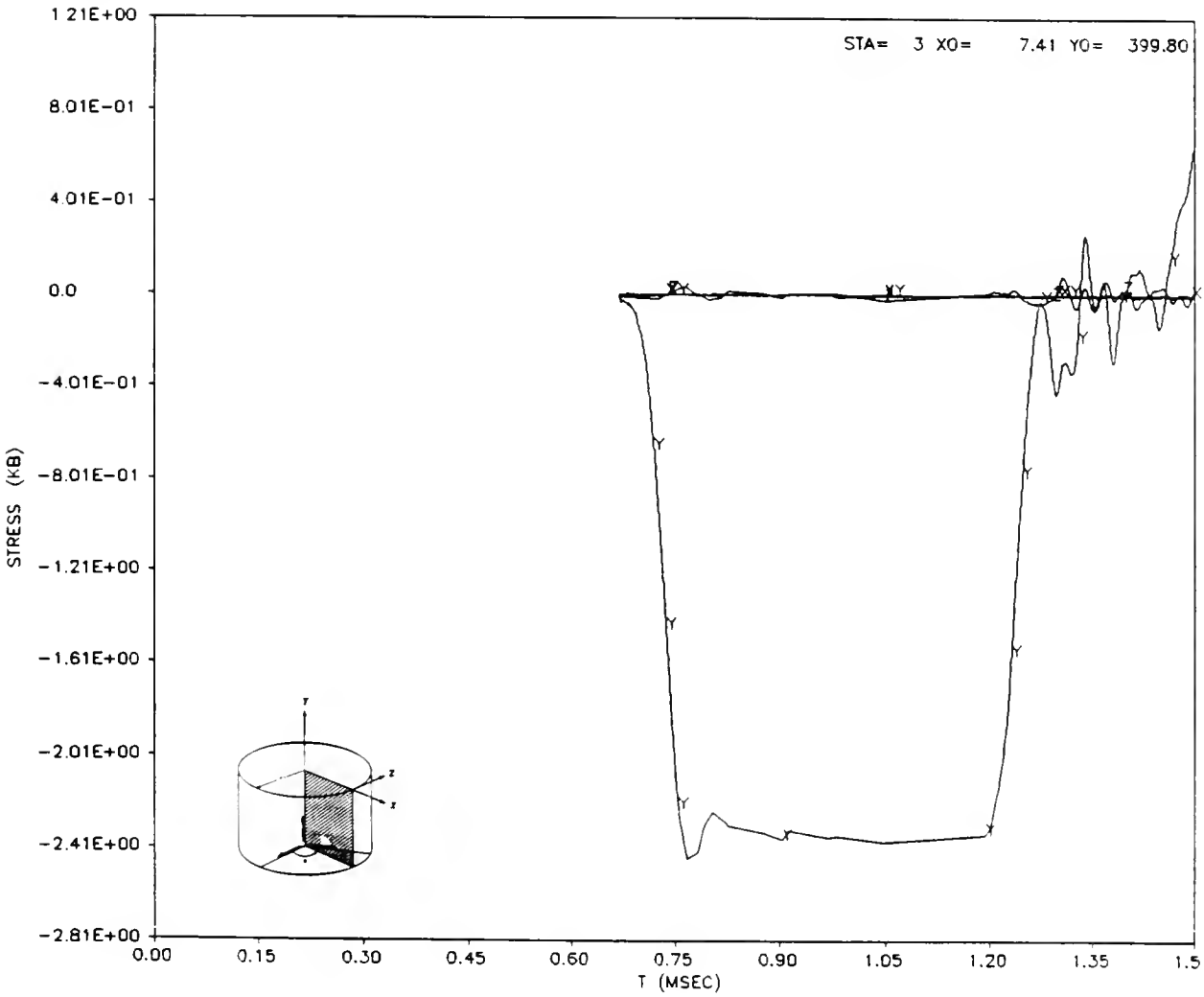

Figure 34. HULL Output. 6-inch Bar, Transmitted Stress with Zero Friction

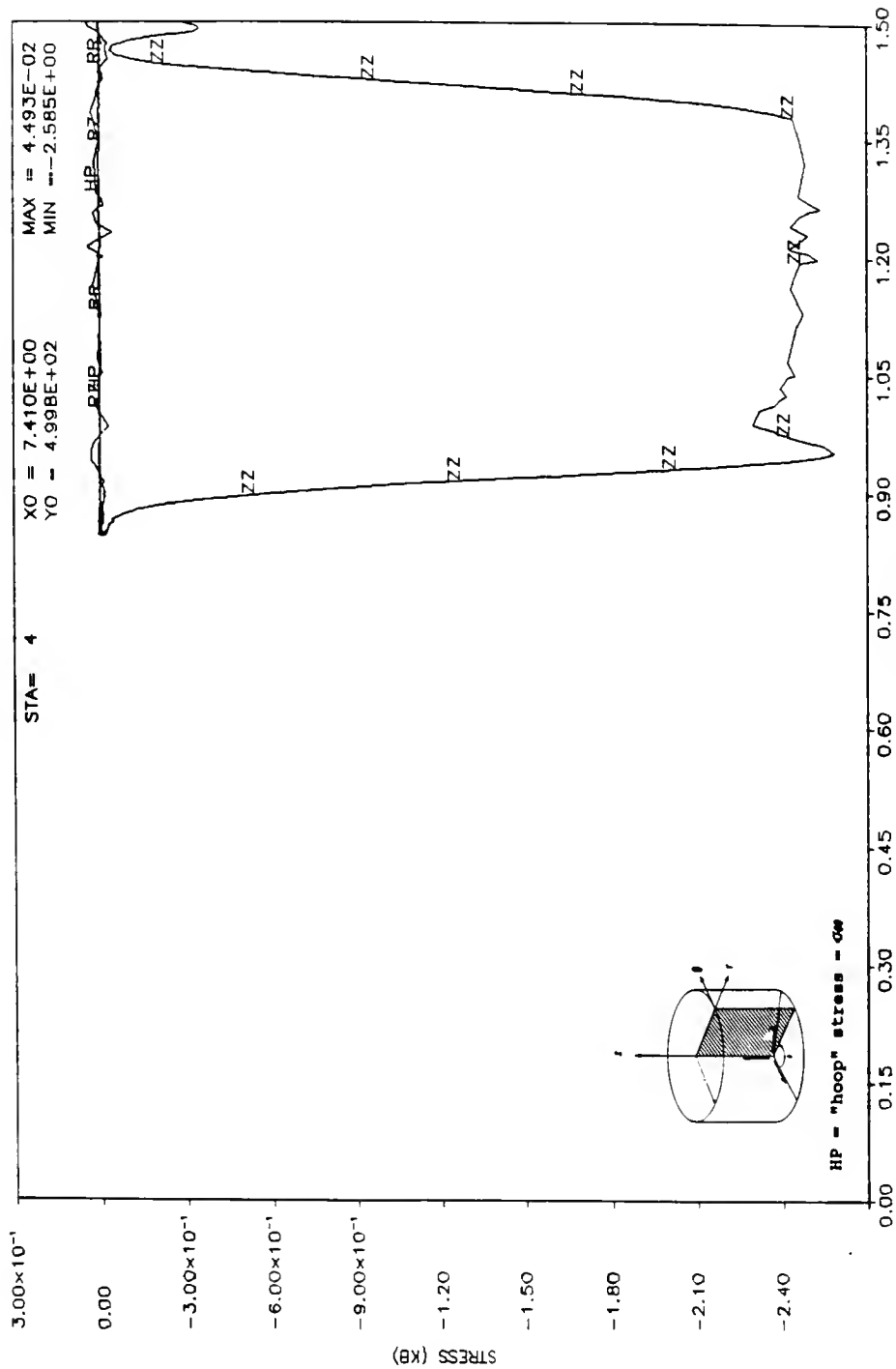

Figure 35. HULL Output. 6-inch Bar, Transmitted Stress with Infinite Friction

CHAPTER 4

SIX-INCH SHPB FEASIBILITY

Summary

The objective of this effort was to assess the feasibility of a 6-inch SHPB. There is an abundance of experimental data for existing SHPB systems, and it was used in this study to test the accuracy and reliability of the numerical finite difference code HULL.

The first part of this work researched the multitude of efforts conducted on the subject in the past years. In particular, it was established that it was important to look at the two-dimensional equations of motion as the simplified one-dimensional case may not be adequate for a larger system. The Pochhammer-Chree solution for an infinitely long bar was used as the baseline for the mathematical analysis. Early papers on inertia and friction effects were studied, and the methodology extended to the 6-inch bar system, primarily to have a feel for the magnitude of the errors introduced by those factors.

Taking a closer look at the governing equations and at the Pochhammer-Chree frequency equation, it became apparent that the problem of wave propagation in a cylindrical bar is independent of scale if the ratio of the diameter over the wavelength of the traveling pulse is kept constant. This is not a new idea, but the implications in this study are crucial. It means that in theory at least, an SHPB can be scaled up or down as long as the input pulse is also scaled up or down. It does not mean the SHPB response is one dimensional, rather it implies that since the simple one-dimensional analysis

has been proven reliable for the existing systems, it should apply just as well to the proposed 6-inch SHPB.

The next part of this effort looked at three methodologies in order to compare and contrast the results. The goal was to have a firm understanding of the implications of increasing the size of an SHPB. The first two included a finite difference numerical technique, and experimental traces obtained at Tyndall AFB. The third method, called the Modified Pochhammer-Chree method for elastic systems, consisted of computationally following each Fourier component of the input pulse as it reflects and transmits at the bar-specimen interfaces. Each pulse has a unique velocity and wavelength, which enables one to calculate its position in time. The complete pulse can then be reconstructed at any time. Furthermore, the distribution of displacements and stresses along the radial direction can also be calculated if the wavespeeds of the Fourier components are known. It was shown how this methodology gives surprisingly good results, considering the many orders of magnitude difference in computing time compared to the finite difference technique.

All three methodologies reaffirmed the initial statement of scale invariance of any SHPB. It was shown how if the input pressure pulse has a wavelength of 500 microseconds, a 6-inch SHPB will behave as a one-dimensional wave propagation system, and thus all the current data reduction schemes and the current assumptions will be valid.

Finally, the effects of friction and inertia were analyzed. It turns out friction causes only a few percent error, even for a large 6-inch bar. Inertia however, will affect the results of an SHPB, and must be accounted for in the data analysis of a new 6-inch system. Inertia effects increase as strain-rate increases.

Conclusions and Recommendations

The following conclusions can be drawn from this analytical study.

1. A 6-inch SHPB is theoretically feasible, and in fact identical to any existing system if the input pressure pulse duration is scaled appropriately. Specifically, a 500 microsecond wavelength is recommended.

2. The modified Pochhammer-Chree method can be used to assess the validity and study the wave propagation in any size SHPB. The results give the incident, transmitted and reflected pulses for different diameters, wavelengths and materials. This method can be applied to any input pressure if it can be described by a Fourier series.

3. If the specimen length and diameter are kept in the same order of magnitude, one need not worry about friction in the proposed 6-inch SHPB. It will cause only a small error in the analysis.

4. The new proposed 6-inch SHPB will need a correction in the data analysis to account for inertia. This is true especially if the input pulse is a step function and if strain rates higher then 10-20 1/sec are desired. Davies and Hunter [7] derived an equation to correct for inertia which has been shown to be fairly accurate. It is recommended this equation be incorporated in the existing data reduction algorithm. A Fortran subroutine has been written by the author, is included in Appendix E, and can be directly integrated in the existing data reduction programs in use at the University of Florida and at Tyndall AFB.

By following the guidelines in steps 1 through 4, the test engineer has in effect removed or corrected for any rate, friction, or two-dimensional effects due to the testing apparatus itself, and thus the results will permit the

observation of the true material behavior. The intrinsic characteristics of the material will be separated from any other effects inherent to the way the specimen is being tested. Therefore, the Split Hopkinson Pressure Bar has been and remains a reliable, accurate and useful tool to study material response to loading, even for a new proposed system 6 inches in diameter.

REFERENCES

1. Kolsky, H., "An Investigation of the Mechanical Properties of Materials at Very High Rates of Loading," Proceedings of the Physics Society, Vol. 62, pp. 676-700, 1949.

2. Hauser, F.E., Simmons, J.A., and Dorn, J.E., "Response of Metals to High Velocity Deformation," Proceedings of the Metallurgical Society Conference, Vol. 9, pp. 93-101, 1960.

3. Lindholm, U.S., "Some Experiments with the Split Hopkinson Pressure Bar," Journal of the Mechanics and Physics of Solids, Vol. 12, pp. 317-335, 1964.

4. Malvern, L.E., and Ross C.A., "Dynamic Response of Concrete and Concrete Structures," Final Technical Report, AFOSR Contract F49620-83-K007, University of Florida, Gainesville, FL, May 1986.

5. Robertson, K.D., Chou, S. and Rainey, J.H., "Design and Operating Characteristics of a Split Hopkinson Pressure Bar Apparatus," Technical Report AMMRC TR 71-49, Army Materials and Mechanics Research Center, Watertown, MA, November 1971.

6. Kolsky, H., Stress Wave in Solids, Dover Publications, New York, 1963.

7. Davies, E.D.H., and Hunter, S.C., "The Dynamic Compression Testing of Solids by the Method of the Split Hopkinson Pressure Bar," Journal of the Mechanics and Physics of Solids, Vol. 11, pp. 155-179, 1963.

8. Rand, J.L., "An Analysis of the Split-Hopkinson Pressure Bar," U.S. Naval Ordnance Laboratory , White Oak, MD, NOLTR67-156, 1967.

9. Dharan, C.K.H. and Hauser, F.E., "Determination of Stress-Strain Characteristics at Very High Strain Rates," Experimental Mechanics, Vol. 10, pp. 370-382, 1970.

10. Samanta, S.K., "Dynamic Deformation of Aluminum and Copper at Elevated Temperatures," Journal of the Mechanics and Physics of Solids, Vol. 19, pp. 117-124, 1971.

11. Jahsman, W.E., "Re-examination of the Kolsky Technique for Measuring Dynamic Material Behavior," Journal of Applied Mechanics, Vol. 38, pp. 75-82, 1971.

12. Chiu, S.S. and Neubert, V.H., "Difference Method for Wave Analysis of the Split Hopkinson Pressure Bar with a Viscoelastic Specimen", Journal of the Mechanics and Physics of Solids, Vol. 15, pp. 177-193, 1967.

13. Young, C. and Powell, C.N., "Lateral Inertia Effects on Rock Failure in Split Hopkinson-Bar Experiments," 20th U.S. Symposium on Rock Mechanics, Austin, TX, pp. 299-303, 1979.

14. Nicholas, T., "An Analysis of the Split Hopkinson Bar Technique for Strain-Rate-Dependent Material Behavior", Journal of Applied Mechanics, Vol. 1, pp. 277-282, March 1973.

15. Lawson, J.E., "An Investigation of the Mechanical Behavior of Metals at High Strain Rates in Torsion," Ph.D. Dissertation, Air Force Institute of Technology, Wright-Patterson AFB, OH, June 1971.

16. Baker, W.E. and Yew, C.H., "Strain-Rate Effects in the Propagation of Torsional Plastic Waves", Journal of Applied Mechanics, Vol. 33, pp. 917-923, 1966.

17. Jones, R.P.N., "The Generation of Torsional Stress Waves in a Circular Cylinder", Quarterly Journal of Mechanics and Applied Mathematics, Vol. 12, pp. 208-211, 1959.

18. Okawa, K., "Mechanical Behavior of Metals Under Tension-Compression Loading at High Strain Rate," International Journal of Plasticity, Vol. 1, pp. 347-358, 1985.

19. Ross, C.A., Nash, P.T., Friesenhahn, G.H., "Pressure Waves in Soils Using a Split-Hopkinson Pressure Bar," Final Technical Report, ESL-TR-81-29, AFESC, Tyndall AFB, FL, July 1986.

20. Rajendran, A.M., and Bless, S.J., "High Strain Rate Material Behavior," Technical Report, AFWAL-TR-85-4009, AFWAL, Kirtland AFB, NM, December 1985.

21. Ross, C.A., "Split Hopkinson Pressure Bar Tests," Final Technical Report, ESL-TR-88-82, AFESC, Tyndall AFB, FL, March 1989.

22. Follansbee, P.S. and Frantz, C., "Wave Propagation in the Split Hopkinson Pressure Bar", ASME Journal of Engineering Materials and Technology, Vol. 105, pp. 61-66, 1983.

23. Redwood, M., Mechanical Waveguides, Pergamon Press, New York, 1960.

24. Bertholf, L.D. and Karnes, C.H., "Two-dimensional Analysis of the Split Hopkinson Pressure Bar System," Journal of the Mechanics and Physics of Solids, Vol. 23,pp. 1-19, 1975.

25. Bancroft D., "The Velocity of Longitudinal Waves in Cylindrical Bars," Physical Review, Vol. 59, pp. 588-593, April 1941.

26. Mindlin, R.D. and Herrmann G., A One-Dimensional Theory of Compressional Waves in an Elastic Rod, Pro. 1st U.S. Nat. Cong. App. Mech., Chicago, pp. 187-191, 1951.

27. Davies, R.M., "A Critical Study of the Hopkinson Pressure Bar," Philosophical Transactions Royal Society, Vol. A240, pp. 375-457, 1948.

28. Kolsky, H., "The Propagation of Stress Pulses in Viscoelastic Solids," Phil. Mag. Vol. 1, pp. 693-710, 1956.

29. Love, A. E. H., 1927, The Mathematical Theory of Elasticity, Dover Publications, New York.

30. Karal, F.C., "Propagation of Elastic Waves in a Semi-infinite Cylindrical Rod Using Finite Difference Methods," Journal of Sound Vibration, Vol. 13, pp. 115-145, 1970.

31. Gong, J.C., Malvern, L.E., and Jenkins, D.A., "Dispersion Investigation in the Split Hopkinson Pressure Bar," Journal of Engineering Materials and Technol ogy, Vol. 112, pp. 309-314, July 1990.

32. Jerome, E.L., "Feasibility of a 6-inch Split Hopkinson Pressure Bar (SHPB)," Final Technical Report, ESL-TR-90-44, AFESC, Tyndall AFB, FL, August 1990.

33. Hopkinson, B., "A Method of Measuring the Pressure Produced in the Detonation of High Explosives or by the Impact of Bullets," Philosophical Transactions of the Royal Society of London, Vol. 213, pp. 437-456, 1914.

34. Osborne, J.J., and Matuska, D.A., "HULL, Finite Difference Code," Orlando Technology, Inc., Shalimar, Florida, 1987.

35. Rinehart, J.S., Stress Transients in Solids, HyperDynamics, Santa Fe, New Mexico, May, 1975.

36. Chree, C., "The Equations of an Isotropic Elastic Solid in Polar and Cylindrical Coordinates, Their Solutions and Applications," Cambridge Philosophical Society, Transactions, Vol. 14, 1889, pp.250-369.

37. Pochhammer, L., "On the Propagation Velocities of Small Oscillations in an Unlimited Isotropic Circular Cylinder," Journal fur die Reine und Angewandte Mathematik, Vol. 81, 1876, pp. 324-326.

APPENDIX A
MODIFIED POCHHAMMER-CHREE PROGRAM AND SAMPLE OUTPUTS

This program uses the Pochhammer-Chree frequency equation solution to the two-dimensional equations of motion in cylindrical coordinates to analyze the wave propagation of an arbitrary trapezoidal input pulse in a bar of varying dimensions and material properties. The wave is carried through a typical compressive SHPB. Multiple reflections and transmissions at the interfaces between the specimen and bars are calculated and the waves reconstructed in the incident and in the transmitter bar.

The program logic is organized as follows:

- The user is asked to enter the areas, densities, and wave speeds for the bars and the specimen. This information is used to calculate the characteristic impedances of the materials.

- The user is asked to enter the pulse duration, number of time steps (each 0.5e-6 seconds long), the diameter of the bar, and the dimensions of the specimen.

- The input pulse is represented via a Fourier series. 55 terms are retained. Amplitude of the incident pulse is normalized to 1.0. Each component has a unique phase angle, frequency, and amplitude and they are all in phase at the onset.

- The Pochhammer-Chree solution for mode $M_{1,1}$ is used to calculate the wave speed of each Fourier component in the bar material as well as in the specimen material.

- Each pulse is then started at a distance of 2 meters from the specimen and is followed to the incident bar-specimen interface through the multiple reflections and transmissions that occur at that point and is followed into the specimen to the specimen-transmitter bar interface where more reflections and transmissions take place. Since the speed of each

component of the pulse is known, and since the characteristic impedances are known, the program calculates the amount that gets reflected and transmitted each time, as well as how long it takes for each component to travel any distance. All 55 terms are treated in this way, and then the waveform is reconstructed both in the incident and in the transmitter bar at the strain gage locations both 1 meter from the specimen.

- The output is in numerical form. The incident, transmitted, and reflected waves are represented by values one-half microsecond apart. These data can be easily plotted with any available software. LOTUS 123 was used by the author.

- Additionally, the program calculates the cross sectional variations of the stresses derived from the Pochhammer-Chree frequency solution. Bessel functions are evaluated numerically. For each radial value the 55 terms making up the traveling wave are added for each time increment. The portion of each stress dependent on r, discussed in chapter 3, are essentially multiplied to each Fourier component at each time step. All the terms, at their particular frequency are added up in time to form the complete waveform at each radial location. Longitudinal, radial, and shear stresses are calculated, and their amplitudes are all normalized to the longitudinal stress at the center.

- Figures 36 and 37 are examples of cross sectional variations of the longitudinal stress for a 2-inch and a 6-inch SHPB. Reflected and transmitted pulses are shown.

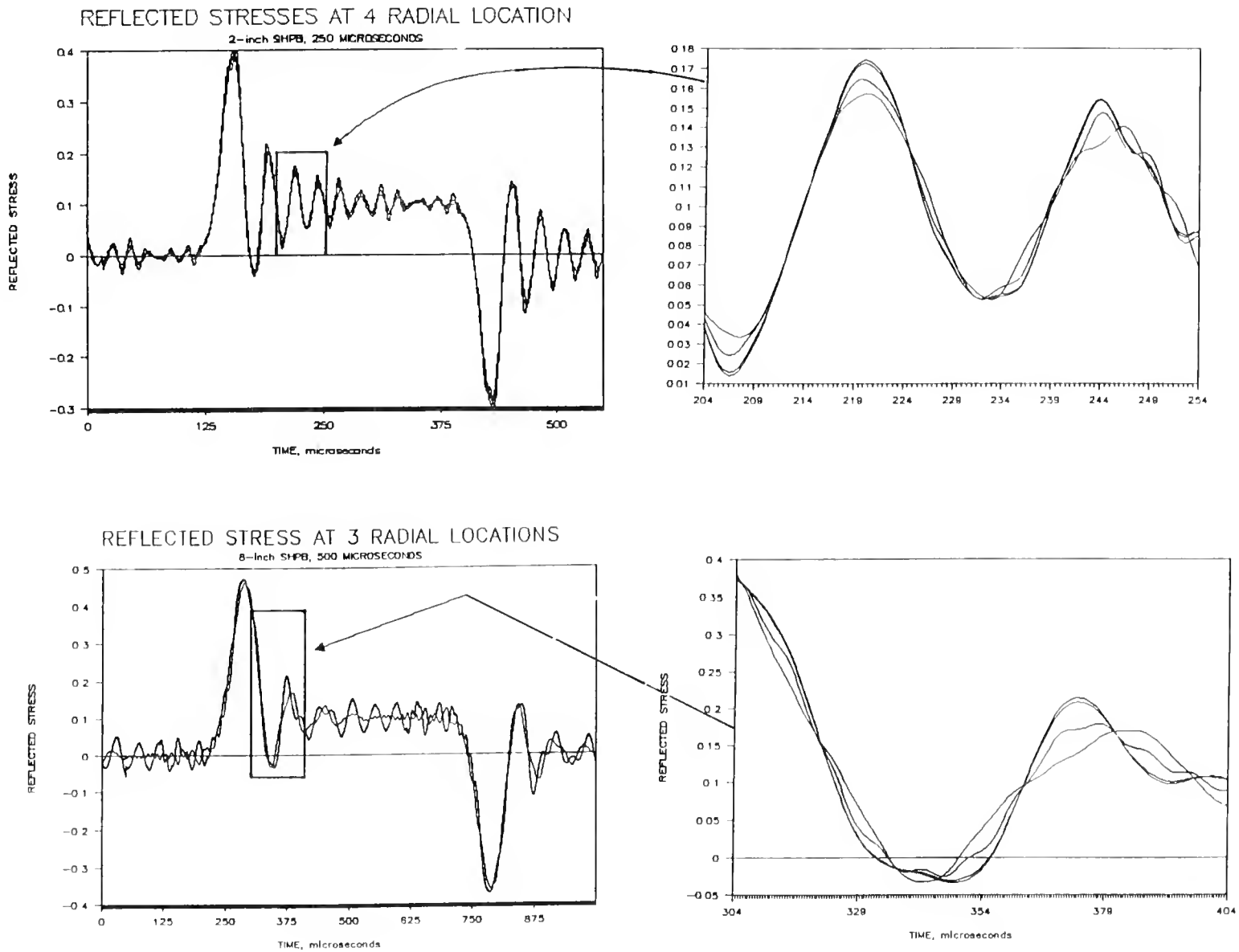

Figure 36. Modified Pochhammer-Chree Results. Radial Variations of Reflected Stresses. 2-inch SHPB (Top), 6-inch SHPB (Bottom)

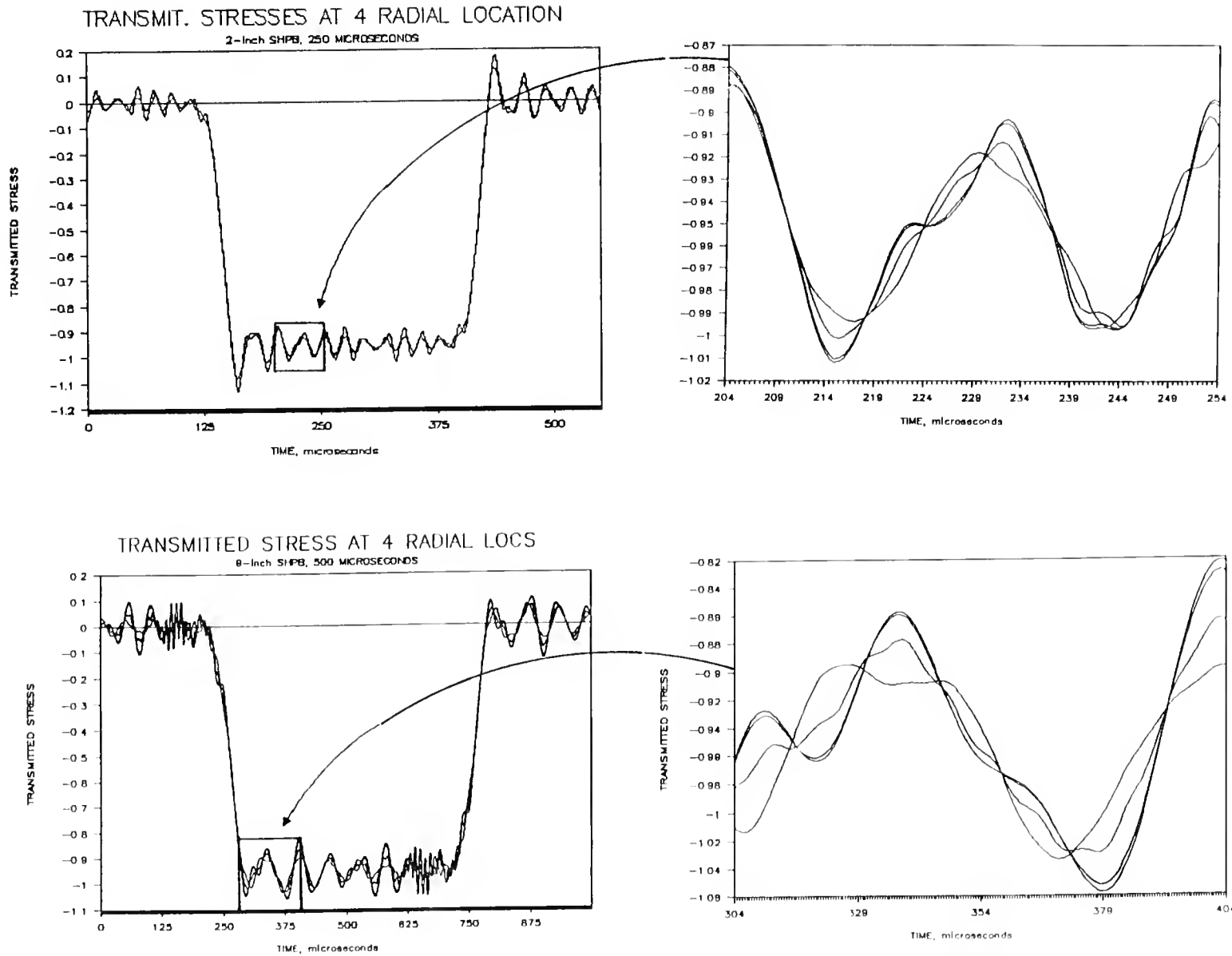

Figure 37. Modified Pochhammer-Chree Results. Radial Variations of Transmitted Stresses. 2-inch SHPB (Top), 6-inch SHPB (Bottom)

```
C       THIS PROGRAM USES POCHHAMMER AND CHREE
C       FREQUENCY SOLUTION OF THE TWO DIMENSIONAL
C       EQUATIONS OF MOTION IN CYLINDRICAL COORDINATES
C       TO ANALYZE THE WAVE PROPAGATION OF AN ARBITRARY
C       TRAPEZOIDAL INPUT PULSE IN A BAR OF VARYING
C       DIMENSIONS AND MATERIAL PROPERTIES.
C
C       FURTHERMORE, IT CALCULATES THE RESPONSE DUE
C       TO THE MULTIPLE REFLECTIONS AND TRANSMISSIONS
C       AS THE WAVE ENCOUNTERS A SPECIMEN OF DIFFERENT
C       MATERIAL, SAME DIAMETER, AND SPECIFIED LENGTH.
C
C       THE OUTPUT CONSISTS OF THE INCIDENT, REFLECTED
C       AND TRANSMITTED PULSES AT STATIONS ONE METER
C       FROM THE SPECIMEN BOTH ON THE INCIDENT AND ON THE
C       TRANSMITTER BAR.  SOLUTIONS ARE GIVEN AT THE CENTER
C       OF THE BAR (FILE FOR001.DAT), AND AT THE SURFACE
C       (FILE FOR010.DAT) TO CHECK FOR RADIAL UNIFORMITY
C       OF THE MOTION.  ALL AMPLITUDES ARE NORMALIZED.
C
      dimension d(3000,40),f(3000),ph1(200),ph2(200)
      dimension time(3000,40),u(3000),fr(3000),c(200),dl(200)
      dimension frr(3000),ut(3000),frrr(3000),utt(3000)
      dimension sig(100,200)
      s=0.014
      pi=3.14159
C     WAVE SPEEDS, AREAS, AND DENSITIES ARE ENTERED TO
C     CALCULATE CHARACTERISTIC IMPEDANCES

      write(*,*)' input speeds, densities, and areas'
      write(*,*)' co1,co2,(m/sec),ro1,ro2,A1,A2'
      write(*,*)' bar is 1, specimen is 2'
      Read(*,*)co1,co2,ro1,ro2,a1,a2

      a=2.0/(pi**2*s)

      tr=2*a1*ro2*co2/(ro2*co2*a2+ro1*co1*a1)
      ref=(a2*ro2*co2-a1*ro1*co1)/(ro2*co2*a2+ro1*co1*a1)
      tr2=2*a2*ro1*co1/(ro2*co2*a2+ro1*co1*a1)
      ref2=-ref

      write(*,*)tr,ref,tr2,ref2
      n=-1
      write(*,*)' input nn,wo (1/sec),diameter (mm),spec. length(m)'
      read(*,*)nn,wo,diam,z12
      dia=diam/1000.0
C     STRAIN GAGE LOCATION IS ASSUMED AT ONE METER
C     FROM IMPACTED END, AND ONE METER FROM EITHER
C     SIDES OF THE SPECIMEN
      z1=1.0
      z13=1.0
      z24=1.0

C     55 TERMS ARE USED IN THE FOURIER ANALYSIS

      mm=55
      do 5 j=1,mm
      n=n+2
      ne=(n-1)/2
```

```
C       CALCULATE THE AMPLITUDES OF EACH PULSE
C       AS THEY CROSS THE INTERFACES BACK AND FORTH
C
C       AT STATION ON THE INCIDENT BAR:

        d(j,1)=(-a*(-1)**ne/n**2)*sin(n*pi*s)
        d(j,2)=ref*d(j,1)
c       THIS NEXT PIECE IS THE FIRST REFLECTION BACK
C       WHICH WILL ADD TO THE REFLECTED STRESS
        d(j,3)=tr*ref2*tr2*d(j,1)
        d(j,6)=d(j,3)*ref2**2

C       AT STATION ON THE TRANSMITTER BAR:

        d(j,4)=tr*tr2*d(j,1)
c       PLUS WHAT BOUNCES BACK AND FORTH IN THE SPECIMEN
C       AND ADDS TO THE TRANSMITTED STRESS
        d(j,5)=tr*ref2*ref2*tr2*d(j,1)
        d(j,7)=d(j,5)*ref2**2


   5    continue

C       SUBROUTINE ANGLE CALCULATES PHASE CHANGES, VELOCITIES
C       AND WAVELENGTHS FOR EACH TERM IN THE FOURIER SERIES

        call angle(dia,co1,co2,wo,mm,ph1,ph2,c,dl)

C       SUBROUTINE CROSS CALCULATES THE CROSS SECTIONAL VARIATION
C       OF THE DISPLACEMENTS AND STRESSES.  ONLY LONGITUDINAL STRESSES
C       ARE BROUGHT BACK INTO THE MAIN PROGRAM
C       SIGMA RR AND SIGMA ZZ ARE OUTPUTED TO FILE FOR002.DAT

        call cross(dia,c,dl,mm,sig)

c
c       CALCULATE THE TIMES EACH PULSE TAKES TO
C       REACH THE STRAIN GAGES

        n=-1
        do 10 j=1,mm
        n=n+2
        time(n,1)=z1*((-1.0/co1)+ph1(n))
        time(n,2)=time(n,1)+2.0*z13*((-1.0/co1)+ph1(n))
        time(n,3)=time(n,2)+z12*((-1.0/co2)+ph2(n))*2.0
        time(n,4)=time(n,1)+z24*2.0*((-1.0/co1)+ph1(n))
     1            +z12*((-1.0/co2)+ph2(n))
        time(n,5)=time(n,4)+2*z12*((-1.0/co2)+ph2(n))
        time(n,6)=2*z12*ph2(n)/(0.5*1.e-6)

   10   continue
```

```
C       k REPRESENTS THE RADIAL VARIATION OF THE STRESSES
C       k=1 IS AT THE CENTER OF THE BAR
C       k=10 IS AT THE SURFACE OF THE BAR

        do 80 k=1,10,9

C       nn IS THE NUMBER OF POINTS MAKING UP THE PULSE

        do 20 i=1,nn

c       this is time -- delta t is half a microsecond

        t=i*0.5*1.e-6

        f(i)=0.5
        fr(i)=0.5*ref
        u(i)=0.5*tr*tr2
        frr(i)=0.5*tr*ref2*tr2
        ut(i)=0.5*tr*ref2*ref2*tr2
        frrr(i)=frr(i)*ref2**2
        utt(i)=ut(i)*ref2**2
        n=-1
        do 20 j=1,mm
        n=n+2


        phi=t-time(n,1)
        f(i)=f(i)+sig(j,k)*d(j,1)*cos(n*wo*phi)
        phir=t-time(n,2)
        phir2=t-time(n,3)

        fr(i)=fr(i)+sig(j,k)*d(j,2)*cos(n*wo*phir)
        frr(i)=frr(i)+sig(j,k)*d(j,3)*cos(n*wo*phir2)
        frrr(i)=frrr(i)+sig(j,k)*d(j,6)*cos(n*wo*phir2)

        phit=t-time(n,4)
        phit2=t-time(n,5)

        u(i)=u(i)+sig(j,k)*d(j,4)*cos(n*wo*phit)
        ut(i+iii)=ut(i+iii)+sig(j,k)*d(j,5)*cos(n*wo*phit2)
        utt(i+jjj)=utt(i+jjj)+sig(j,k)*d(j,7)*cos(n*wo*phit2)
   20   continue
```

```
      i=0
      ii=0
      jj=time(1,6)
      jjj=jj*2
      do 45 j=jj,nn
      i=i+1
      if(j.ge.jjj)ii=ii+1
      if(j.lt.jjj)x=0.0
      fr(j)=fr(j)+frr(i)+x*frrr(ii)
      u(j)=u(j)+ut(i)+x*utt(ii)
   45 continue

C     OUTPUT THE THREE PULSES TO FILES 1 AND 10

      do 40 j=1,nn

      write(k,100)f(j),fr(j),u(j)
   40 continue
   80 continue
  100 format(3f10.6)

      stop
      end
```

```
      subroutine angle (d,co1,co2,wo,mm,ph1,ph2,c1,dl)
      dimension c(200),ph1(200),ph2(200),c1(200),dl(200),dll(200)
      cp(v)=.5764+(.4236/(2.148*v**4+.736*v*v*v-.276*v*v+
     *      .3065*v**1.5+1.0))

      do 10 ncount=1,2
      co=co1
      if(ncount.eq.2)co=co2

      pi=3.14159
c     z=0.61
      m=mm*2+2

      w=d*wo/co
      v=0.0
      i=0
   70 i=i+1
      x=i*w
   80 v=v+0.0001
      xp=2.0*pi*cp(v)*v
   83 if(xp-x)80,85,85
   85 c(i)=cp(v)
      dll(i)=v
   88 if(i-m)70,90,90
   90 do 100 i=1,m
      if(ncount.eq.2)go to 20
      dl(i)=dll(i)
      c1(i)=c(i)
      ph1(i)=1/(c(i)*co)
   20 ph2(i)=1/(c(i)*co)
  100 continue

   10 continue
      return
      end
```

```
      subroutine cross(dia,c,dl,mm,signo)
      dimension c(200),dl(200),sig(100,200),signo(100,200)
      dimension sigr(100,200),signr(100,200),sigrz(100,200)
      dimension sinrz(100,200)
      real*8 j0r,j1r,j1a,j0kr,j1kr,j1ka,ha,ak
      pi=3.14159

      r=0.0
      do 30 ii=1,10
      r=r+dia/20.
      beta=0.59
      a=dia/2.
      amu=8.1
      n=-1
      do 60 j=1,mm
      n=n+2
      x=c(n)**2*1.29
      gam=2.*pi*dl(n)/dia
      if (gam.le.0.0)go to 60
      ha=pi*dl(n)*sqrt(abs(beta*x-1.0))

      ak=pi*dl(n)*sqrt(abs(2.*x-1.0))

      hh=beta*x-1.0
      akk=2.*x-1.0
      if (hh.lt.0.0)go to 15
      j1r=bessj1(ha*r/a)
      j0r=bessjo(ha*r/a)
      j1a=bessj1(ha)
      ratio1=j0r/j1a
      go to 12
15    j1r=bessi1(ha*r/a)
      j0r=bessio(ha*r/a)
      j1a=bessi1(ha)
      ratio1=j0r/j1a
12    if (akk.lt.0.0)go to 25
      j1kr=bessj1(ak*r/a)
      j0kr=bessjo(ak*r/a)
      j1ka=bessj1(ak)
      ratio2=j0kr/j1ka

      go to 35
25    j1kr=bessi1(ak*r/a)
      j0kr=bessio(ak*r/a)
      j1ka=bessi1(ak)
      ratio2=j0kr/j1ka

35    sig(j,ii)=(-2.0*amu*gam**2*j1a/(ha))*
     +     ((1.0+x-beta*x)*(ha)*ratio1+(1.0-beta*x)*
     +     (ak)*ratio2/(x-1.0))

      signo(j,ii)=sig(j,ii)/sig(j,1)
```

```
      sigr(j,ii)=(2.0*amu*gam**2*j1a/(ha))*
     +     ((1.0-x)*(ha)*ratio1+(1.0-beta*x)*
     +     (ak)*ratio2/(x-1.0)+(beta*x-1.0)*(a/r)*j1r/j1a
     +     -(beta*x-1.0)*(a/r)*(j1kr/j1ka)/(1.0-x))

      signr(j,ii)=sigr(j,ii)/sig(j,1)

      sigrz(j,ii)=-2.0*amu*gam*(ha/a)*j1a*((j1r/j1a)-(j1kr/j1ka))
      sinrz(j,ii)=sigrz(j,ii)/sig(j,1)

   60 continue
   30 continue
      do 90 i=1,mm
       write(2,100)(signo(i,ii),ii=1,10)
   90  continue
      do 190 i=1,mm
       write(3,100)(sinrz(i,ii),ii=1,10)
       write(2,100)(signr(i,ii),ii=1,10)
  190  continue
c
c
  100  format(10e8.2)
      return
      end
```

```
C       THIS CALCULATES THE BESSEL FUNCTION OF ORDER 0
C
        function bessjo(x)
        real*8 y,p1,p2,p3,p4,p5,q1,q2,q3,q4,q5,r1,r2,r3,r4,r5,r6,
     *         s1,s2,s3,s4,s5,s6
        data p1,p2,p3,p4,p5/1.d0,-.1098628627d-2,.2734510407d-4,
     *    -.2073370639d-5,.2093887211d-6/,q1,q2,q3,q4,q5/-.1562499995d-1,
     *    .1430488765d-3,-.6911147651d-5,.7621095161d-6,-.934945152d-7/
        data r1,r2,r3,r4,r5,r6/57568490574.d0,-13362590354.d0,65161964
     *       0.7d0,-11214424.18d0,77392.33017d0,-184.9052456d0/,
     *       s1,s2,s3,s4,s5,s6/57568490411.d0,1029532985.d0,
     *       9494680.718d0,59272.64853d0,267.8532712d0,1.d0/
c
        if(abs(x).lt.8.)then
            y=x**2
            bessjo=(r1+y*(r2+y*(r3+y*(r4+y*(r5+y*r6)))))
     *           /(s1+y*(s2+y*(s3+y*(s4+y*(s5+y*s6)))))
        else
           ax=abs(x)
           z=8./ax
           y=z**2
           xx=ax-.785398164
           bessjo=sqrt(.636619772/ax)*(cos(xx)*(p1+y*(p2+y*(p3+y*(p4+y
     *          *p5))))-z*sin(xx)*(q1+y*(q2+y*(q3+y*(q4+y*q5)))))
        endif
        return
        end
c
C
C       THIS CALCULATES THE BESSEL FUNCTION OF ORDER 1
C
        function bessj1(x)
        real*8 y,p1,p2,p3,p4,p5,q1,q2,q3,q4,q5,r1,r2,r3,r4,r5,r6,
     *       s1,s2,s3,s4,s5,s6
        data r1,r2,r3,r4,r5,r6/72362614232.d0,-7895059235.d0,242396853.
     *       1d0,-2972611.439d0,15704.48260d0,-30.16036606d0/,
     *       s1,s2,s3,s4,s5,s6/144725228442.d0,2300535178.d0,
     *       18583304.74d0,99447.43394d0,376.9991397d0,1.d0/
        data p1,p2,p3,p4,p5/1.d0,.183105d-2,-.3516396496d-4,.2457520174d-
     *  5,-.240337019d-6/,q1,q2,q3,q4,q5/.04687499995d0,-.2002690873d-3,
     *       .8449199096d-5,-.88228987d-6,.105787412d-6/
        if(abs(x).lt.8.)then
            y=x**2
            bessj1=x*(r1+y*(r2+y*(r3+y*(r4+y*(r5+y*r6)))))
     *           /(s1+y*(s2+y*(s3+Y*(s4+y*(s5+y*s6)))))
        else
            ax=abs(x)
            z=8./ax
            y=z**2
            xx=ax-2.356194491
            bessj1=sqrt(.636619772/ax)*(cos(xx)*(p1+y*(p2+y*(p3+y*(p4+y
     *           *p5))))-z*sin(xx)*(q1+y*(q2+Y*(q3+y*(q4+y*q5)))))
     *           *sign(1.,x)
            endif
        return
        end
c
```

```
C
C       THIS CALCULATES THE MODIFIED BESSEL FUNCTION OF ORDER 0
C
        function bessio(x)
        real*8 y,p1,p2,p3,p4,p5,p6,p7,
     *       q1,q2,q3,q4,q5,q6,q7,q8,q9
        data p1,p2,p3,p4,p5,p6,p7/1.0d0,3.5156229d0,3.0899424d0,1.206749
     *       2d0,0.2659732d0,0.360768d-1,0.45813d-2/
        data q1,q2,q3,q4,q5,q6,q7,q8,q9/0.39894228d0,0.1328592d-1,
     *       0.225319d-2,-0.157565d-2,0.916281d-2,-0.2057706d-1,
     *       0.2635537d-1,-0.1647633d-1,0.392377d-2/
        if(abs(x).lt.3.75)then
           y=(x/3.75)**2
           bessio=p1+y*(p2+y*(p3+y*(p4+Y*(p5+y*(p6+y*p7)))))
        else
           ax=abs(x)
           y=3.75/ax
           bessio=(exp(ax)/sqrt(ax))*(q1+y*(q2+y*(q3+y*(q4
     *          +y*(q5+y*(q6+y*(q7+y*(q8+y*q9))))))))
        endif
        return
        end
c
C
C       THIS CALCULATES THE MODIFIED BESSEL FUNCTION OF ORDER 1
C
        function bessi1(x)
        real*8 y,p1,p2,p3,p4,p5,p6,p7,
     *         q1,q2,q3,q4,q5,q6,q7,q8,q9
        data p1,p2,p3,p4,p5,p6,p7/0.5d0,0.87890594d0,0.51498869d0,
     *       0.15084934d0,0.2658733d-1,0.301532d-2,0.32411d-3/
        data q1,q2,q3,q4,q5,q6,q7,q8,q9/0.39894228d0,-0.3988024d-1,
     *       -0.362018d-2,0.163801d-2,-0.1031555d-1,0.2282967d-1,
     *       -0.2895312d-1,0.1787654d-1,-0.420059d-2/
        if(abs(x).lt.3.75)then
           y=(x/3.75)**2
           bessi1=x*(p1+Y*(p2+Y*(p3+Y*(p4+Y*(p5+y*(p6+Y*p7))))))
        else
           ax=abs(x)
           y=3.75/ax
           bessi1=(exp(ax)/sqrt(ax))*(q1+Y*(q2+Y*(q3+Y*(q4+
     *          y*(q5+Y*(q6+Y*(q7+Y*(q8+y*q9))))))))
           endif
           return
           end
```

SAMPLE OUTPUT FROM MODIFIED POCHHAMMER-CHREE PROGRAM
2 INCH SHPB, 250 MICROSECONDS PULSE

ILES FOR002.DAT AND FOR003.DAT

STRESS VALUES ALONG THE CROSS SECTION

LONGITUDINAL STRESS:

R=0 (CENTER).....R=A (SURFACE)

55 FOURIER TERMS

.10E+010.10E+010.10E+010.10E+010.10E+010.10E+010.10E+010.10E+010.10E+010.10E+01
.10E+010.10E+010.10E+010.10E+010.10E+010.10E+010.10E+010.10E+010.10E+010.10E+01
.10E+010.10E+010.10E+010.10E+010.10E+010.10E+010.10E+010.10E+010.99E+000.99E+00
.10E+010.10E+010.10E+010.10E+010.10E+010.10E+010.99E+000.99E+000.99E+000.99E+00
.10E+010.10E+010.10E+010.10E+010.99E+000.99E+000.99E+000.99E+000.98E+000.98E+00
.10E+010.10E+010.10E+010.99E+000.99E+000.99E+000.98E+000.98E+000.97E+000.97E+00
.10E+010.10E+010.10E+010.99E+000.99E+000.98E+000.98E+000.97E+000.96E+000.95E+00
.10E+010.10E+010.99E+000.99E+000.98E+000.97E+000.97E+000.96E+000.94E+000.93E+00
.10E+010.10E+010.99E+000.98E+000.98E+000.96E+000.95E+000.94E+000.92E+000.91E+00
.10E+010.10E+010.99E+000.98E+000.97E+000.95E+000.94E+000.92E+000.90E+000.87E+00
.10E+010.99E+000.98E+000.97E+000.96E+000.94E+000.91E+000.89E+000.86E+000.83E+00
.10E+010.99E+000.98E+000.96E+000.94E+000.91E+000.88E+000.85E+000.82E+000.78E+00
.10E+010.99E+000.97E+000.95E+000.92E+000.89E+000.85E+000.80E+000.76E+000.71E+00
.10E+010.99E+000.96E+000.93E+000.90E+000.85E+000.80E+000.74E+000.69E+000.62E+00
.10E+010.98E+000.95E+000.91E+000.86E+000.81E+000.74E+000.67E+000.59E+000.51E+00
.10E+010.98E+000.94E+000.89E+000.83E+000.75E+000.67E+000.58E+000.48E+000.38E+00
.10E+010.97E+000.92E+000.86E+000.78E+000.69E+000.58E+000.47E+000.35E+000.22E+00
.10E+010.97E+000.91E+000.83E+000.74E+000.62E+000.50E+000.35E+000.20E+000.46E-01
.10E+010.96E+000.90E+000.81E+000.70E+000.57E+000.41E+000.25E+000.62E-01-.13E+00
.10E+010.96E+000.89E+000.79E+000.67E+000.52E+000.35E+000.16E+00-.63E-01-.30E+00
.10E+010.96E+000.89E+000.79E+000.66E+000.50E+000.31E+000.90E-01-.16E+00-.46E+00
.10E+010.96E+000.89E+000.79E+000.66E+000.49E+000.29E+000.48E-01-.24E+00-.59E+00
.10E+010.96E+000.89E+000.79E+000.66E+000.50E+000.28E+000.22E-01-.30E+00-.70E+00
.10E+010.96E+000.90E+000.80E+000.67E+000.51E+000.29E+000.69E-02-.35E+00-.80E+00
.10E+010.97E+000.90E+000.81E+000.69E+000.52E+000.30E+00-.39E-03-.39E+00-.90E+00
.10E+010.97E+000.91E+000.83E+000.71E+000.54E+000.31E+00-.23E-02-.42E+00-.10E+01

.10E+010.97E+000.92E+000.84E+000.72E+000.56E+000.33E+00-.25E-03-.46E+00-.11E+01

.10E+010.97E+000.93E+000.85E+000.74E+000.58E+000.35E+000.50E-02-.48E+00-.12E+01

.10E+010.98E+000.94E+000.87E+000.76E+000.61E+000.37E+000.13E-01-.51E+00-.13E+01

.10E+010.98E+000.95E+000.88E+000.79E+000.63E+000.39E+000.23E-01-.53E+00-.14E+01

.10E+010.98E+000.95E+000.90E+000.81E+000.66E+000.42E+000.36E-01-.56E+00-.15E+01

.10E+010.99E+000.96E+000.91E+000.83E+000.69E+000.44E+000.50E-01-.58E+00-.16E+01

.10E+010.99E+000.97E+000.93E+000.85E+000.71E+000.47E+000.66E-01-.60E+00-.17E+01

.10E+010.99E+000.98E+000.95E+000.88E+000.74E+000.50E+000.85E-01-.62E+00-.18E+01

.10E+010.10E+010.99E+000.96E+000.90E+000.78E+000.54E+000.11E+00-.65E+00-.19E+01

.10E+010.10E+010.10E+010.98E+000.93E+000.81E+000.57E+000.13E+00-.67E+00-.20E+01

.10E+010.10E+010.10E+010.10E+010.95E+000.84E+000.61E+000.15E+00-.69E+00-.22E+01

.10E+010.10E+010.10E+010.10E+010.98E+000.88E+000.65E+000.18E+00-.71E+00-.23E+01

.10E+010.10E+010.10E+010.10E+010.10E+010.92E+000.69E+000.21E+00-.73E+00-.25E+01

.10E+010.10E+010.10E+010.11E+010.10E+010.95E+000.73E+000.24E+00-.75E+00-.26E+01

.10E+010.10E+010.10E+010.11E+010.11E+010.99E+000.78E+000.27E+00-.76E+00-.28E+01

.10E+010.10E+010.11E+010.11E+010.11E+010.10E+010.82E+000.31E+00-.78E+00-.29E+01

.10E+010.10E+010.11E+010.11E+010.11E+010.11E+010.87E+000.35E+00-.80E+00-.31E+01

.10E+010.10E+010.11E+010.11E+010.12E+010.11E+010.93E+000.39E+00-.82E+00-.33E+01

.10E+010.10E+010.11E+010.12E+010.12E+010.12E+010.98E+000.43E+00-.84E+00-.35E+01

.10E+010.10E+010.11E+010.12E+010.12E+010.12E+010.10E+010.48E+00-.85E+00-.37E+01

.10E+010.10E+010.11E+010.12E+010.13E+010.13E+010.11E+010.53E+00-.87E+00-.40E+01

.10E+010.10E+010.11E+010.12E+010.13E+010.13E+010.12E+010.59E+00-.88E+00-.42E+01

.10E+010.11E+010.11E+010.12E+010.13E+010.14E+010.12E+010.65E+00-.90E+00-.45E+01

.10E+010.11E+010.11E+010.13E+010.14E+010.14E+010.13E+010.71E+00-.91E+00-.47E+01

.10E+010.11E+010.12E+010.13E+010.14E+010.15E+010.14E+010.77E+00-.92E+00-.50E+01

.10E+010.11E+010.12E+010.13E+010.14E+010.15E+010.14E+010.84E+00-.93E+00-.53E+01

.10E+010.11E+010.12E+010.13E+010.15E+010.16E+010.15E+010.92E+00-.94E+00-.57E+01

.10E+010.11E+010.12E+010.14E+010.15E+010.17E+010.16E+010.10E+01-.95E+00-.60E+01

.10E+010.11E+010.12E+010.14E+010.16E+010.17E+010.17E+010.11E+01-.96E+00-.64E+01

RADIAL STRESS:

-.19E-02-.19E-02-.19E-02-.19E-02-.19E-02-.18E-02-.18E-02-.18E-02-.17E-02-.17E-02
-.58E-02-.57E-02-.56E-02-.54E-02-.52E-02-.49E-02-.46E-02-.42E-02-.37E-02-.33E-02
-.12E-01-.11E-01-.11E-01-.11E-01-.99E-02-.91E-02-.82E-02-.71E-02-.59E-02-.45E-02
-.19E-01-.19E-01-.18E-01-.17E-01-.16E-01-.14E-01-.13E-01-.10E-01-.80E-02-.53E-02
-.30E-01-.29E-01-.28E-01-.26E-01-.24E-01-.21E-01-.18E-01-.14E-01-.10E-01-.58E-02

-.42E-01-.41E-01-.39E-01-.37E-01-.33E-01-.29E-01-.25E-01-.19E-01-.13E-01-.62E-02
-.59E-01-.57E-01-.54E-01-.51E-01-.46E-01-.40E-01-.33E-01-.25E-01-.16E-01-.67E-02
-.79E-01-.77E-01-.73E-01-.68E-01-.61E-01-.53E-01-.43E-01-.33E-01-.21E-01-.77E-02
-.10E+00-.10E+00-.96E-01-.89E-01-.80E-01-.69E-01-.57E-01-.42E-01-.26E-01-.92E-02
-.14E+00-.13E+00-.12E+00-.12E+00-.10E+00-.89E-01-.73E-01-.54E-01-.34E-01-.12E-01
-.17E+00-.17E+00-.16E+00-.15E+00-.13E+00-.11E+00-.92E-01-.69E-01-.42E-01-.15E-01
-.22E+00-.21E+00-.20E+00-.19E+00-.17E+00-.14E+00-.12E+00-.86E-01-.53E-01-.18E-01
-.28E+00-.27E+00-.25E+00-.23E+00-.21E+00-.18E+00-.14E+00-.11E+00-.65E-01-.22E-01
-.34E+00-.33E+00-.31E+00-.28E+00-.25E+00-.22E+00-.17E+00-.13E+00-.77E-01-.26E-01
-.41E+00-.40E+00-.37E+00-.34E+00-.30E+00-.26E+00-.21E+00-.15E+00-.89E-01-.28E-01
-.49E+00-.47E+00-.44E+00-.40E+00-.36E+00-.30E+00-.24E+00-.17E+00-.10E+00-.28E-01
-.56E+00-.54E+00-.51E+00-.46E+00-.41E+00-.34E+00-.27E+00-.19E+00-.11E+00-.25E-01
-.62E+00-.60E+00-.56E+00-.51E+00-.45E+00-.37E+00-.29E+00-.20E+00-.11E+00-.20E-01
-.67E+00-.64E+00-.60E+00-.55E+00-.48E+00-.40E+00-.31E+00-.22E+00-.12E+00-.16E-01
-.69E+00-.66E+00-.62E+00-.57E+00-.50E+00-.42E+00-.33E+00-.23E+00-.12E+00-.13E-01
-.69E+00-.67E+00-.63E+00-.58E+00-.51E+00-.43E+00-.34E+00-.24E+00-.13E+00-.14E-01
-.68E+00-.66E+00-.63E+00-.58E+00-.52E+00-.45E+00-.36E+00-.26E+00-.15E+00-.16E-01
-.67E+00-.65E+00-.62E+00-.58E+00-.53E+00-.46E+00-.38E+00-.28E+00-.16E+00-.18E-01
-.66E+00-.64E+00-.62E+00-.58E+00-.53E+00-.47E+00-.39E+00-.29E+00-.17E+00-.20E-01
-.64E+00-.63E+00-.61E+00-.58E+00-.54E+00-.48E+00-.41E+00-.31E+00-.19E+00-.21E-01
-.63E+00-.62E+00-.60E+00-.58E+00-.54E+00-.49E+00-.42E+00-.33E+00-.20E+00-.21E-01
-.62E+00-.61E+00-.60E+00-.58E+00-.55E+00-.51E+00-.44E+00-.35E+00-.21E+00-.20E-01
-.61E+00-.60E+00-.60E+00-.58E+00-.56E+00-.52E+00-.46E+00-.37E+00-.23E+00-.19E-01
-.60E+00-.60E+00-.59E+00-.58E+00-.57E+00-.54E+00-.48E+00-.39E+00-.24E+00-.18E-01
-.59E+00-.59E+00-.59E+00-.59E+00-.58E+00-.55E+00-.50E+00-.41E+00-.26E+00-.16E-01
-.58E+00-.59E+00-.59E+00-.59E+00-.59E+00-.57E+00-.52E+00-.44E+00-.28E+00-.13E-01
-.58E+00-.58E+00-.59E+00-.60E+00-.60E+00-.59E+00-.55E+00-.46E+00-.30E+00-.11E-01
-.57E+00-.58E+00-.59E+00-.60E+00-.61E+00-.60E+00-.57E+00-.49E+00-.32E+00-.82E-02
-.56E+00-.57E+00-.59E+00-.61E+00-.62E+00-.62E+00-.60E+00-.52E+00-.34E+00-.53E-02
-.56E+00-.57E+00-.59E+00-.61E+00-.64E+00-.64E+00-.62E+00-.55E+00-.37E+00-.22E-02
-.55E+00-.57E+00-.59E+00-.62E+00-.65E+00-.67E+00-.65E+00-.58E+00-.39E+000.11E-02
-.55E+00-.57E+00-.60E+00-.63E+00-.67E+00-.69E+00-.68E+00-.61E+00-.42E+000.45E-02
-.55E+00-.57E+00-.60E+00-.64E+00-.68E+00-.71E+00-.72E+00-.65E+00-.45E+000.80E-02
-.54E+00-.57E+00-.60E+00-.65E+00-.70E+00-.74E+00-.75E+00-.69E+00-.48E+000.12E-01
-.54E+00-.57E+00-.61E+00-.66E+00-.72E+00-.77E+00-.79E+00-.73E+00-.51E+000.15E-01
-.54E+00-.56E+00-.61E+00-.67E+00-.73E+00-.80E+00-.83E+00-.77E+00-.55E+000.19E-01
-.53E+00-.56E+00-.61E+00-.68E+00-.75E+00-.82E+00-.87E+00-.82E+00-.59E+000.23E-01
-.53E+00-.56E+00-.62E+00-.69E+00-.77E+00-.86E+00-.91E+00-.87E+00-.63E+000.28E-01
-.53E+00-.57E+00-.62E+00-.70E+00-.79E+00-.89E+00-.95E+00-.92E+00-.68E+000.32E-01
-.53E+00-.57E+00-.63E+00-.71E+00-.82E+00-.92E+00-.10E+01-.98E+00-.72E+000.36E-01
-.53E+00-.57E+00-.63E+00-.73E+00-.84E+00-.96E+00-.10E+01-.10E+01-.78E+000.41E-01
-.53E+00-.57E+00-.64E+00-.74E+00-.86E+00-.99E+00-.11E+01-.11E+01-.83E+000.46E-01
-.52E+00-.57E+00-.65E+00-.75E+00-.89E+00-.10E+01-.12E+01-.12E+01-.89E+000.51E-01
-.52E+00-.57E+00-.65E+00-.77E+00-.91E+00-.11E+01-.12E+01-.12E+01-.95E+000.56E-01
-.52E+00-.57E+00-.66E+00-.78E+00-.94E+00-.11E+01-.13E+01-.13E+01-.10E+010.62E-01
-.52E+00-.57E+00-.67E+00-.80E+00-.96E+00-.12E+01-.13E+01-.14E+01-.11E+010.67E-01
-.52E+00-.58E+00-.67E+00-.81E+00-.99E+00-.12E+01-.14E+01-.15E+01-.12E+010.73E-01
-.52E+00-.58E+00-.68E+00-.83E+00-.10E+01-.12E+01-.15E+01-.16E+01-.13E+010.80E-01
-.52E+00-.58E+00-.69E+00-.84E+00-.10E+01-.13E+01-.15E+01-.16E+01-.13E+010.86E-01
-.52E+00-.58E+00-.70E+00-.86E+00-.11E+01-.13E+01-.16E+01-.17E+01-.14E+010.93E-01

SHEAR STRESS:

-.14E-06-.28E-06-.39E-06-.48E-06-.54E-06-.55E-06-.51E-06-.41E-06-.25E-060.00E+00
-.39E-05-.75E-05-.11E-04-.13E-04-.15E-04-.15E-04-.14E-04-.11E-04-.67E-050.00E+00
-.18E-04-.35E-04-.50E-04-.61E-04-.68E-04-.70E-04-.65E-04-.52E-04-.31E-040.00E+00
-.50E-04-.96E-04-.14E-03-.17E-03-.19E-03-.19E-03-.18E-03-.14E-03-.85E-040.00E+00
-.11E-03-.21E-03-.29E-03-.36E-03-.40E-03-.41E-03-.38E-03-.31E-03-.18E-030.00E+00
-.20E-03-.38E-03-.54E-03-.66E-03-.74E-03-.75E-03-.70E-03-.56E-03-.33E-030.00E+00
-.33E-03-.63E-03-.90E-03-.11E-02-.12E-02-.13E-02-.12E-02-.94E-03-.55E-030.00E+00
-.51E-03-.98E-03-.14E-02-.17E-02-.19E-02-.19E-02-.18E-02-.14E-02-.85E-030.00E+00
-.74E-03-.14E-02-.20E-02-.25E-02-.28E-02-.28E-02-.26E-02-.21E-02-.12E-020.00E+00
-.10E-02-.20E-02-.28E-02-.35E-02-.39E-02-.39E-02-.36E-02-.29E-02-.17E-020.00E+00
-.14E-02-.26E-02-.38E-02-.46E-02-.51E-02-.52E-02-.48E-02-.38E-02-.23E-020.00E+00
-.17E-02-.33E-02-.47E-02-.58E-02-.64E-02-.65E-02-.60E-02-.48E-02-.28E-020.00E+00

-.20E-02-.39E-02-.55E-02-.68E-02-.75E-02-.76E-02-.70E-02-.56E-02-.33E-020.00E+00
-.21E-02-.41E-02-.58E-02-.71E-02-.78E-02-.79E-02-.73E-02-.58E-02-.34E-020.00E+00
-.17E-02-.33E-02-.47E-02-.57E-02-.63E-02-.64E-02-.59E-02-.47E-02-.27E-020.00E+00
-.32E-03-.62E-03-.88E-03-.11E-02-.12E-02-.12E-02-.11E-02-.88E-03-.51E-030.00E+00

.28E-020.53E-020.75E-020.92E-020.10E-010.10E-010.95E-020.76E-020.44E-020.00E+00

.84E-020.16E-010.23E-010.28E-010.31E-010.32E-010.29E-010.23E-010.14E-010.00E+00

.17E-010.33E-010.47E-010.58E-010.64E-010.65E-010.60E-010.48E-010.28E-010.00E+00

.29E-010.56E-010.79E-010.97E-010.11E+000.11E+000.10E+000.83E-010.49E-010.00E+00

.42E-010.81E-010.11E+000.14E+000.16E+000.16E+000.15E+000.12E+000.75E-010.00E+00

.54E-010.11E+000.15E+000.19E+000.21E+000.22E+000.21E+000.17E+000.10E+000.00E+00

.66E-010.13E+000.18E+000.23E+000.26E+000.27E+000.26E+000.22E+000.13E+000.00E+00

.77E-010.15E+000.22E+000.27E+000.31E+000.32E+000.31E+000.26E+000.16E+000.00E+00

.86E-010.17E+000.24E+000.31E+000.35E+000.37E+000.36E+000.31E+000.19E+000.00E+00

.95E-010.19E+000.27E+000.34E+000.40E+000.42E+000.41E+000.35E+000.22E+000.00E+00

.10E+000.20E+000.30E+000.38E+000.44E+000.47E+000.46E+000.40E+000.26E+000.00E+00

.11E+000.22E+000.32E+000.41E+000.48E+000.52E+000.51E+000.45E+000.29E+000.00E+00

.12E+000.23E+000.34E+000.44E+000.52E+000.56E+000.56E+000.49E+000.32E+000.00E+00

.13E+000.25E+000.37E+000.47E+000.55E+000.61E+000.61E+000.54E+000.36E+000.00E+00

.13E+000.26E+000.39E+000.50E+000.59E+000.66E+000.67E+000.60E+000.40E+000.00E+00

.14E+000.28E+000.41E+000.53E+000.63E+000.70E+000.72E+000.65E+000.44E+000.00E+00

.15E+000.29E+000.43E+000.56E+000.67E+000.75E+000.77E+000.71E+000.48E+000.00E+00

.15E+000.30E+000.45E+000.59E+000.71E+000.80E+000.83E+000.76E+000.52E+000.00E+00

.16E+000.31E+000.47E+000.62E+000.75E+000.85E+000.89E+000.82E+000.57E+000.00E+00

.16E+000.33E+000.49E+000.64E+000.79E+000.90E+000.95E+000.89E+000.62E+000.00E+00

.17E+000.34E+000.51E+000.67E+000.83E+000.95E+000.10E+010.95E+000.67E+000.00E+00

.17E+000.35E+000.53E+000.70E+000.87E+000.10E+010.11E+010.10E+010.73E+000.00E+00

.18E+000.36E+000.55E+000.73E+000.91E+000.11E+010.11E+010.11E+010.79E+000.00E+00

.19E+000.37E+000.57E+000.76E+000.95E+000.11E+010.12E+010.12E+010.85E+000.00E+00

.19E+000.39E+000.59E+000.79E+000.99E+000.12E+010.13E+010.13E+010.92E+000.00E+00

.20E+000.40E+000.61E+000.82E+000.10E+010.12E+010.14E+010.13E+010.99E+000.00E+00

.20E+000.41E+000.63E+000.85E+000.11E+010.13E+010.14E+010.14E+010.11E+010.00E+00

.21E+000.42E+000.65E+000.88E+000.11E+010.14E+010.15E+010.15E+010.12E+010.00E+00

.21E+000.43E+000.67E+000.91E+000.12E+010.14E+010.16E+010.16E+010.12E+010.00E+00

.22E+000.44E+000.68E+000.95E+000.12E+010.15E+010.17E+010.17E+010.13E+010.00E+00

.22E+000.46E+000.70E+000.98E+000.13E+010.16E+010.18E+010.18E+010.14E-010.00E+00

.23E+000.47E+000.72E+000.10E+010.13E+010.16E+010.19E+010.20E+010.15E+010.00E+00

.23E+000.48E+000.74E+000.10E+010.14E+010.17E+010.20E+010.21E+010.16E+010.00E+00

.24E+000.49E+000.77E+000.11E+010.14E+010.18E+010.21E+010.22E+010.18E+010.00E+00

.24E+000.50E+000.79E+000.11E+010.15E+010.19E+010.22E+010.23E+010.19E+010.00E+00

.25E+000.51E+000.81E+000.11E+010.15E+010.19E+010.23E+010.25E+010.20E+010.00E+00

.25E+000.52E+000.83E+000.12E+010.16E+010.20E+010.24E+010.26E+010.22E+010.00E+00

.26E+000.53E+000.85E+000.12E+010.16E+010.21E+010.26E+010.28E+010.23E+010.00E+00

.26E+000.55E+000.87E+000.12E+010.17E+010.22E+010.27E+010.30E+010.25E+010.00E+00

SAMPLE OUTPUT FROM POCHHAMMER-CHREE PROGRAM
FILE FOR001.DAT (first page only)

incident	reflected	transmitted	stresses
-0.000927	-0.037942	0.066404	
-0.001246	-0.035632	0.066411	
-0.003111	-0.032091	0.063479	
-0.004295	-0.027605	0.058842	
-0.002979	-0.022447	0.053575	
0.001690	-0.016882	0.048329	
0.009385	-0.011174	0.043237	
0.018760	-0.005606	0.038004	
0.027920	-0.000466	0.032121	
0.035026	0.003985	0.025112	
0.038826	0.007562	0.016738	
0.038968	0.010201	0.007095	
0.035998	0.011988	-0.003407	
0.031091	0.013132	-0.014154	
0.025609	0.013917	-0.024470	
0.020658	0.014618	-0.033750	
0.016783	0.015420	-0.041529	
0.013884	0.016365	-0.047491	
0.011361	0.017349	-0.051440	
0.008407	0.018158	-0.053255	
0.004341	0.018550	-0.052874	
-0.001133	0.018336	-0.050314	
-0.007837	0.017451	-0.045719	
-0.015190	0.015971	-0.039412	
-0.022402	0.014091	-0.031913	
-0.028718	0.012063	-0.023897	
-0.033595	0.010114	-0.016098	
-0.036785	0.008377	-0.009175	
-0.038289	0.006866	-0.003573	
-0.038227	0.005478	0.000559	
-0.036702	0.004052	0.003378	
-0.033709	0.002430	0.005275	
-0.029141	0.023570	0.019545	
-0.022886	0.020394	0.021017	
-0.014981	0.015843	0.021732	
-0.005739	0.011028	0.022070	
0.004193	0.007046	0.022322	
0.013897	0.004653	0.022646	
0.022349	0.004054	0.023051	
0.028651	0.004873	0.023434	
0.032242	0.006303	0.023628	
0.033028	0.007369	0.023465	
0.031396	0.007234	0.022825	
0.028090	0.005430	0.021667	
0.024005	0.001965	0.020042	
0.019960	-0.002721	0.018075	
0.016519	-0.007927	0.015941	
0.013907	-0.012910	0.013825	
0.012039	-0.017096	0.011881	
0.010630	-0.020197	0.010199	
0.009339	-0.022230	0.008777	
0.007894	-0.023427	0.007513	
0.006150	-0.024102	0.006222	
0.004077	-0.024511	0.004668	
0.001691	-0.024761	0.002624	
-0.001023	-0.024795	-0.000067	
-0.004157	-0.024445	-0.003432	
-0.007870	-0.023514	-0.007337	
-0.012310	-0.021867	-0.011486	
-0.017499	-0.019478	-0.015469	
-0.023238	-0.016424	-0.018838	
-0.029051	-0.012840	-0.021208	
-0.034228	-0.008856	-0.022342	

APPENDIX B

AMPLITUDES AND RADIUS OVER WAVELENGTH VALUES

Ratio of Fourier Coefficients for Given a/Λ of 3 Bar Diameters
2, 3, AND 6 INCH BARS

Duration -->		250 μsec	250 μsec	1000 μsec
Bar Diameter -->		2-inch	3-inch	6-inch
n	D_n/A_o	$\frac{a}{\Lambda}$		
1	-.635	.0105	.0154	.0076
2	.2116	.0316	.0464	.0228
3	-.1263	.0528	.0776	.038
4	.0895	.0741	.1092	.0533
5	-.0689	.0956	.1418	.0686
6	.0556	.1174		.0841
7	-.0463	.1397		.0997
8	.0394			.1154
9	-.0340			.1314
10	.0297			

APPENDIX C

MISCELLANEOUS HULL PLOTS

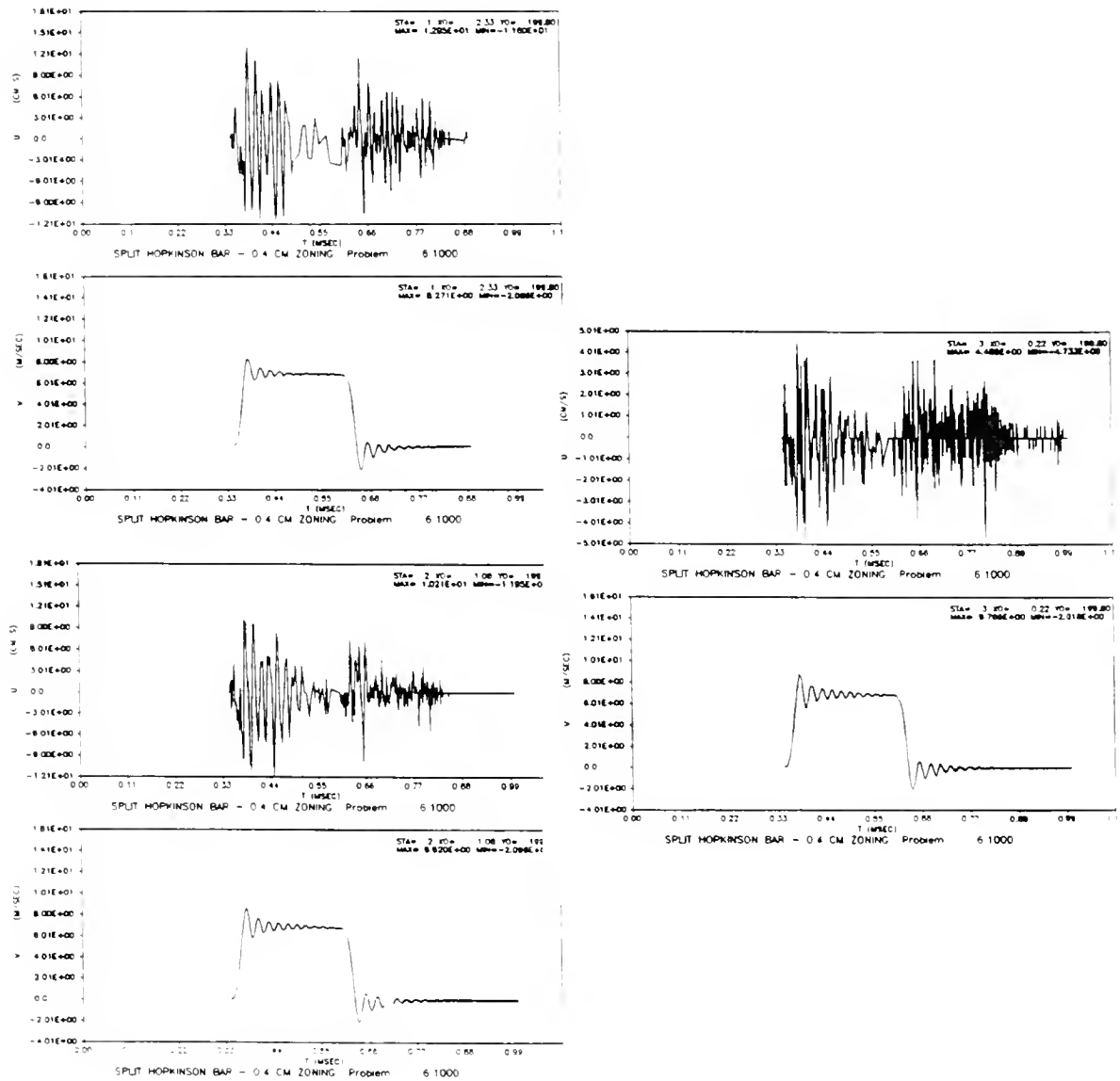

Figure 38. HULL Output. 2-inch SHPB. Radial and Longitudinal Velocities at Incident Bar - Specimen Interface. (Bar Surface: Top , Middle of the Bar: Bottom , Bar Center: Right)

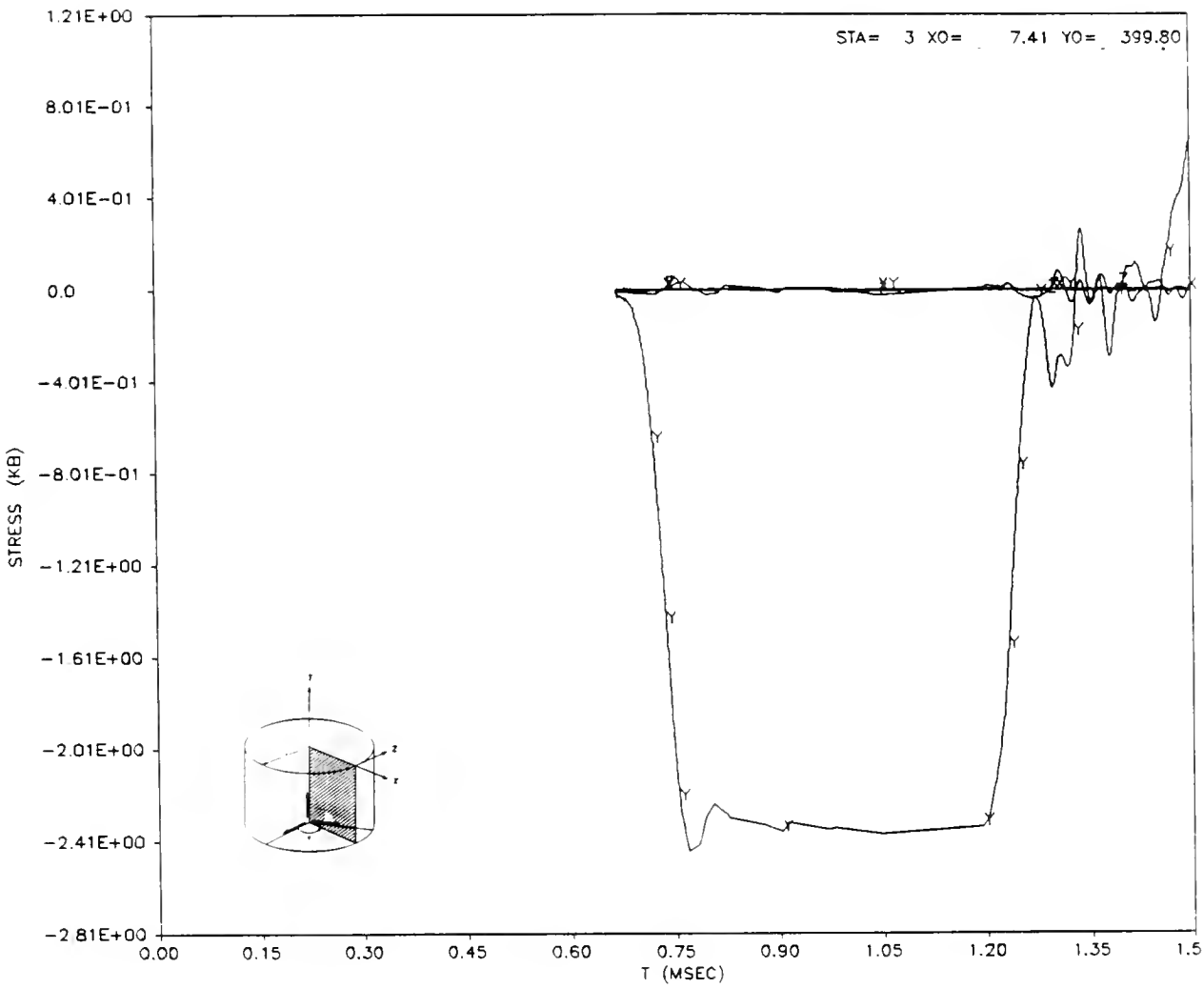

Figure 39. HULL Output. 6-inch SHPB. All Transmitted Stresses at Bar Surface

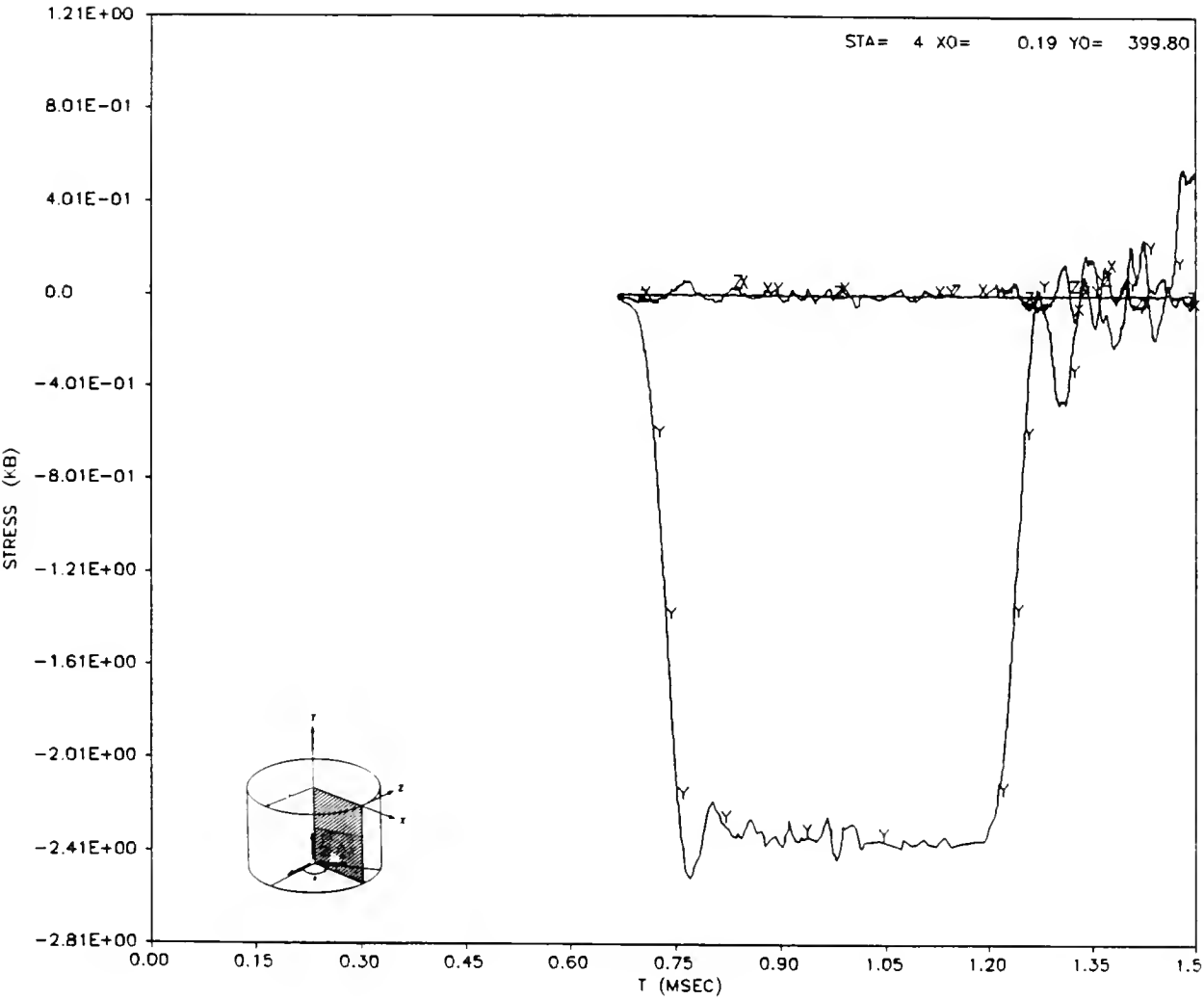

Figure 40. HULL Output. 6-inch SHPB. All Transmitted Stresses at Bar Center Compare with Figure 37

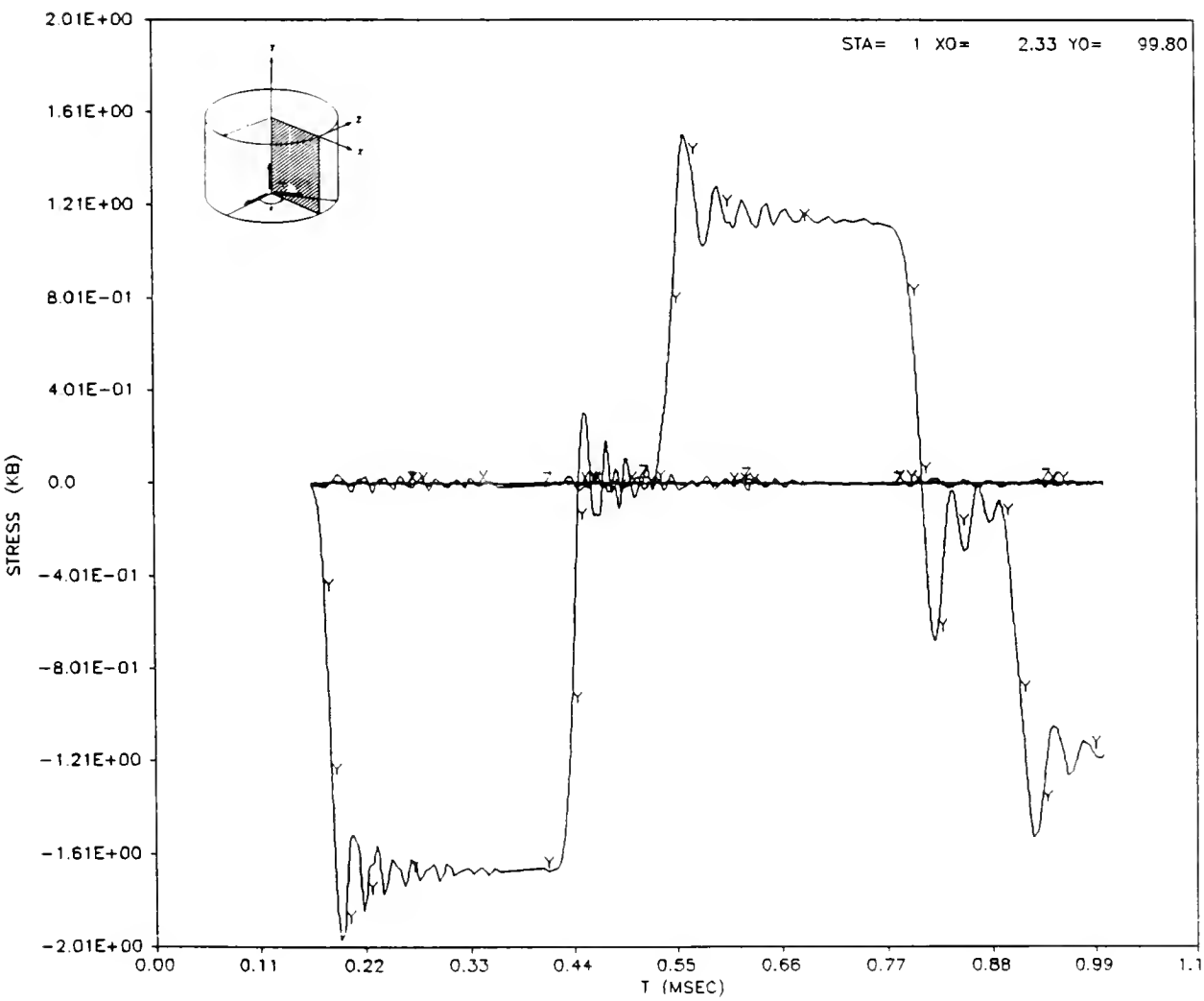

Figure 41. HULL Output. 2-inch SHPB. 1-inch Aluminum Specimen. Incident and Reflected Stresses

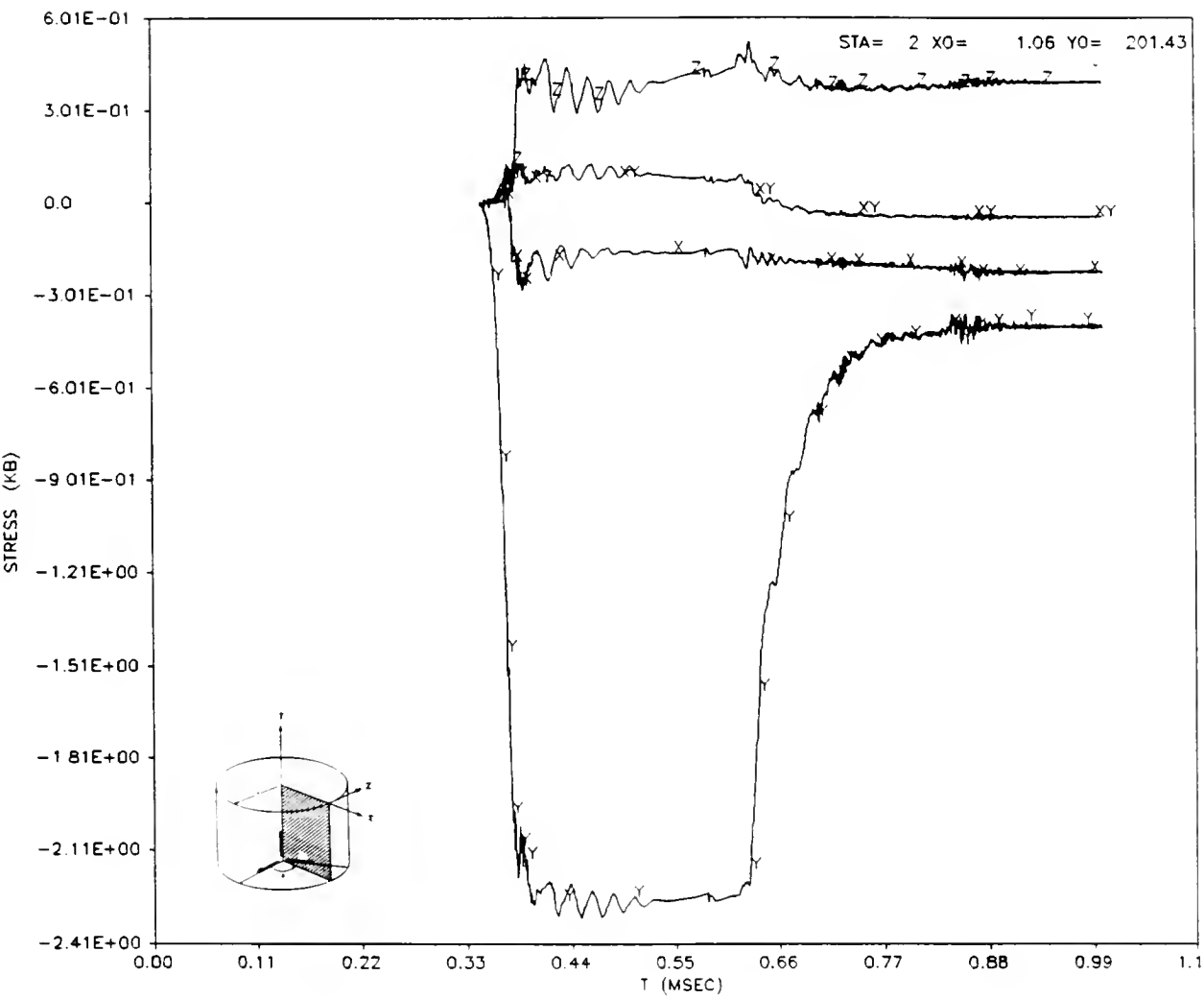

Figure 42. HULL Output. 2-inch SHPB. 1-inch Aluminum Specimen. All Stresses Within the Specimen

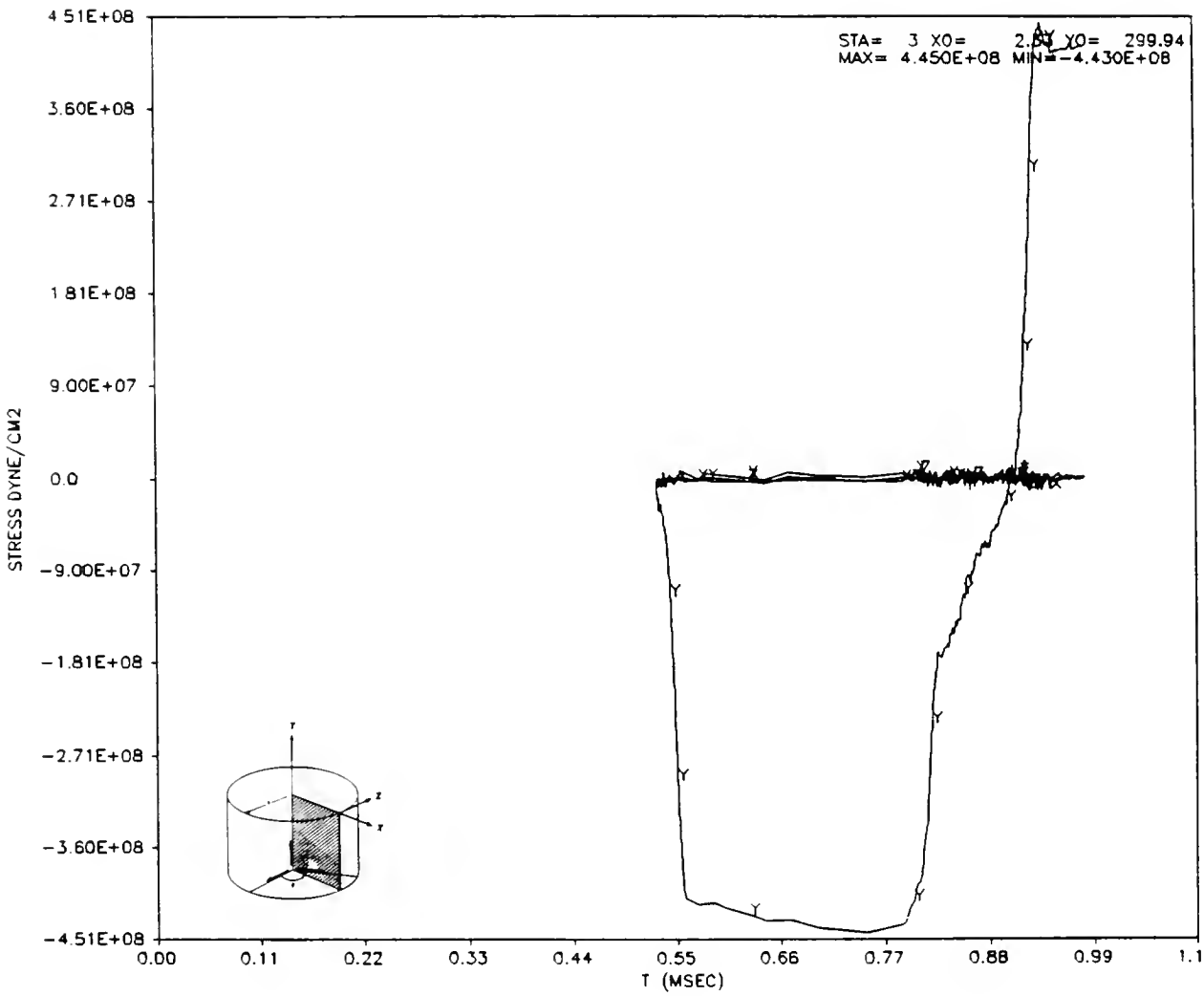

Figure 43. HULL Output. 2-inch SHPB. 1-inch Aluminum Specimen. All Stresses in the Transmitter Bar

APPENDIX D

HULL SAMPLE INPUT FILES

```
KEEL LAGRANGE PROB 6.1
INMEML=1
XLBOW=10000
HEADER
 SPLIT HOPKINSON BAR - 0.4 CM ZONING
NM=2 FE=1  AL=2
NLREG=3
REGION 1
NXI=7 NYJ=501
NT=FIXX NX=1,1 NY= 2,501
NT=FREE NX=7,7 NY=2,501
NT=MASTER NX=1,4 NY=501,501
NT=FREE NX=5,7 NY=501,501
NT=PRES NX=1,7 NY=1,1
MAT=1 NX=1,7 NY=1,501
NS=QUAD NX=1,7 NY=1,501
X1=2.54 X2 2.54 X3 0 X4 0
Y1 200 Y2 0 Y3 0 Y4 200
REGION 2
NXI=7 NYJ=501
NT=FIXX NX=1,1 NY=2,501
NT=FREE NX=7,7 NY=2,501
NT=FREE NX=2,7 NY=501,501
NT=FREE NX=5,7 NY=1,1
NT=MASTER NX=1,4 NY=1,1
MAT=1 NX=1,7 NY=1,501
NS=QUAD NX=1,7 NY=1,501
X1 2.54 X2 2.54 X3 0 X4 0
Y1 401.92 Y2 201.92 Y3 201.92 Y4 401.92
REGION 3
NXI=4 NYJ=9
NT=FIXX NX=1,1 NY=1,9
NT=FREE NX=4,4 NY=2,9
NT=SLAVE MASTREG=1 NX=1,4 NY=1,1
NT=SLAVE MASTREG=2 NX=1,4 NY=9,9
MAT=2 NX=1,4 NY=1,9
NS=QUAD NX=1,4 NY=1,9
X1 0.96 X2 0.96 X3 0 X4 0
Y1 201.92 Y2 200 Y3 200 Y4 201.92
STATIONS
XL 2.54 YL 200
XL 0.96 YL 200
XL 0.02 YL 200
XL 2.54 YL 201.92
END
```

```
HULL LAGRANGE
PROB 6.1
CYCLE=0
NPRES=3
P=28.0E8 T=0
P=28.0E8 T=257.E-6
P=0 T=257.5E-6
PTSTOP=1500.E-6
```

APPENDIX E

FORTRAN LISTING FOR INERTIA CORRECTION

```
      ******************************************************
      *LINES WITH ** ARE THOSE ADDED TO CORRECT FOR INERTIA*
      ******************************************************

C     THE PHASE CORRECTIONS HAVE BEEN DONE. THE USER HAS NOW THE
C     OPTION TO STOP THE PROGRAM, OR TO CONTINUE  TO CALCULATE
C     STRESSES, STRAINS, ETC...
c
 72   write(*,*)'THE CORRECTIONS ON',ks ,' SET(S) OF DATA HAVE'
      write(*,*)'BEEN CALCULATED. DO YOU WISH TO PROCEDE WITH'
      write(*,*)'THE STRESS AND STRAIN CALCULATIONS? Y/N'
      read(*,1001)OP
      if(OP.EQ.'N'.or.op.eq.'n')GO TO 66
      if(op.ne.'Y'.and.op.ne.'y') go to 72
c
 26   ssfac=(velocb**2)*ro*1.0e-6
c
 1011 format(a)
 1002 format(3f10.3)
 1003 format(4f10.3)
c1004 format(f6.2,1h,f10.3)
 1005 format(f10.3)
 1006 format(i2)
 1007 format(' enter # ',i2,' specimen ID')
c
c
      AREAB=3.14159*DIA*DIA/4.
      EGCONS=AREAB*VELOCB*TSTEP*SSFAC
c
  75  write(*,*)'Which set of data is to be used'
      write(*,*)'Original(0) or Corrected(1)'
      read(*,*)l
      if(l.ne.0.and.l.ne.1)GO TO 75
      write(*,*)'Enter the total number of specimens'
      read(*,*)ns
      do 21 i=1,ns
      write(*,1007)i
      read(*,1011)n(i)
      write(*,*)'specimen length, in meters'
      read(*,*)sl(i)
      write(*,*)'Enter cross section area ratio of bars to the specimen'
      read(*,*)ar(i)
  21  continue
c
      do 23 ik=1,ns
      id=n(ik)
      slen=sl(ik)
      aratio=ar(ik)
c
c     using original set of data (uncorrected)
c
      if(l.eq.0)then
      idi=id//'i.dat'
      idr=id//'r.dat'
      idt=id//'t.dat'
c
c     output files:uncorrected.  (example: if ID is test then
c     output will be testsso.dat)
c
```

```
      idsts=id//'sso.dat'
      idstn=id//'sno.dat'
      ideng=id//'eno.dat'
c
c     using corrected set of data

      else
      idif=id//'if.dat'
      idrf=id//'rf.dat'
      idtf=id//'tf.dat'
c
c     ouput files
c
      idsts=id//'ssf.dat'
      idstn=id//'snf.dat'
      ideng=id//'enf.dat'
      endif
c
c
c
      if(l.eq.0)open(1,file=idi,status='old')
      if(l.eq.1)open(1,file=idif,status='old')
      do 15 i=1,ni
      read(1,1005)binc(i)
   15 continue
      close(1)
      if(l.eq.0)open(1,file=idr,status='old')
      if(l.eq.1)open(1,file=idrf,status='old')
      do 16 i=1,ni
      read(1,1005)bref(i)
   16 continue
      close(1)
      if(l.eq.0)open(1,file=idt,status='old')
      if(l.eq.1)open(1,file=idtf,status='old')
      do 27 i=1,ni
      read(1,1005)btra(i)
   27 continue
      close(1)

      flag=1.0                                                    **
      cor=ro*((slen**2)/6.-.09*(dia**2)/8.)*1.0e-6                **

      write(*,*)'DO YOU WANT TO CORRECT FOR INERTIA? Y/N'         **
      read(*,1001)op                                              **
      if(op.eq.'y'.or.op.eq.'Y')go to 45                          **
      flag=0.0                                                    **
c
   73 write(*,*)'DO YOU WANT TO CALCULATE STRESSES? Y/N'
      read(*,1001)op
      if(op.eq.'N'.or.op.eq.'n')go to 44
      if(op.ne.'Y'.and.op.ne.'y')go to 73
      open(11,file=idsts,status='unknown')
      do 11 i=1,ni
      strsin=(binc(i)+bref(i))*ssfac*aratio*1.e-6
      strsot=btra(i)*ssfac*aratio*1.e-6

c     CALCULATE STRESS AND CORRECT FOR INERTIA                    **

      stress=(strsin+strsot)/2.+cor*e2dot(i)*flag                 **
```

```
      write(11,1002)strsin,strsot,stress
   11 continue
      close(11)
C
      write(*,*)idsts

      if(flag.eq.1.0) go to 46                                        **
C
   44 write(*,*)'DO YOU WANT TO CALCULATE STRAINS AND VELOCITIES? Y/N'
      read(*,1001)op
      if(op.eq.'N'.or.op.eq.'n') go to 23
      if(op.ne.'Y'.and.op.ne.'y')go to 44
   45 open(22,file=idstn,status='unknown')
      do 112 i=1,ni
      velin=(binc(i)-bref(i))*velocb*1.e-06
      velot=btra(i)*velocb*1.e-06
      strnrt=(velin-velot)/slen
      if(i-1)118,118,19
  118 strain=0.
      e2dot(1)=strnrt/(tstep*1.e-06)                                  **
      go to 20
   19 strain=strain+strnrt*tstep*1.e-04
      ii=i-1                                                          **

C     CALCULATE THE SECOND DERIVATIVE OF THE STRAIN                   **
C     TO CORRECT FOR INERTIA                                          **

      e2dot(i)=strnrt/(tstep*1.e-06)-e2dot(ii)                        **
   20 write(22,1003)strnrt,strain,velin,velot
  112 continue
      close(22)

      if(flag.eq.1.0) go to 73                                        **
C
   46 write(*,*)idstn
C
C
   23 continue

   66 CONTINUE
```

BIOGRAPHICAL SKETCH

Elisabetta Lidia Landi was born in Torino, Italy. She first came to the United States to attend her last year of high school. She entered the Ohio State University in January 1978 and graduated with a Bachelor of Science in Mechanical Engineering in August 1981, and with a Master of Science degree in mechanical engineering in June 1983.

In the summer of 1983 Elisabetta married David Mark Jerome and moved to Florida, and subsequently was employed as a research engineer at Eglin Air Force Base. She and her husband moved to Gainesville, Florida, between August 1986 and August 1987 to attend graduate school at the University of Florida in the Aerospace Engineering, Mechanics and Engineering Science department. During that year she completed her residency requirements for the Doctor of Philosophy degree. They moved back to Eglin Air Force Base where she got a job with Sverdrup Technology as a research engineer. While working there, she completed the requirements for her doctoral degree. Elisabetta and David plan to make Florida their home in the years to come.

I certify that I have read this study and that in my opinion it conforms to acceptable standards of scholarly presentation and is fully adequate, in scope and quality, as a dissertation for the degree of Doctor of Philosophy

C. Allen Ross, Chair
Professor Emeritus of Aerospace Engineering, Mechanics and Engineering Science

I certify that I have read this study and that in my opinion it conforms to acceptable standards of scholarly presentation and is fully adequate, in scope and quality, as a dissertation for the degree of Doctor of Philosophy.

Ulrich H. Kurzweg
Professor of Aerospace Engineering, Mechanics and Engineering Science

I certify that I have read this study and that in my opinion it conforms to acceptable standards of scholarly presentation and is fully adequate, in scope and quality, as a dissertation for the degree of Doctor of Philosophy.

Daniel C. Drucker
Graduate Research Professor of Aerospace Engineering, Mechanics and Engineering Science

I certify that I have read this study and that in my opinion it conforms to acceptable standards of scholarly presentation and is fully adequate, in scope and quality, as a dissertation for the degree of Doctor of Philosophy.

Lawrence E. Malvern
Professor Emeritus of Aerospace Engineering, Mechanics and Engineering Science

I certify that I have read this study and that in my opinion it conforms to acceptable standards of scholarly presentation and is fully adequate, in scope and quality, as a dissertation for the degree of Doctor of Philosophy.

Bruce H. Edwards
Associate Professor of Mathematics

This dissertation was submitted to the Graduate Faculty of the College of Engineering and to the Graduate School and was accepted as partial fulfillment of the requirements for the degree of Doctor of Philosophy.

August 1991

for Winfred M. Phillips
Dean, College of Engineering

Madelyn M. Lockhart
Dean, Graduate School